2013

ACTIVE OPTIMAL CONTROL STRATEGIES FOR INCREASING THE EFFICIENCY OF PHOTOVOLTAIC CELLS

Sharif Aljoaba
Univesrity of Kentucky, sharif.aljoaba@uky.edu

Recommended Citation

STUDENT AGREEMENT:

I represent that my thesis or dissertation and abstract are my original work. Proper attribution has been given to all outside sources. I understand that I am solely responsible for obtaining any needed copyright permissions. I have obtained and attached hereto needed written permission statements(s) from the owner(s) of each third-party copyrighted matter to be included in my work, allowing electronic distribution (if such use is not permitted by the fair use doctrine).

I hereby grant to The University of Kentucky and its agents the non-exclusive license to archive and make accessible my work in whole or in part in all forms of media, now or hereafter known. I agree that the document mentioned above may be made available immediately for worldwide access unless a preapproved embargo applies.

I retain all other ownership rights to the copyright of my work. I also retain the right to use in future works (such as articles or books) all or part of my work. I understand that I am free to register the copyright to my work.

REVIEW, APPROVAL AND ACCEPTANCE

The document mentioned above has been reviewed and accepted by the student's advisor, on behalf of the advisory committee, and by the Director of Graduate Studies (DGS), on behalf of the program; we verify that this is the final, approved version of the student's dissertation including all changes required by the advisory committee. The undersigned agree to abide by the statements above.

<div align="right">

Sharif Aljoaba, Student

Dr. Bruce L. Walcott, Major Professor

Dr. Zhi David Chen, Director of Graduate Studies

</div>

ACTIVE OPTIMAL CONTROL
STRATEGIES FOR INCREASING
THE EFFICIENCY OF PHOTOVOLTAIC CELLS

DISSERTATION

A dissertation submitted in partial fulfillment of the
requirements for the degree of Doctor of Philosophy in the
College of Engineering at the University of Kentucky

By

Sharif Zidan Ahmad Aljoaba

Lexington, Kentucky

Co-Directors: Dr. Bruce Walcott, Professor of Engineering Alumni Association
and   Dr. Aaron Cramer, Professor of Electrical Engineering

Lexington, Kentucky

ABSTRACT OF DISSERTATION

ACTIVE OPTIMAL CONTROL
STRATEGIES FOR INCREASING
THE EFFICIENCY OF PHOTOVOLTAIC CELLS

Energy consumption has increased drastically during the last century. Currently, the worldwide energy consumption is about 17.4 TW and is predicted to reach 25 TW by 2035. Solar energy has emerged as one of the potential renewable energy sources. Since its first physical recognition in 1887 by Adams and Day till nowadays, research in solar energy is continuously developing. This has lead to many achievements and milestones that introduced it as one of the most reliable and sustainable energy sources. Recently, the International Energy Agency declared that solar energy is predicted to be one of the major electricity production energy sources by 2035.

Enhancing the efficiency and lifecycle of photovoltaic (PV) modules leads to significant cost reduction. Reducing the temperature of the PV module improves its efficiency and enhances its lifecycle. To better understand the PV module performance, it is important to study the interaction between the output power and the temperature. A model that is capable of predicting the PV module temperature and its effects on the output power considering the individual contribution of the solar spectrum wavelengths significantly advances the PV module designs toward higher efficiency.

In this work, a thermoelectrical model is developed to predict the effects of the solar spectrum wavelengths on the PV module performance. The model is characterized and validated under real meteorological conditions where experimental temperature and output power of the PV module measurements are shown to agree with the predicted results.

The model is used to validate the concept of active optical filtering. Since this model is wavelength-based, it is used to design an active optical filter for PV applications. Applying this filter to the PV module is expected to increase the output power of the module by filtering the spectrum wavelengths. The active filter performance is optimized, where different cutoff wavelengths are used to maximize the module output power. It is predicted that if the optimized active optical filter is applied to the PV module, the

module efficiency is predicted to increase by about 1%. Different technologies are considered for physical implementation of the active optical filter.

KEY WORDS: Thermoelectrical Modeling, Photovoltaic Energy, Experimental Parameterization, Active Optical Filtering, Performance Optimization

Sharif Z. Aljoaba
_____
Student's Signature

April 11, 2013
_____
Date

ACTIVE OPTIMAL CONTROL
STRATEGIES FOR INCREASING
THE EFFICIENCY OF PHOTOVOLTAIC CELLS

By

Sharif Zidan Ahmad Aljoaba

Bruce L. Walcott, Ph.D
_____
Co-Director of Dissertation

Aaron M. Cramer, Ph.D
_____
Co-Director of Dissertation

David Z. Chen, Ph.D
_____
Director of Graduate Studies

April 11, 2013
_____

To my wife, Hadeel

Your endless support, love, and encouragement have been my
continuous source of inspiration and patience. You are the
light that helps me to see when darkness shades my trip
through that tunnel that finally I saw its end

To my parents, Zidan and Maha

Your continuous encouragement has helped me to start my trip
and your endless support has been my boat that helped me to
reach my goals

ACKNOWLEDGEMENTS

TABLE OF CONTENTS

LIST OF TABLE

LIST OF FIGURES

CHAPTER 1.

PREFACE

1.1. Introduction

Energy demand and consumption has increased drastically during the last century. Currently, the worldwide energy consumption is about 17.4 TW and it is predicted to increase to 25 TW by 2035 as shown in Figure 1.1. The energy consumption of the United States between 2004 and 2008 is demonstrated in Table 1.1. The data calculation shows that the United States has consumed 3.3242 TW in 2008. The main contribution to this consumption is fossil fuels. According to the International Energy Agency (IEA), the dominance of fossil fuels in the fuel mix through 2035 is a consistent theme in the global demand analysis [1]. As shown in Figure 1.2, IEA indicates a continuing reliance of fossil fuel use through 2035. This predicted continued reliance will lead to a quicker depletion of our known fossil fuel reserved as well as continued emission of carbon dioxide. In fact, the world's energy-related carbon dioxide emissions in 2007, as stated by the Energy Information Administration (EIA), were 29,914 million metric tons of carbon dioxide. In 2008 only, the United States emitted 5.405 million metric tons of carbon dioxide [2]. The current and the predicted data of carbon dioxide release increase the pollution and further affect the global warming issue.

Given the current and the predicted world reliance on fossil fuels, the energy research community has devoted more attention to finding new sources of energy. These new sources not only need to be environmentally friendly and clean, but also renewable, sustainable, and reliable.

Renewable energy can be generated from several resources such as wind, solar, geothermal, and hydro. These sources are clean, reliable, renewable, and freely available. Recently, the energy organizations and research communities have focused more attention to develop and utilize the renewable energy resources in order to reduce the

reliance on fossil fuels. IEA stated in 2010, that the net consumption of electricity power generated from renewable energy sources increases over time to become by 2015 the major portion as shown in Figure 1.3. Consequently, the growth rates in renewable energy sources are higher than the growth rates in the non-renewable sources.
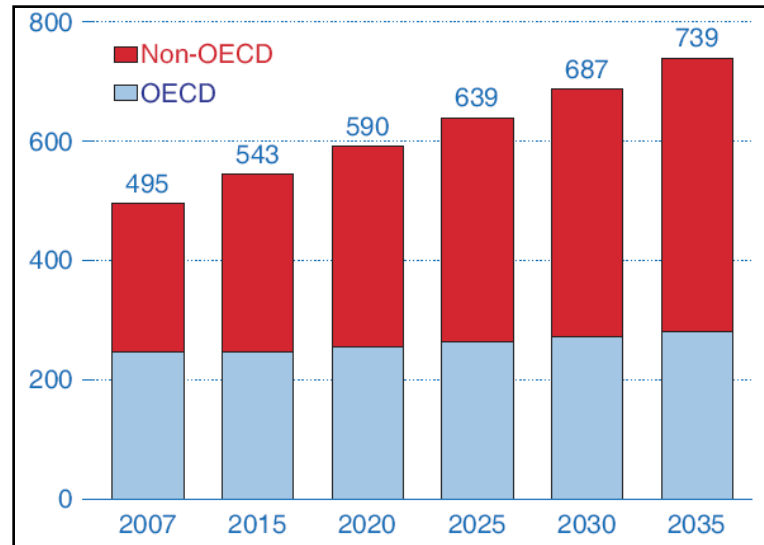
Figure 1.1. World energy consumption, 2007–2035 (QB, 1QB / year = 33.43 GW) [1]

Table 1.2. U.S. Energy consumption by energy source, 2004 to 2008 (QB) [3]

Energy Source	2004	2005	2006	2007	2008
Total	100.334	100.468	99.790	101.502	99.438
Fossil Fuels	85.828	85.815	84.687	86.223	83.532
Coal	22.466	22.797	22.447	22.749	22.398
Coal Coke Net Imports	0.137	0.045	0.061	0.025	0.040
Natural Gas[1]	22.931	22.583	22.224	23.679	23.814
Petroleum[2]	40.292	40.391	39.955	39.769	37.279
Electricity Net Imports	0.039	0.084	0.063	0.106	0.113
Nuclear Electric Power	8.222	8.161	8.215	8.455	8.427
Renewable Energy	6.247	6.407	6.825	6.719	7.367
Biomass[3]	3.010	3.117	3.277	3.503	3.852
Biofuels	0.500	0.577	0.771	0.991	1.372
Waste	0.389	0.403	0.397	0.413	0.436
Wood and Derived Fuels	2.121	2.136	2.109	2.098	2.044
Geothermal Energy	0.341	0.343	0.343	0.349	0.360
Hydroelectric Conventional	2.690	2.703	2.869	2.446	2.512
Solar Thermal/PV Energy	0.065	0.066	0.072	0.081	0.097
Wind Energy	0.142	0.178	0.264	0.341	0.546

[1]Includes supplemental gaseous fuels.
[2]Petroleum products supplied, including natural gas plant liquids and crude oil burned as fuel.
[3]Biomass includes: biofuels, waste (landfill gas, MSW biogenic, and other biomass), wood and wood derived fuels.
PV = Photovoltaic.

The energy generation in the United States from renewable sources increases as the demand increases in most of the states [1]. In fact, the predicted future share of energy generation from renewable sources will grow from 8.5% in 2007 to 17.0% in 2035 as shown in Figure 1.4.
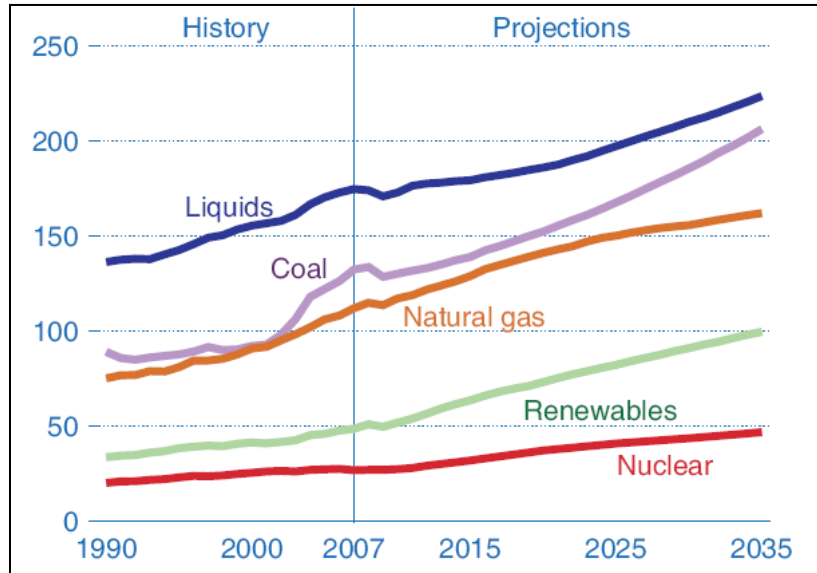
Figure 1.2. World marketed energy use by fuel type, 1990-2035 (QB) [1]
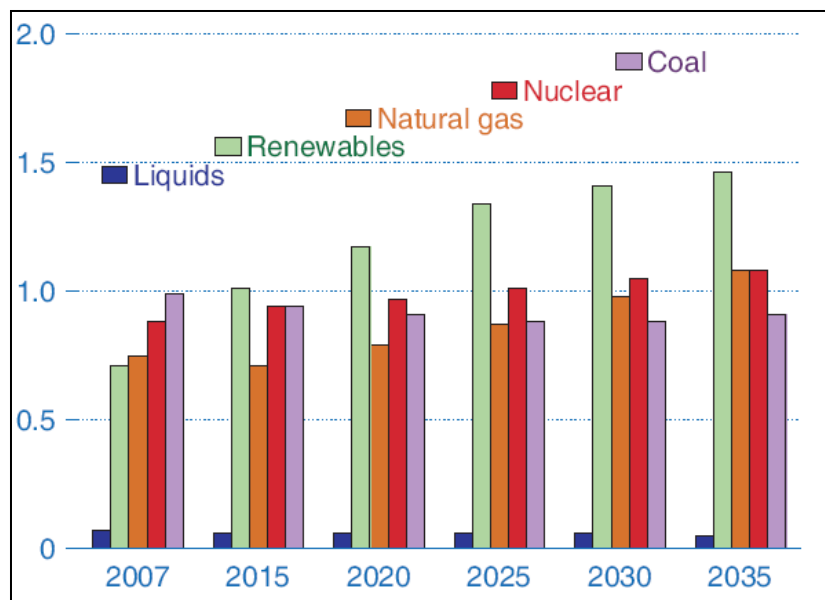
Figure 1.3. Net electricity generation in OECD (Organization for Economic Co-operation and Development) Europe, 2007-2035 (Trillion KWh) [1]
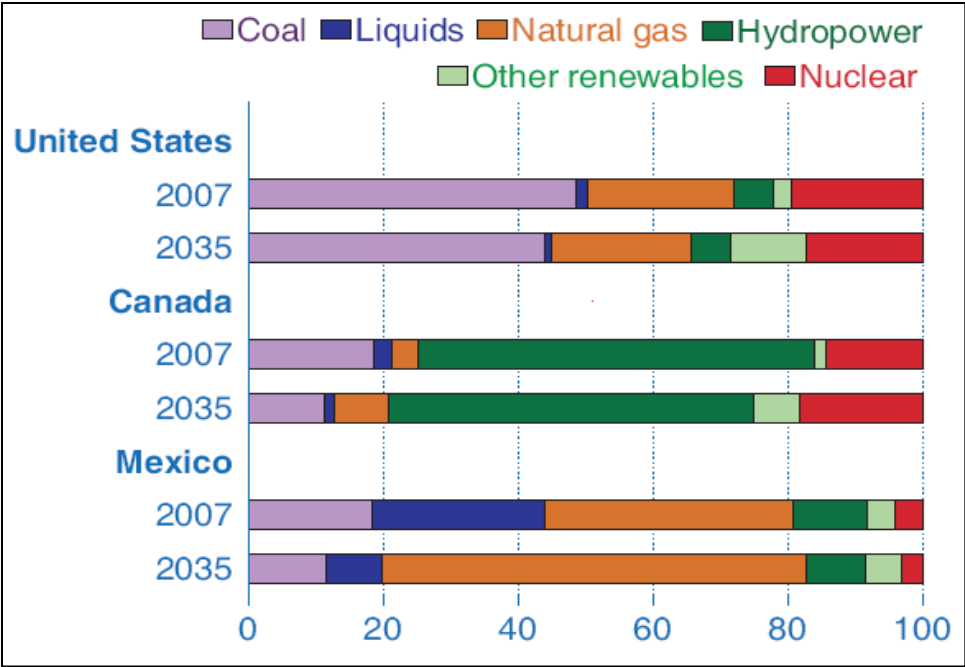
Figure 1.4. Net electricity generation in North America, 2007 and 2035 (percent) [1]

One of the most important energy sources is the sun. One could argue that all energy on earth is derived from the sun with the exception of volcanic and tide based energy. The solar energy is increasingly becoming more efficient to produce electricity. As shown in Figure 1.5, IEA projected that the contribution of solar energy in producing electricity will rapidly increase over the projected period. This can be attributed to the incentives offered and policies adopted by governments in order to construct new solar power generation fields and facilities. While fossil fuel and nuclear power plants generally produce heat to create steam to drive electric turbines, contrastingly, solar energy is far more versatile and can be utilized to create electricity through photovoltaic cells, heat water, and even produce steam.

More specifically, solar energy can be collected to heat the water in pipes which could be supplied to buildings for daily use and also could be used for heating purposes. The solar thermal power plants focus the sun rays using mirrors to heat a fluid to high temperatures. The fluid is then circulated through pipes to transfer the heat to the water in order to produce steam. The steam, in turn, is converted into mechanical energy in a turbine and

into electricity by a conventional generator coupled to the turbine [1]. Furthermore, solar energy can be used to produce electricity using photovoltaic effect which can be obtained by solar or also known as photovoltaic (PV) cells. Briefly, when light hits these cells, electrons in the PV cell material are excited and collected to produce electrical current.
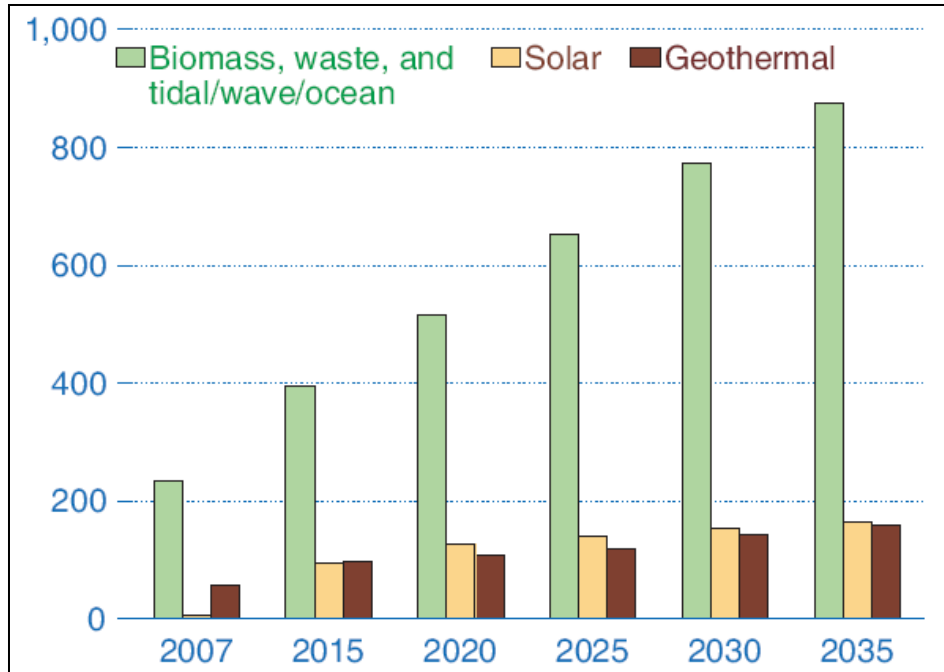
Figure 1.5. World renewable electricity generation by energy source, excluding wind and hydropower, 2007-2035 (Billion KWh) [1]

At the end of 2008, the United States had the largest solar energy plant in the world in California. Out of total 11 plants, nine of them in California, one in Arizona, and one in Nevada. Larger plants are proposed for construction in the future.

While solar power plants need to be located in areas that are highly exposed to sunlight, these plants are quiet, safe, and require a minimal number of workers to maintain them. At the recently opened Sempra 48 MW Solar Plant in El Dorado, Nevada only four workers are needed to staff the facility.

1.2. Photovoltaic cells, motivation historical view

Photovoltaic (PV) is the process of converting sunlight directly into electricity using solar cells. In these cells, when the light photons hit the semiconductor material (the material of the solar cells) excite the electrons to break the bonds and leave their atoms. These electrons in addition to the impurities (doped in the semiconductor material) are called free carriers which cause a current flow (short circuit current) and built in voltage (open circuit voltage) as shown in Figure 1.6.
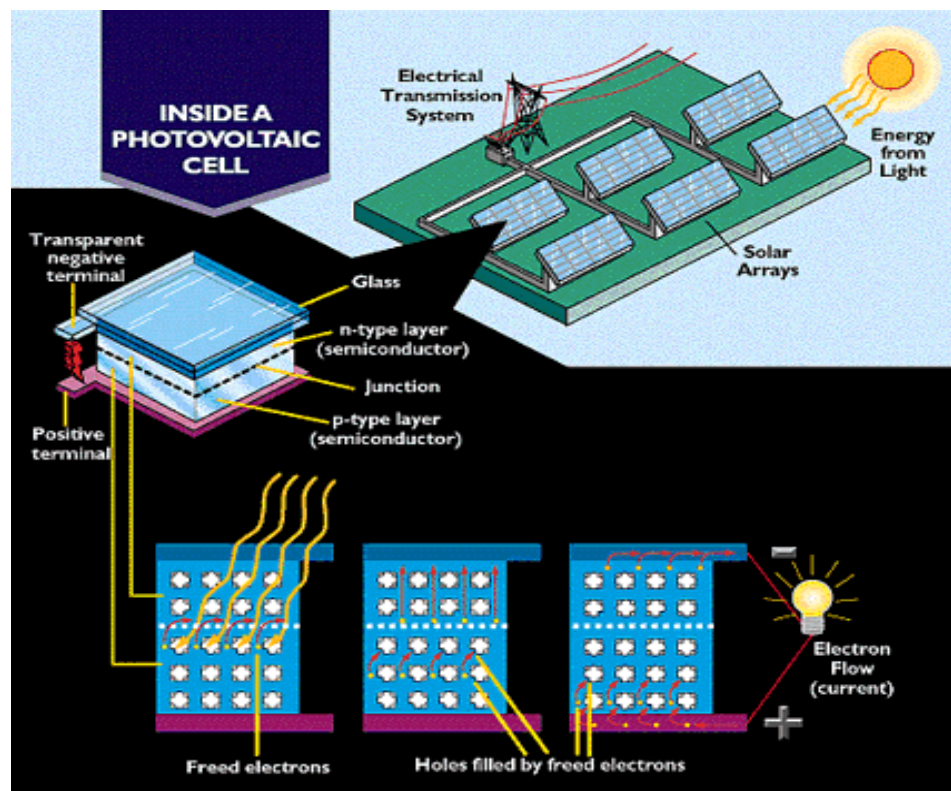
Figure 1.6. Illustration for the photovoltaic effect

The photovoltaic effect is based on the fundamental physical phenomena that are firstly observed in the 19th century. In 1839, Edmond Bequerel observed that when metal plates (platinum or silver) were immersed in a suitable solution (electrolyte) then were exposed to light, small voltage and current were produced [4]. Later in 1878, Adams and Day followed up on the Smith's work [5] on selenium photoconductivity, and published the first report directly attributed to the PV effect in a solid state substrate. In 1954, Chapin,

Fuller, and Pearson of Bell Telephone Laboratories developed a silicon solar cell [6], which generated a significant amount of current when it was exposed to light. The efficiency of this solar cell is about 6% under the irradiance condition that was used.

Solar energy these days is rapidly growing as renewable alternative source to the conventional fossil fuel electricity generation. However, compared to other electricity generating technologies, it is relatively novel, with the first practical photovoltaic devices demonstrated in the 1950s as mentioned above. Research and development of photovoltaics received its first major boost from the space industry in the 1960s which required a power supply separated from the grid power for satellite applications. These space solar cells were more expensive than they are today by several thousand times. The perceived need for an electricity generation method apart from grid power was still a decade away. Solar cells became an exciting scientific variation to the rapidly expanding silicon transistor development with several potentially specialized niche markets [7]. The oil crisis in the 1970s focused the attention on the desirability of alternate energy sources for terrestrial use. This in turn promoted the exploration of photovoltaics as means to generate terrestrial power. Despite the oil crisis did not last long and the financial incentives to develop solar cells abated, solar cells had entered the arena as a power generating technology. Their application and usefulness to the remote power supply area was recognized by the investors and prompted the development of terrestrial photovoltaics industry. Small scale transportable applications (such as calculators and watches) were utilized and remote power applications began to benefit from photovoltaics. [7]

The efficiency of photovoltaics is affected and most probably reduced by several factors. Some of them are related to design issues such as the semiconductor material and the mismatching resistances, and others are related to irradiance conditions. Temperature was found to be a critical factor that significantly affects the PV cell efficiency since temperature is part of the physics that control its operational performance. The temperature increases mainly due to the excess photonic energy in the desired spectrum wavelengths. In addition, the undesired spectrum wavelengths might be absorbed by the

PV module layers and convert into heat that accumulates by time causing efficiency reduction.

Increasing the efficiency of photovoltaics to reduce the production costs is the most important issue for the researchers. In the 1980s research in silicon solar cells produced an increase in solar cell efficiency. In 1985 silicon solar cells achieved the milestone of 20% efficiency [7]. Over the next decade, the photovoltaic industry experienced steady growth rates of between 15% and 20%, largely promoted by the remote power supply market. In the year 1997 the growth rate jumped into 38% [7]. In theory, the maximum efficiency of a solar cell made of single semiconductor layer reported by researchers is limited to 40%. [8]

Today, solar cells are recognized as means to produce power and to enhance the quality of life to those who do not have grid access. Moreover, they significantly reduce the environmental damage caused by conventional electricity generation technologies in the advanced industrial countries [7]. It was found that covering 4% of the world's desert area with photovoltaic panels could supply the equivalent of all of the world's electricity. The Gobi Desert (area of 1,295,000 km^2 (500,002 sq mi)) alone could supply almost all of the world's total electricity demand. [9]

According to Lowis [10], out of the 1.2×10^5 TW of solar energy that strikes the earth's surface, only 600 TW is the practical power potential. To produce 20 TW of carbon-free power using 10% efficient photovoltaic modules, 0.16% of the earth's surface should be covered or equivalently 5×10^{11} m^2.

The estimate of energy consumption of the United States in 2000 was 3.3 TW [10]. The total land area of USA including Alaska is 9.1×10^{12} m^2. The area of the land that should be covered by 10% efficient photovoltaic modules with nominal output power 200W/m^2 will be 1.6×10^{11} m^2. This represents 1.7% of the USA lands. So increasing the efficiency will highly reduce the needed area to produce the demanded power. For instance, if the efficiency of the modules enhanced to 20%, the needed land will be reduced to half.

1.3. Research statement

The main objective of this research is to enhance the efficiency of the photovoltaic cells using optimal control strategies to design an active filtering process that increases the output power through controlling the input power. In this research, lean and sustainable design and implementation of the filtering process will be highly considered and utilized. This helps to satisfy the sub-objectives of this research which are not only decreasing the manufacturing and implementation costs of the active filter, but also increasing the lifecycle of the PV module. These sub-objectives can be accomplished by achieving the following research goals:

1. Understanding and observing the photovoltaic effect of converting light into electricity

2. Understanding the limitations of light-to-electricity conversion efficiency especially the ones that are related to thermal aspects, and addressing the conducted efforts of the researchers to override these limitation

3. Developing a mathematical wavelength-based model that uses computational methods to predict the temperature of the PV module, and its effects on the output power. This model should reflect the individual contribution of the solar spectrum wavelengths on the module efficiency

4. Designing and building the required experimental setup to validate the developed model

5. Using the validated model to proof that active filtering scheme would be effective in increasing the productivity of the photovoltaic process

6. Obtaining a penalty function that accurately reflects the contribution of various parameters to the photovoltaic process

7. Designing an active controller filter using the optimization techniques to find the optimal values of variables of the penalty function obtained in number 6

8. Exploring different means that can be used to physically implement the designed active controlling filter

9. Building the described filter if it is physically and economically feasible

1.4. Dissertation layout

The dissertation consists of seven chapters. In **Chapter one**, an introductory preface, historical preview of the photovoltaic cells, research objectives, and dissertation layout are presented. In **Chapter two,** the literature review of the research efforts in the areas of temperature effects, modeling PV cells, spectrum splitting and filtering, active filtering of solar spectrum, and optimization are presented. The problem to be solved in this research and the concept of active filtering and its effects on the PV module efficiency are introduced in **Chapter three**. The detailed mathematical derivation and description of the proposed wavelength-based thermoelectrical model are discussed in **Chapter four**. An optical model that predicts the overall light absorption, reflection, and transmission of the PV module layers is also introduced in **Chapter four.** In **Chapter five**, characterization procedures for the different unknown quantities of the model introduced in **Chapter four** are proposed. The experimental setups and measurements used to characterize the model, the validation of this proposed model, and the results of the different covers for the PV module simulation are also described in **Chapter five**. **Chapter six** focuses on the optical filtering and its benefits on the PV module efficiency. The optimization process to find the optimal cutoff wavelength and the optical technologies that can be used to implement the active filter are also discussed in **Chapter six. Chapter seven** comprises the conclusions, the contributions of this research, and the recommendations for future work.

CHAPTER 2.

BACKGROUND

2.1. Introduction

As a renewable energy source and environmentally friendly technology, photovoltaic (PV) energy is considered one of the most important sustainable energy sources. This motivated researchers to enhance the performance of the PV cells by thoroughly investigating, understanding, and studying the physics that control their performance. The first PV effect was reported in 1878 and the first PV cell was made in 1954 [6] with an efficiency rating of approximately 6%. Since that time, several breakthroughs and milestones have been accomplished with theoretical efficiencies crossing 40%.

Recent development in photovoltaics research resulted in decreasing their manufacturing costs, increasing their lifecycle, and more importantly, enhancing their efficiencies. Specifically, researches ([11], 1987), ([12], 1981), ([13], 2000), ([14], 2005), ([15], 2004), ([16], 2005) on various semiconductor materials has led to economically viable and more efficient photovoltaic cells. Even greater efficiency can be fulfilled by using better lattice match alloys and different band gap materials. Other studies ([17], 2004) show that by concentrating the amount of incident light, using concentrators, solar cell efficiency is further enhanced. The concentrators are used to increase the incident irradiance from one sun (1000 W/m^2) to several hundred suns. This enhances the output power, but also increases the PV cell temperature. Another approach to enhance the output power is to employ special invertors and better load-resistance matching devices. Furthermore, researchers enhanced the PV cell efficiency by tracking the maximum power point of its current/voltage characteristic diagram using special devices designed for this purpose ([18], 2006), ([19], 2010). Moreover, some efforts were exerted to increase the PV efficiency by increasing the amount of light that hits the cell's surface using solar tracking systems, and light trapping coatings to confine the light ([20], 2009). Other researchers worked on splitting the spectrum into bands in order to take the

advantage of all wavelengths of the incident light by stacking several solar cells of different band gab semiconductor materials ([21], 2010).

Temperature is a critical parameter that considerably affects the PV cell performance. Controlling the temperature is an approach that has been followed in order to increase the PV efficiency. Reducing the temperature of the solar cells enhances its efficiency. It is reported that PV module loses up to 23% of its output power when its temperature increase is about 35 K [22]. Several experimental and theoretical methodologies were conducted to reduce the module temperature. These efforts can be classified as one of the following:

1. Coating filters (passive filters) were designed in order to split the solar spectrum into accepted and unaccepted bands ([21], 2010), ([17], 2004). The accepted band contains the part of light (short wavelengths) that is converted into electricity, while the unaccepted one contains the part of light (long wavelengths) that may convert into heat.

2. Active cooling systems as water and air conditioning were integrated with the PV arrays. This created combination is called photovoltaic/thermal hybrid system ([23], 2010), ([22], 2003). In the hybrid PV/T system, the coolant (water or air) flows through pipes in the back of the module. The coolant in one hand cools the PV panel down and on the other hand, it can be used for heating purposes.

3. Finally, employing phase change materials to absorb the produced heat ([23], 2010), [24], 2010). These materials change their physical state when the heat accumulates in the module. This accordingly reduces the module temperature.

Part of these methods were conducted theoretically using models for PV cells, modules, and arrays ([25], 1985), ([26], 1999), ([27], 2010). Some researchers used simulation models from literature to study the effects of their contributions on the PV cell performance ([28], 2007), and ([29], 2008). Others presented thermal models to study the effects of irradiance and temperature on PV modules performance ([30], 2001), ([31], 2008), ([32], 2007).

In general, these subjects inspire researchers in the different fields of the photovoltaics. Therefore, more detailed reviews are presented in the next section to cover the efforts that are highly related to the objectives and motivation of this research. Mainly these fields include: the early efforts of PV cells, modeling, temperature effects, filtering structures, and optimizations.

2.2. Literature review

This section presents a detailed literature review of the theoretical and experimental efforts that are directly related to the main objective of this research. As discussed in chapter one, our main goal is to enhance the efficiency of the photovoltaic modules using optimal control strategies to design an active filtering process that increases the output power through controlling the input power. The most significant works that were conducted in the fields of temperature and thermal effects, temperature control, spectral filtering and controlling processes, and modeling and optimization attempts will be reviewed.

2.2.1. Introduction to photovoltaics

Green ([33], 1993), ([34], 2009) presented a review of the progress that has been made on silicon solar cells from 1874, with its rectifying properties, to the date of his reports in 1993 and 2009. Green discussed the milestones achieved by researchers which increased the solar cell efficiency from less than 1% to 25% as shown in Figure 2.1. These accomplishments will be discussed by their importance to the history of photovoltaic cells as Green introduced them.

Oh1 of Bell Laboratories, ([35], 1941) discovered the wells defined as barriers in polycrystalline ingots that were grown from some lots of commercial high-purity silicon. The grown-in junctions resulted from impurity segregation during the recrystallization process. Oh1 found that one side of the junction reached a negative potential when samples were illuminated or heated. The same side had to be biased negatively to show

low resistance to current flow across the barrier or across the point of contact to this material. This led to the terminology of 'negative' or 'n-type' silicon for the material on this side of the junction and the material of the opposite side was named 'positive' or 'p-type'. Apparently, it was only after this initial experimental work that the role of donor and acceptor impurities in producing these properties was shown.
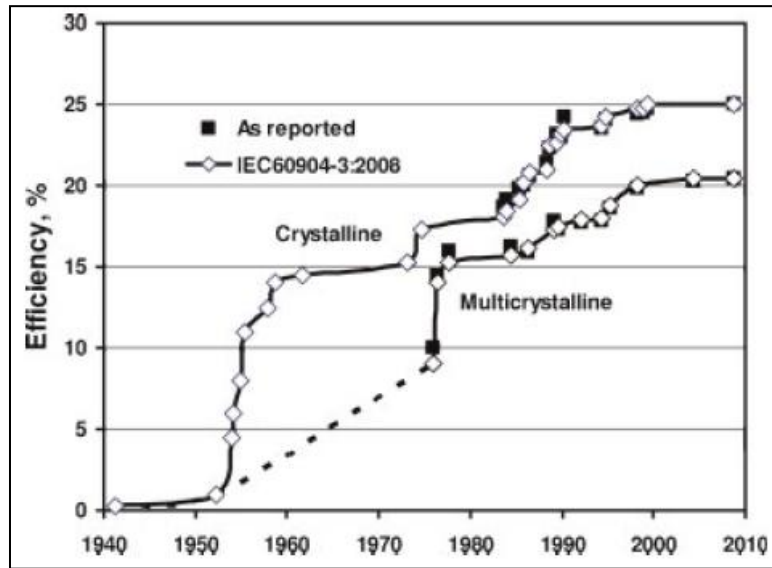
Figure 2.1. Evolution of silicon solar cell efficiency [34]

In 1941, the first photovoltaic devices based on these grown-in junctions were described [35]. Figure 2.2 shows the geometry of cells cut from the recrystallized material. Contact was made at the periphery of the top of the device, and over the entire rear surface. No energy conversion efficiency figures were reported for these cells, although an analysis of the data suggests the efficiency is well below 1%.

Kingsbury and Oh1 reported more controllable method of junction formation in 1952 [36]. These cells used recrystallized silicon fabricated from pure source material to prevent grown-in junctions being formed. They used helium ion bombardment of the surface to form the rectifying junction. The used contacting scheme is similar to the earlier devices. These devices showed quite respectable spectral responsiveness, although

energy conversion efficiencies were also not reported. Efficiency was estimated to be somewhere around 1%.

Improved techniques for crystal growth producing single-crystal wafers of silicon were developed at Bell Laboratories, as were techniques for doping using high-temperature diffusion of impurities. This led to the first report of a modern silicon cell in 1954 by Pearson, Fuller and Chapin of Bell Laboratories [6]. In the first cells lithium diffusion is used to form the junction and had an efficiency of about 4.5%. The lithium diffusion was soon replaced by boron diffusion with a 6% efficiency increase. These cells had the dual rear contact structure and opened up the first real prospects for power generation using photovoltaics as shown in Figure 2.3. Improvement in the cell structure led to demonstration of 10% efficiency within 18 months of the initial report [37] in 1954. An application was identified in space on satellites, and this formed the major application of the PV cells until the early 1970s and provided the major incentive for their continued development.
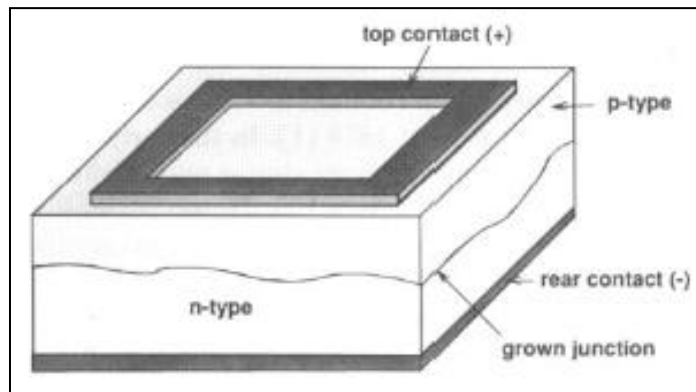
Figure 2.2. Si solar cell reported in 1941 with junction formed by impurity segregation in the recrystallized Si melts [33]

The development of cells for space resulted in further refinements such as the use of contact grids on the top surface presented by Mandelkorn *et al.* ([38], 1962). This increased the cell efficiency to 14% at live sunlight illumination in the early 1960s.
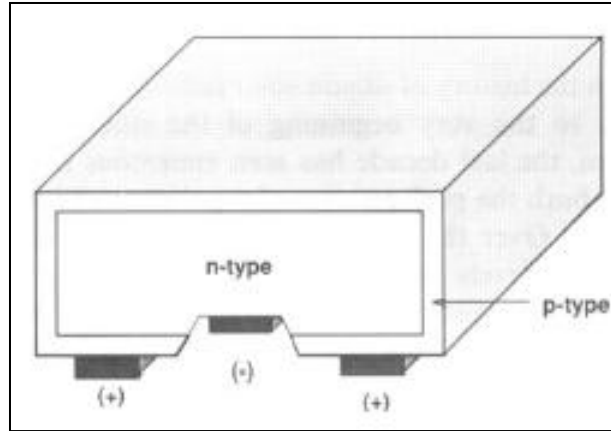
Figure 2.3. First modern Si cell fabricated on single-crystalline Si wafers in 1954 [33]

In the early 1960s, the superior radiation resistance of boron-doped substrates became apparent. This led to a shift from the phosphorus-doped substrates that were previously preferred. Despite this change, reduced initial cell efficiency, it created a cell capable of withstanding the high-energy particles present in the space environment [33]. Cell design then stabilized, for a decade, to the structure shown in Figure 2.4. Cell size was standardized at 2 cm x 2 cm, six metal contact fingers formed by the vacuum evaporation of a Ti/Ag multilayer (subsequently Ti/Pd/Ag) and were generally used to conduct carriers generated over this area to a 1 mm wide busbar (not shown). In addition, a silicon monoxide quarter-wavelength antireflection coating was used to reduce reflection from the top surface of the cell [33].
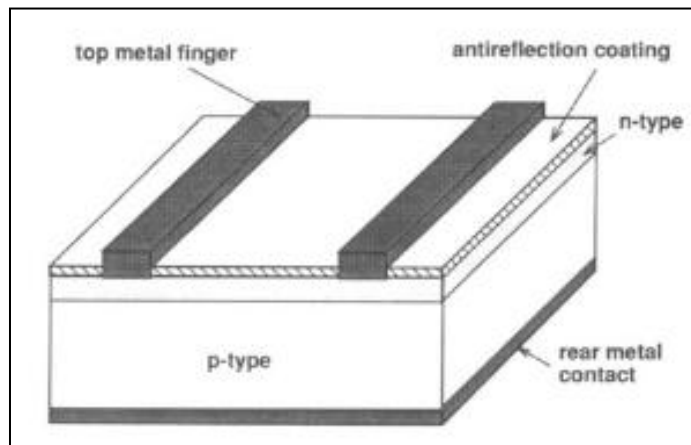
Figure 2.4. Space Si cell design developed in early 1960s [33]

16

In the first half of the 1970s several innovations were introduced into cell design. The first results observed from alloying the aluminum into the rear of the produced cell improved current and voltage output. The effect was initially attributed to the settling of impurities in the cell bulk by the aluminum ([39], 1973). It was subsequently explained in terms of the heavily doped p-type layer produced at the rear surface by the alloyed aluminum [40], [41]. Recently, this is commonly described as "back surface field effect", although the effect can be more usefully described in terms of reduction in the effective recombination velocity at the rear of the cell.

Further improvement was obtained at Comsat Laboratories by Lindmayer and Allison ([42], 1973) by applying the photolithographic techniques developed for microelectronics to the definition of the top metal contact. This produced much finer metallization fingers than possible with the previous technique of evaporation through a metal shadow mask. Finer metal fingers meant that fingers could be more closely spaced without excessive shadowing of the top surface of the cell. This allowed much shallower diffusions to be used to form the top junction, eliminating dead layers which resulted from excessive dopant concentrations near the surface in earlier cells [42]. Using this approach, the response of the cells to light of wavelengths at the blue end of the spectrum was greatly improved, since this light is strongly absorbed near the surface of silicon. Furthermore, new antireflection coatings which do not absorb such light were developed to take advantage of this new ability [42]. Meanwhile, the use of anisotropic etching to expose crystal planes in silicon was being explored in microelectronics. This technique was extended, also by Comsat Laboratories ([43], 1974), to produce pyramids randomly located on the top surface of (100) plane silicon. In this approach, the square-based pyramids are formed by intersecting (111) plane crystallographic planes. This approach reduces reflection from the top surface of the cell as well as coupling the light obliquely into the cell, allowing it to be absorbed closer to the most active region of the cell near the top junction. Figure 2.5 shows a cell incorporating all the previous advanced features, which resulted in cells of approximately 17% efficiency under terrestrial sunlight ([44], 1976). This performance figure was unrivaled for nearly a decade [33].
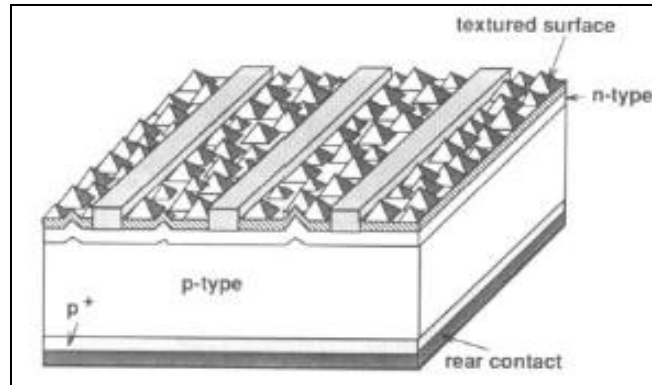
Figure 2.5. Textured top surface with antireflection coated Si solar cell developed in 1976 [33]

The next improvement in cell performance came primarily as a result of increased output voltage due to improved passivation of the electronic activity at the top surface of the cell. This improved passivation resulted from the use of thermally grown oxide to pacify non-contacted areas of the cell and the use of a variety of techniques to reduce the activity at the interface with the top metal contact. The pacified emitter solar cell (PESC) used a reduced area of contact at the top surface to minimize the effects of such activity. Due to the improved top-surface properties of this cell, it was able to take fuller advantage of high-quality starting wafers than earlier designs. By using high-quality float-zone wafers relatively highly doped with boron, 20% efficiency was surpassed with this structure in 1985 ([45], 1985).

The next advance in cell design resulted from extending oxide passivation to both front and rear surfaces of the cell. The first successful design of this type was the point contact solar cell developed by Sinton *et al.* ([46], 1985). In this design, the effects of contact recombination were further reduced by localizing contacts to small points on the non-illuminated surface of the cell. These cells depend on having both extremely good passivation of cell surfaces and extremely high-quality bulk properties. Processing the cells presents challenges, not only does bulk and surface quality have to be maintained during processing, but excellent rear oxide integrity is also essential. Defects in this oxide can cause shunting between the rear contacts and the substrate ([47], 1990). These novel

cells were the first to exceed 22% efficiency under normal terrestrial testing, although 27% efficiency has been demonstrated under highly concentrated sunlight ([48], 1986).

The highest terrestrial silicon cell efficiency confirmed till 1993 has been developed by Green *et al.* ([49], 1987) and obtained by the pacified emitter, rear locally diffused (PERL) cell as shown in Figure 2.6. This cell essentially combines the best features of the two previously discussed designs which gave cell efficiencies above 23% [49].

The previous discussion presents the most significant progress that was accomplished by different researchers since the first interest in photovoltaics in 1878 until the early 1990s. Beyond this period more developments have been carried out by different researchers using different cell designs and materials (i.e. tandem cells, thin film cells...etc). These efforts will not be reviewed here since they are beyond the scope of this research.
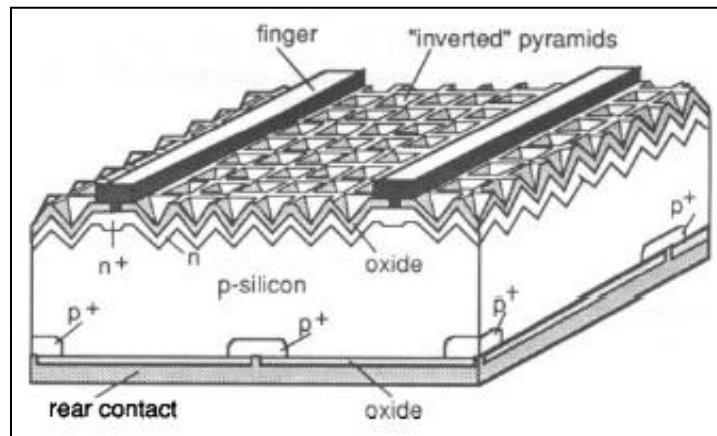
Figure 2.6. Pacified emitter, rear locally-diffused cell with 23% efficiency [33]

2.2.2. Temperature effect

It is well known that PV cell temperature considerably affects the cell performance, i.e., voltage, output power, fill factor, and conversion efficiency.

From the physical aspects, the deteriorations of the PV cell output power and conversion efficiency when temperature increases are attributed to ([50], 2003):

➢ Increase of the thermal lattice vibrations, leading to electron-phonon scattering

➢ Decrease of charge carriers mobility

➢ Reduction of the p-n junction built-in voltage and junction ability to separate electrons from holes in the photogenerated pairs

In order to reduce these effects, it is useful to decrease the module temperature by removing the heat produced by [50]:

➢ Non-active absorption of photons, which do not generate pairs

➢ Recombination of electron-hole pairs

➢ Photocurrent (Joule's heat generated during the current flow in the series resistance of the p-n junction) and parasitic currents

➢ Lack of effective cooling of the module

The following paragraphs represent detailed samples of the work that have been theoretically and experimentally conducted by researchers in order to demonstrate the effects of temperature on PV modules performance.

Radziemska ([50], 2003), ([22], 2003) studied the influence of temperature and wavelength on electrical parameters of crystalline silicon solar cell and a solar module. Radziemska experimentally and theoretically investigated the temperature influence on the light absorption mechanism and the radiation performance of silicon solar cell working at constant temperature. Furthermore, he experimentally investigated the temperature performance of a PV silicon solar module working at constant irradiance. Radziemska used a copper plate as heat sink in order to cool the PV cell when it becomes overheated (80 ℃). As shown in Figures 2.7 and 2.8, Radziemska found that output power and efficiency of the solar cell decrease dramatically as temperature increases. He also observed that the decrease of the output power is -0.65% / K, the fill factor is -0.2% / K, and the conversion efficiency is -0.08% / K. He concluded that PV modules should be well designed and cooled in order to reduce the temperature increase to enhance its performance.
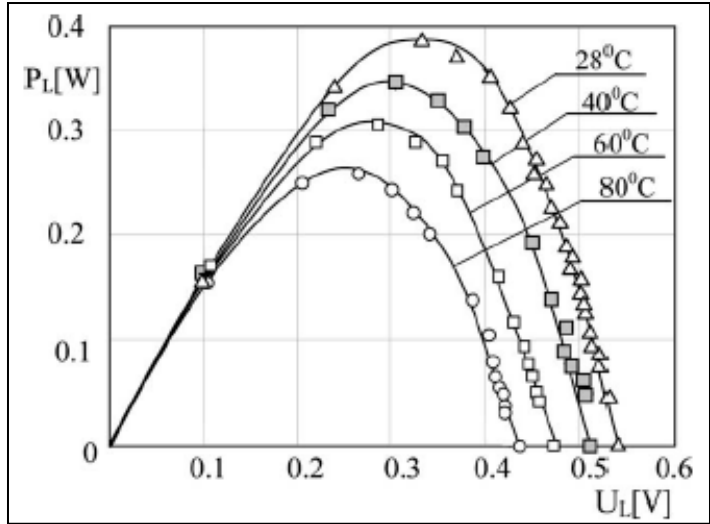
Figure 2.7. Output power as a function of open-circuit voltage at different temperatures [50]
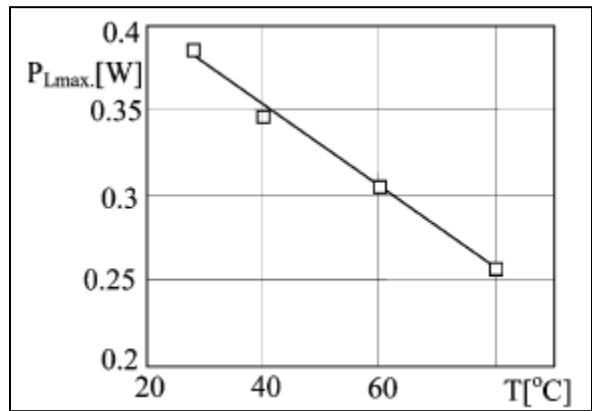
Figure 2.8. Maximum power of single crystalline Si PV cell as function of temperature [50]

Shaltout *et al.* ([51], 2000) measured the spectral response of monocrystalline silicon solar cell at different cell temperatures. They also measured other cell parameters: maximum power, fill factor, and cell efficiency at different illumination levels (1154, 1329, 1740, 2812, and 4010 W/m^2). Figures 2.10, 2.11, and 2.12 show the short circuit current, open circuit voltage and cell maximum power as a function of the cell back temperature. They reported that the temperature has a direct influence on the cell performance, and its spectral response is temperature dependent. They also concluded

21

that when high illumination is applied on a one-sun Si solar cell, at high temperatures, high illumination is of no use in the cell unless some type of cooling is used. Furthermore, they found that at high temperature and illumination values, the cell has its lowest value of efficiency.
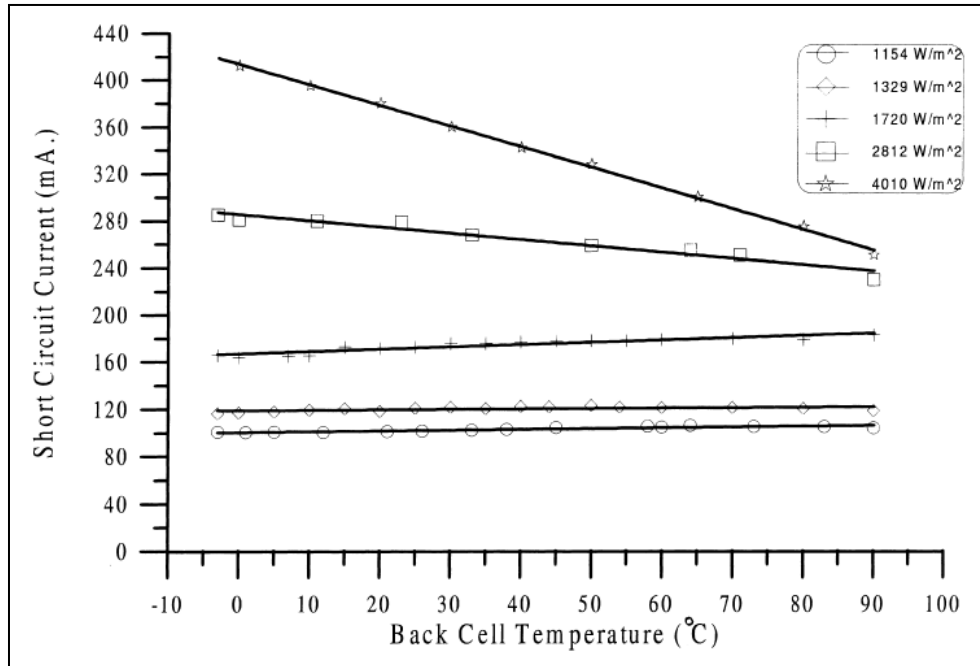
Figure 2.9. Variation of short-circuit current as a function of cell temperature at different illuminations [51]
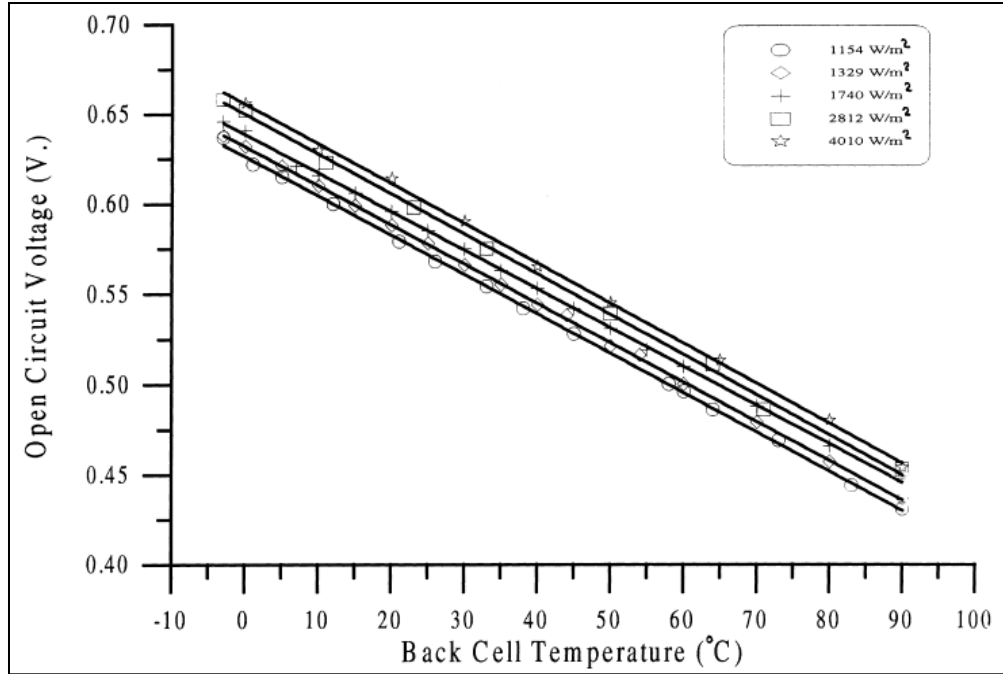
Figure 2.10. Variation of open-circuit voltage as a function of cell temperature at different illuminations [51]
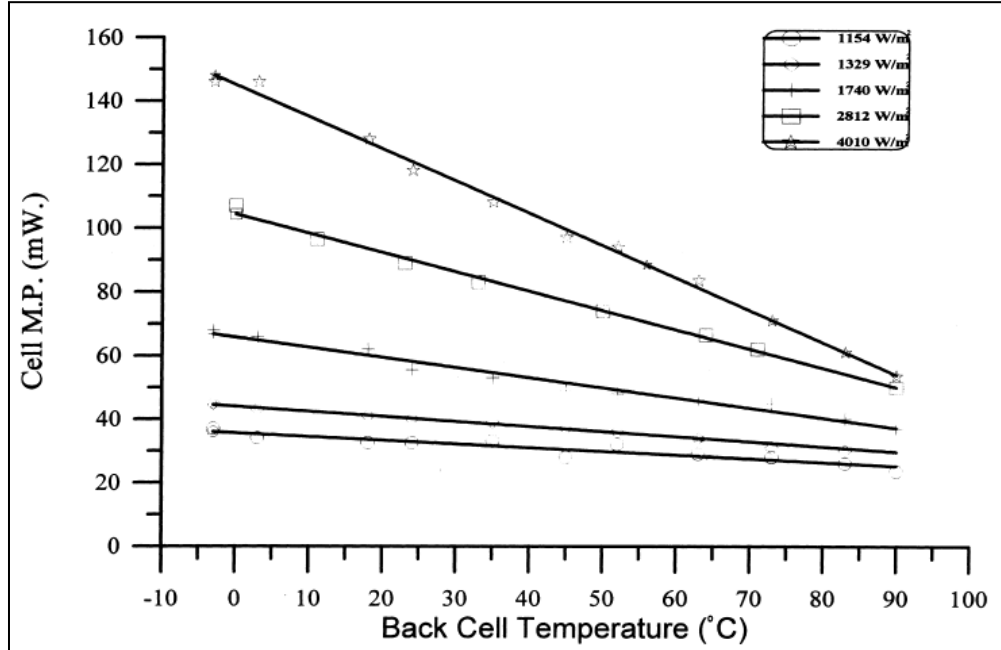
Figure 2.11. Variation of M.P as a function of cell temperature at different illuminations [51]

Akopalki and Palyovs ([52], 2009) provided a review comparison of several researchers efforts conducted in order to study the operating temperature of one-sun commercial grade silicon based solar cells/modules and its effect upon their electrical performance. They gave tabulations for most of the known algebraic forms proposed by different researchers which express the temperature dependence of PV cells efficiency and, equivalently, solar power. They also provided the temperature coefficients measured and calculated by those researchers, which could be used to find the PV efficiency correlation coefficients. In their review, Akopalki and Palyovs concluded that the operating temperature plays a central role in the photovoltaic conversion process. Both the electrical efficiency and the power output of a PV module depend linearly on its operating temperature and decrease as it increases. The various correlations that were proposed in the literature represent simplified working equations which apply to PV modules or PV arrays mounted on free-standing frames, to PV/Thermal collectors, and to BIPV arrays. These correlations involved basic environmental variables, while the numerical parameters are not only material dependent but also system dependent. Thus, care should be exercised in applying a particular expression for the electrical efficiency or the power output of a PV module or array.

Gaitho *et al.* ([53], 2009) investigated the effect of heat flow through the solar cell materials in order to determine the thermal conductivity of the silicon film since it is a factor of operating temperature of the solar cell. They have used a single crystal silicon solar cell coated with zinc oxide thin film, where this coating offers an optical improvement. They used the transient line heat source (TLHS) method to measure the thermal conductivity where the heat source is placed against the inner and outer surfaces of the solar cell to provide heating and to sense the temperature changes at the same time. Figures 2.13 and 2.14 show the thermal conductivity as a function of temperature and thermal conductivity as a function of the efficiency respectively. They found that there is rapid decrease in thermal conductivity from 1.26×10^2 Wm^{-1} K^{-1} to 9.63e2 Wm^{-1} K^{-1} as temperature increases from 297 K to 320 K. Then there is a small decrease to 8.84×10^2 Wm^{-1} K^{-1} at elevated temperatures. They have reported that the general trend is that as the temperature increases thermal conductivity decreases. They have attributed that decrease

in thermal conductivity to the increase in operating temperature of the cell. Their conclusion for the single crystal silicon cell performance is that low temperatures present more efficient photo-conversion.
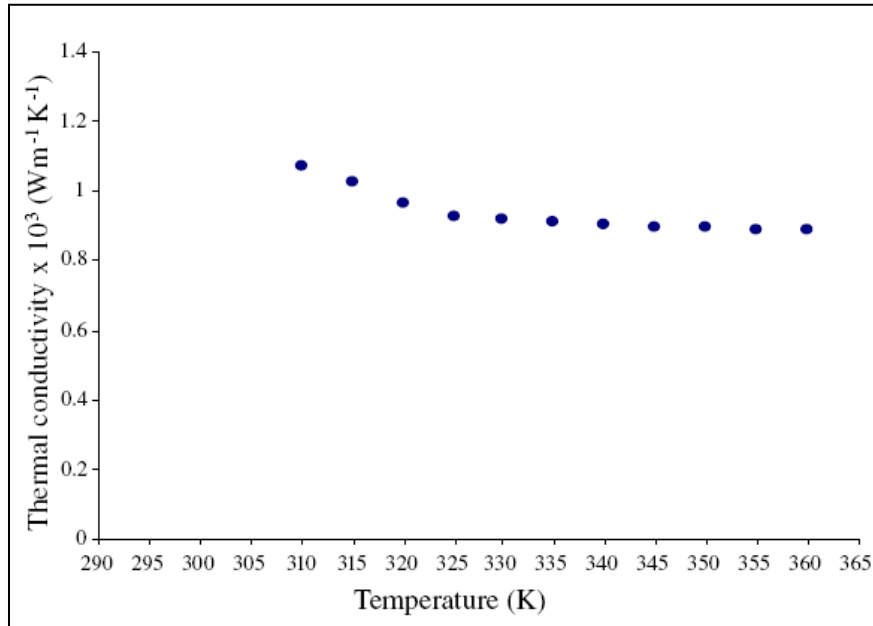
Figure 2.12. Reverse relation between thermal conductivity and temperature [53]
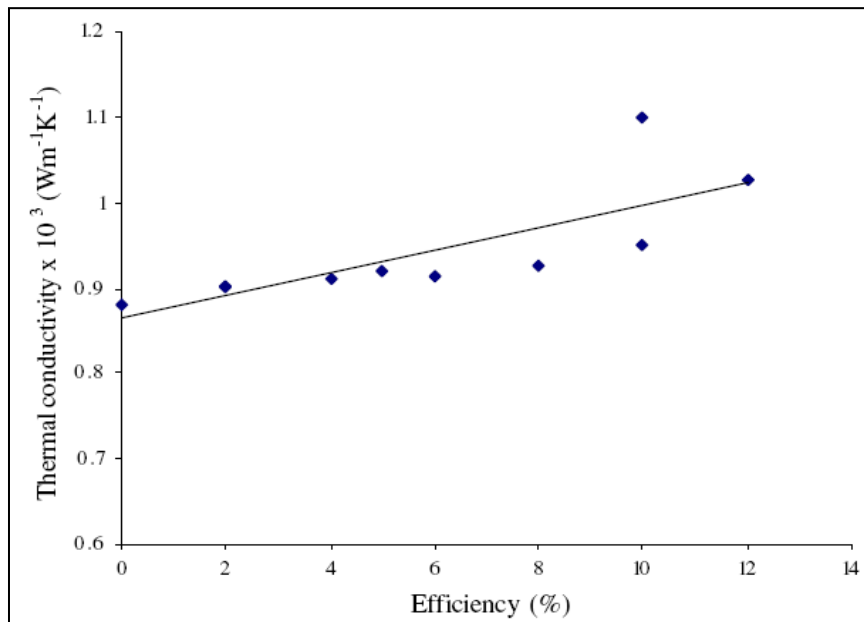
Figure 2.13. Relationship between thermal conductivity and solar cell efficiency [53]

2.2.3. Modeling the photovoltaic cell

Several researchers have introduced numerical models in order to model the solar cell by introducing equivalent circuits and also to simulate the effects of the operating parameters on its performance. These parameters are usually material related, solar irradiance, and temperature. Some other researchers combined thermal and electrical models in one hybrid thermo-electrical model to provide more accurate results. The most related efforts to the research objectives are discussed herein.

Gow and Manning ([26], 1999) developed a general circuit-based model which is the first fundamental model that could be implemented for simulation software programs mainly MATLAB and PSPICE. This model is also designed to be used by power electronics specialists. The inputs to the model are the temperature and irradiance, and the outputs are the current and voltage which form cell characteristics. They proposed two models, the first is double-exponential model given in Equation (2.1), and the second is single-exponential model given in Equation (2.2). The double-exponential model is accepted to reflect the behavior of cells constructed from polycrystalline silicon, while the single-exponential model is used to reflect the behavior of amorphous silicon. Both models are derived from the physics of the pn-junction. From Equation (2.1), the equivalent circuit given in Figure 2.14 is derived. In these non-linear models, five parameters should be found for each module: I_{ph}, I_{D1}, I_{D2}, R_s, and R_{sh}/R_p. Gow and Manning introduced these parameters as functions of temperature and irradiance and some other constants which are given in ([26], 1999). These constants can be found by curve fitting with experimental data, which are different for different PV modules. This modeling effort reflects the significant performance degrading effect of temperature on the PV module parameters.

$$I = I_{ph} - I_{D1}\left[e^{\frac{q(V+IR_s)}{kT}} - 1\right] - I_{D2}\left[e^{\frac{q(V+IR_s)}{AkT}} - 1\right] - \frac{V + IR_s}{R_{sh}} \tag{2.1}$$

$$I = I_{ph} - I_s\left[e^{\frac{q(V+IR_s)}{kT}} - 1\right] - \frac{V + IR_s}{R_p} \tag{2.2}$$
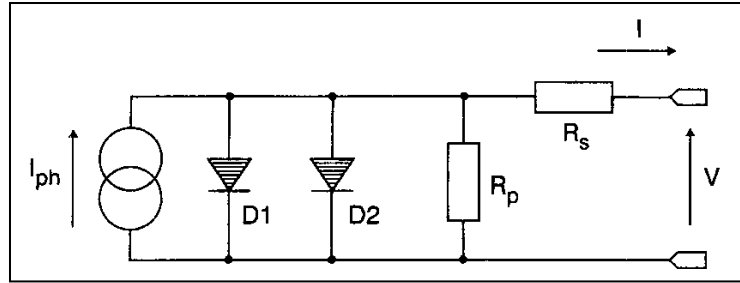
Figure 2.14. Equivalent circuit of PV cell [26]

Shekoofa and Taheraneh ([28], 2007) introduced a circuit-based model for the PV cell, module, and array. They used two diodes to model a single layer silicon cell which is given in Figure 2.15. All the parameters of this model are temperature (T) and irradiance (G) dependent. They implemented the model in Matlab/Simulink in order to find the parameters given in Figure 2.15. The module and array models are based on the cell model. The module model differs from the cell model by the values of the shunt and series resistances (R_p and R_s) , while the array model differs also by the values of photocurrent and diode-current densities as shown in Figures 2.16 and 2.17 respectively. They also conducted some thermal analysis of the solar panel for space satellite applications. Furthermore, they investigated the influence of each panel model's parameters on the simulation results.
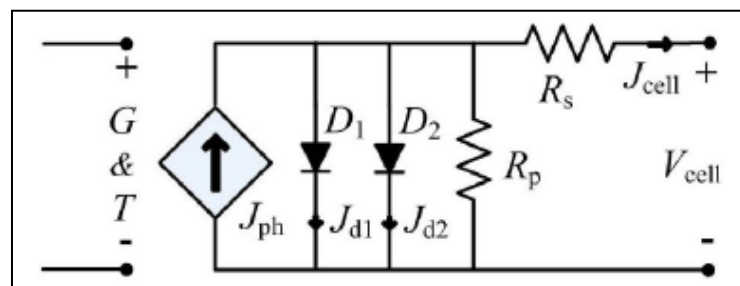
Figure 2.15. Two diode equivalent circuit-based PV cell model [28]

Karatepe *et al.* ([54], 2005) presented a neural network based approach for improving the accuracy of the electrical equivalent circuit of a photovoltaic module. According to them, the conventional PV models are not accurate since their parameters do not depend on

solar irradiation and cell temperature. Therefore, the accuracy and the reliability of the performance estimation cannot be sufficient for all operating conditions. In their approach, the equivalent circuit parameters of a PV module mainly depend on solar irradiation and temperature. They used a set of current–voltage curves to investigate the dependency of the module parameters on environmental factors. They utilized an artificial neural network to overcome the nonlinear relations among these parameters. The equivalent circuit parameters were estimated by only reading samples of the solar irradiation and the temperature very quickly without solving any nonlinear implicit equations. They demonstrated the accuracy and the generalization of their proposed model by comparing the test results with the actual data. The comparison between the measured values and the proposed model results showed higher accuracy than the conventional model for all operating conditions.
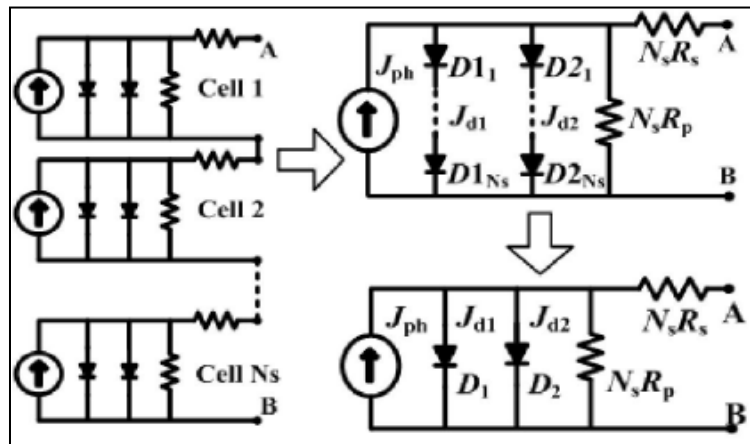
Figure 2.16. Module equivalent circuit [28]

Fahmy and Hefnamwi ([55], 1998) presented a numerical model to calculate the temperature distribution at steady state on the different layers of a PV cell structure at different seasons, solar irradiation and air temperature. Their results showed that the performance of the PV cell is inversely affected by the temperature increase due to the reduction in the open circuit voltage, and reduction in the fill factor despite a slight increase in the short circuit current.
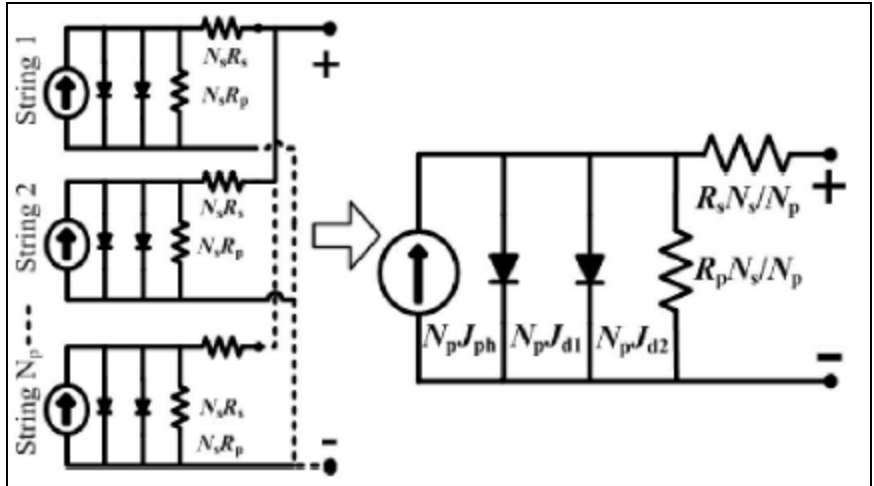
Figure 2.17. Array equivalent circuit [28]

Jones and Underwood ([30], 2001) introduced a non-steady state thermal model for the photovoltaic module. In this model the PV module temperature is predicted considering all energy transfer processes that may affect it. This includes short wave radiation, long wave radiation, convection and electrical energy production as shown in Figure 2.18. The resulting rate of temperature change with time can be expressed as the sum of these contributions as given in Equation (2.3). They developed the expression of each term as given in Equation (2.4) which is the whole thermal model. The model terms given in Equation (2.3) are in the same order that is given in Equation (2.3).
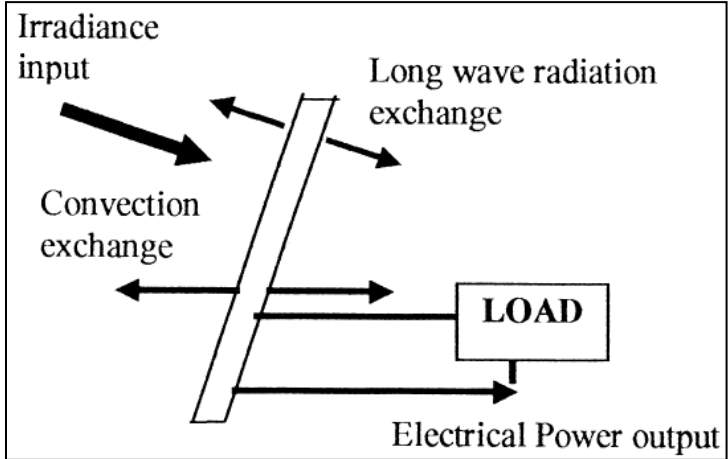
Figure 2.18. Heat transfer and energy exchange at PV module [30]

29

$$C_{module} \frac{dT_m}{dt} = q_{lw} + q_{sw} + q_{conv} - P_{out} \tag{2.3}$$

$$C_{module} \frac{dT_m}{dt} = \sigma A \big(\varepsilon_{sky}(T_{amb} - \delta T)^4 - \varepsilon_m T_m^4 \big) + \alpha \varphi A$$
$$- A \big(h_{c,forced} + h_{c,free} \big)(T_m - T_{amb}) - \frac{C_{FF} \varphi \ln(k_1 \varphi)}{T_m} \tag{2.4}$$

where C_{module} is the module heat capacity, T_m is the module temperature, T_{amb} is the ambient temperature, φ is the incident irradiance (W/m^2), h_c heat transfer coefficient, and C_{FF} is the filling factor of the module. The rest of the symbols are constants and their values given in the reference ([30], 2001). Johns and Underwood found that the predicted results of their model agree with the response of the measured module temperature to transient changes in irradiance. Their model is found to be accurate to within 6 K of the measured temperature values for 95% of the time in cloudy conditions. The best accuracy is obtained in the clear and the overcast conditions when the irradiance is subjected to fewer fluctuations.

Tina and Scrofani ([31], 2008), presented two mathematical models: electrical and thermal. Both models are combined to determine the module temperature based on the field monitored real data, i.e., ambient temperature, wind speed, wind direction, relative humidity and electrical operating point (voltage and current). The parameters of the electrical model are calculated using the least-squares fitting of the equivalent model current-voltage (IV) characteristic curve with the measured one. Further, they studied the module thermal behavior for non-steady state conditions (i.e. considering variations of both environmental and electrical variables). Tina and Scrofani noticed that there are more than one set of parameters to be considered, depending on ambient variables (incident irradiance, ambient temperature…etc). Furthermore, since it is difficult to calculate the optimal parameters, it could be useful to adopt different sets of parameters depending on the range of the main ambient variables. They also found that using a set of parameters formed by parameters close to the average values, regardless the climate

conditions, the IV-characteristic curve of the module is very close to the measured one. Using a set of chosen parameters, Tina and Scrofani claimed that the proposed model allows performing sensitivity analysis for the effect of the meteorological variables on the module performance.

Petal and Agarwal ([56], 2008) presented a Matlab-based modeling and simulation scheme to study the IV and P-V characteristics of a PV array under a non-uniform insolation due to partial shading. They also claimed that their model can be used for developing and evaluating new maximum power point tracking techniques, especially for partially shaded conditions. It can also be used as a tool to study the effects of shading patterns on PV panels having different configurations. They observed that, for a given number of PV modules, the array configuration (how many modules in series and how many in parallel) significantly affects the maximum available power under partially shaded conditions. Their results showed that PV curves have multiple peaks under partially shaded conditions. Therefore, the existing MPPT schemes, which assume a unique maximum power point, remain inadequate. The magnitude of the global peak is dependent on the PV array configuration and shading pattern besides the commonly known factors, i.e., insolation level and array temperature. In addition, they claimed that if the likely shading pattern on the PV array is known, the simulation model is handy to design the most optimum configuration of the PV array to extract the maximum power. They also claimed that the results of this model can be effectively used with off-line capabilities of Matlab/Simulink to investigate the effectiveness of MPPT methods working under non-uniform insolation conditions.

Gonzalez *et al.* ([57], 1994) examined the variation of modeled and observed cell efficiency with the atmospheric variations. They considered that the efficiency of the solar cell is a function of atmospheric conditions, such as, cloudiness, total column ozone, turbidity, and perceptible water because the total intensity and spectral distribution of sunlight. They used the SPCTRAL2 solar spectral radiation model to simulate the effects of turbidity and water vapor content variations. Gonzalez *et al.* coupled the simulation results with spectral response functions of the monocrystalline and amorphous

silicon solar cells then used them to model the efficiency of these cells. They have found that the major factors cause variations in operational efficiency are the ambient temperature and the total irradiance intensity. They also observed an increase of apparent efficiency of the amorphous cell with decreasing the energy in the red region of the solar spectrum. In their simulation results Gonzalez *et al.* have found that beyond 500 W/m^2 the efficiency of the cells is temperature limited. Furthermore, they found that the efficiency of monocrystalline panels decreases approximately 0.06 in absolute value per degree increase, while for the amorphous cells, efficiency increases with temperature especially in humid (low red light) conditions.

Balog *et al.* ([58], 2009) Presented a thermal model and simulation methodology based on the energy conservation principle using historically measured insolation and meteorological data to compute the temperature of the PV module. The principle of their modeling is similar in the essence with the modeling approach proposed by Jones and Underwood ([30], 2001) which is based on energy balance. However, Balog *et al.* did not present a model for the output power term of their thermal model; instead, they assumed a constant efficiency for the module in their modeling ignoring the effects of the temperature on its actual value and accordingly on the predicted temperature. Their results show that the module temperature is lower than 70 ℃ for 99% of its operating time and the peak temperature reached 81 ℃.

Armstrong and Hurley ([59], 2010) proposed a thermal model that incorporates the atmospheric conditions, effects of PV panel material composition and mounting structure. They used the analogy to the RC circuit in their modeling approach. They demonstrated the ability of this model to determine the speed of response the PV panel to changing the input conditions. Their model provides the means of predicting the thermal time constant of a PV panel under varying atmospheric conditions. They expressed the thermal properties of PV panels in terms of their electrical equivalents by means of an RC circuit as shown in Figure 2.19. They investigated the heat transfer from the surface of a PV panel under varying wind conditions. They discussed different models from literature that can be used to determine the free and forced heat transfers of the PV panels. They

measured the time constant for three different wind speeds with a step change of solar irradiance, and compared them with the predicted time constants. Their results show that the worst case accuracy is 13.98% with an average error of 7.26%.
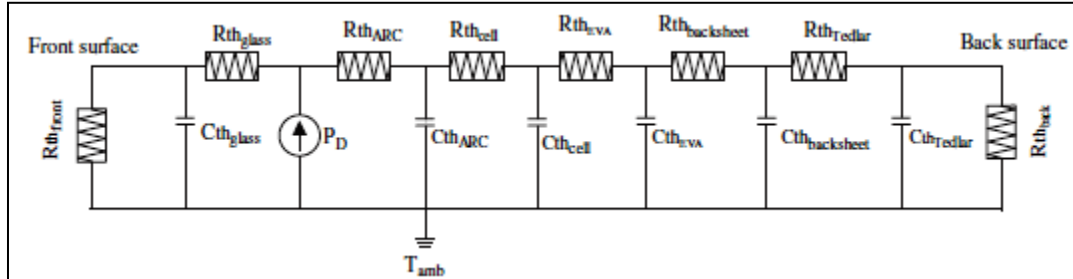
Figure 2.19. Photovoltaic thermal resistance network [59]

2.2.4. Spectrum splitting and filtering

The following paragraphs contain examples of the efforts, approaches, and studies of different researchers who attempted to enhance PVs efficiencies by light filtering and spectrum splitting. Only the passive optical filters and light traps are presented in this section, while the active filtering will be discussed in the next section.

Imenes and Mills ([17], 2004) presented a review of spectral beam splitting techniques and filtering processes used to split the solar spectrum in order to increase the conversion efficiency of the solar concentrating systems. According to their study, there are several filtering categories for PV cells that have been described in the literature, mainly: dielectric multilayer filters, heat reflectors, refraction or prism spectrum splitting, holographic filters, fluorescent methods, and liquid absorption filters. For systems include PV cells only, the filtering techniques that were reported in the literature were carried out using either the tandem-cell approach or splitting approach. In the tandem-cell approach two or more solar cells of different semiconductor materials are mechanically or monolithically stacked in series and arranged in a decreasing order of band-gap energy. In the splitting approach the optical filter separates the light into spectral components directed to individual cells of different band-gap energies. For thermo-photovoltaic systems, the PV cells are built with a thermal solar collector such that part of

the spectrum is filtered out by PV cells for electricity production. The remaining portion is absorbed by a fluid to be used for thermal applications. For more details about these techniques, refer to ([17], 2004).

Fahr *et al.* ([60,61], 2008) suggested a design for a coating to be applied on top of any solar cell having at least one diffusing surface. Their coating acts as an angle and wavelength selective filter. It increases the average path length and absorption at long wavelengths without altering the solar cell performance at short wavelengths as shown in Figure 2.20. Their designed filter should reflect light with wavelengths higher than 870 nm and angle of incidence larger than 2.5^{o} while for other conditions; light should be perfectly transmitted to the solar cell. The base of their filter design is the continuous variation of the refractive index in order to minimize the undesired reflection losses. They used numerical procedures to optimize the filter for a 10 µm thick mono-crystalline silicon solar cell. They also discussed the feasibility of fabricating such filters considering a finite available refractive index range. Fahr *et al.* neglected the absorption and dispersion in the top coating. They used a realistic model for the absorbing layer and had at least one Lambertian surface. They also observed that in order to obtain high transmission, low indices of refraction are necessary. They found that the calculated efficiency could be increased from 28.7% for cell with zero front side reflection up to 30.1% for cell equipped with the angle selective filter.

Green and Ho-Baillie ([62], 2010) implemented an approach in order to enhance the solar cells efficiency. Their approach is to subdivide the broad solar spectrum into smaller energy ranges to convert each range with a cell of appropriately matched bandgap. This can be achieved by using monolithic or mechanical stack of cells arranged in order of increasing bandgap, with the highest bandgap cell uppermost. This represents an automatic filtering of incident sunlight so that each cell absorbs and converts the optimal spectral range. Their schematic diagram is shown in Figure 2.21, where non-stacked cells are used in order to steer light in different wavelength bands. In their work they found that an improved combination of independently confirmed results gives a composite

efficiency of 43% under the global ASTM G173-03 spectrum, the highest reported efficiency to date from any such combination of photovoltaic devices.
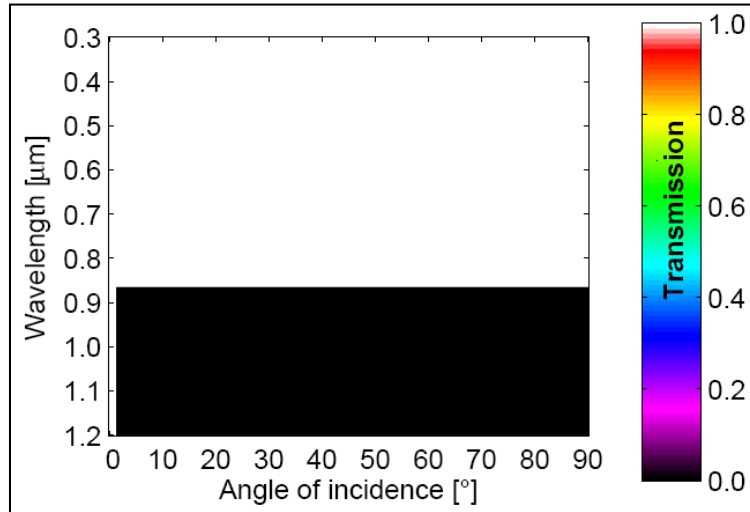
Figure 2.20. Transmission of the unpolarized light in the ideal wavelength and angle selective filter [61]
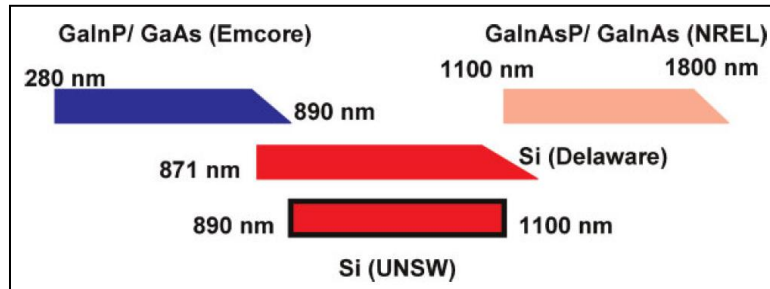
Figure 2.21. Schematic illustration of the spectral ranges involved in the cell measurements [62]

Peters *et al.* ([63], 2009) theoretically and experimentally investigated the photonic light trap which is a combination of angular selective filter and light scattering process. They studied two optical filters: Bragg-like and opal. They have identified that Bragg effect is the principal of creating angular selectivity of the investigated filters. Bragg-like system in addition to the bandgap filter represents the photonic light trap which is applied on a thin-film solar cell of amorphous silicon. Their results showed that the light absorption increased by 25% and accordingly the quantum efficiency is increased by 25%.

Zeng *et al.* ([64], 2006) developed a backside reflector scheme for solar cells in order to enhance the light-trapping efficiency by enhancing the optical path length using textured photonic crystal. As shown in Figure 2.22, the scheme comprises a reflection grating etched on the backside of the substrate and a one-dimensional photonic crystal deposited on the grating. Their scheme works in the following scenario. The grating is dominated by the incidence, diffraction angles, wavelength of the incident light and the refractive index of the solar cell material. Using the 100% reflective Distributed Bragg Reflector (DBR) at the backside of the solar cell (no light escapes the solar cell) increases total internal reflection at the front surface of the cell (active region) for further absorption. Their results showed that the external quantum efficiency (EQE) is significantly improved for light wavelengths within the range of 1000 to 1200 nm, with enhancement up to 135 times. They also concluded that the efficiency can be enhanced much more for cells of smaller thickness and finer grating periods.
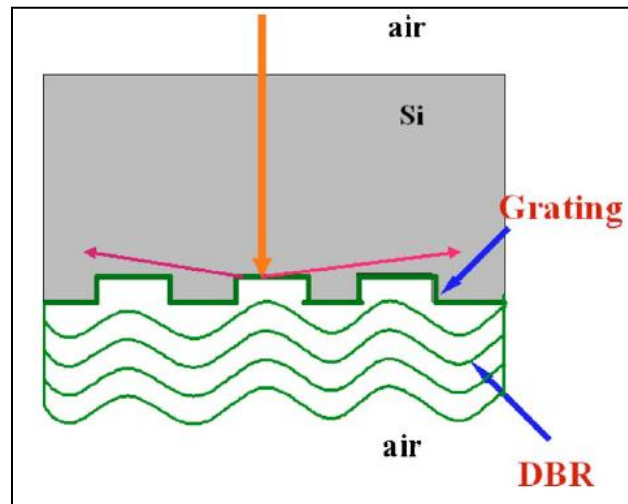
Figure 2.22. Schematic of the back reflector [64]

Goetzberger *et al.* ([65], 2008) introduced a light trap combined of two other light traps. It converts light into voltage with separate solar cells optimized for different frequency bands, which are covered by spectral selective mirrors. Their first light trap as shown in Figure 2.23 employs concentrated radiation incidents on a small volume. The light is focused by the lenses then the concentrated beam enters the light trap through the

36

openings. Then the light is diffused inside the trap. The attached mirrors to the solar cells reflect the light that the solar cells could not use. By this trap, the light is selectively concentrated onto different cells. They concluded that the efficiency of the system depends on the ratio of solar cell area to the input area (aperture area). The second light trap is based on using a photonic structure covering the surface of the system as shown in Figure 2.24. The photonic structure has a critical acceptance angle Θ_c. The light scatters after diffusion into angles larger than Θ_c will be trapped. There are also spectrally selective mirrors covering the solar cells. They showed that the trapping efficiency above 90% is achievable. They also found that the light trapping principle can be applied to large area stationary modules. Their work represents the fundamental theory, and experimental work should be conducted in order to study the feasibility and applicability of this basic principle.
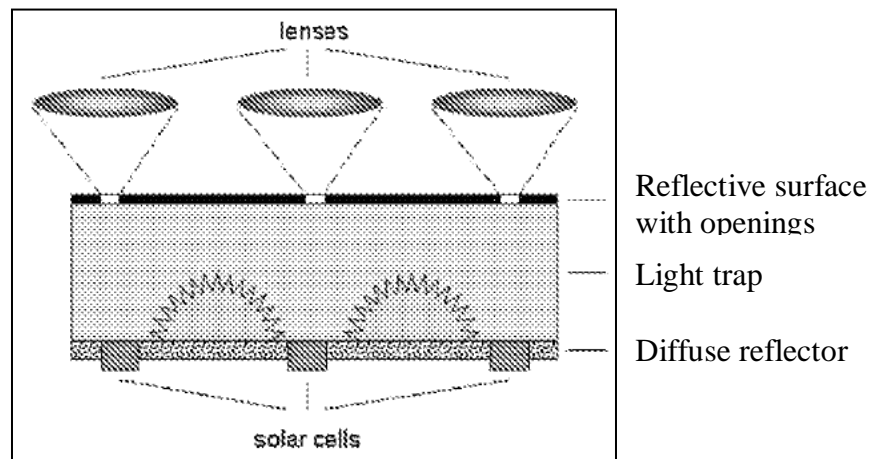
Figure 2.23. Design of first light trap [65]

Barnett *et al.* ([66], 2009) developed an integrated optical system with photovoltaic modules for portable applications in order to operate at efficiency greater than 50%. In their system, they integrated the optical design with the solar cell design. As shown in Figure 2.25, their system architecture is based on a ''parallel or lateral'' optical concentrating system (dichroic mirrors), which splits the incident solar spectrum into several bands, and allows different optical and photovoltaic elements in each band. In their optical system, there is no need for moving tracking system due to the use of high

efficiency (93%) optical system. The module efficiency consists of the optical system efficiency and sum of the solar cells' efficiencies. In their experimental work, they divided the spectrum into three sections with the GaInP/GaAs cell measured above the GaAs band gap, 871 nm, the GaInAsP/GaInAs cell with light beyond 1100 nm, and the silicon below 871 nm. Barnett *et al.* found the efficiencies of these three cells as follows: GaInP/GaAs = 31.7%, Silicon (filtered by GaAs) = 5.4%, GaInAsP/GaInAs (filtered by Si) = 5.6% with total efficiency = 42.7±2.5%.
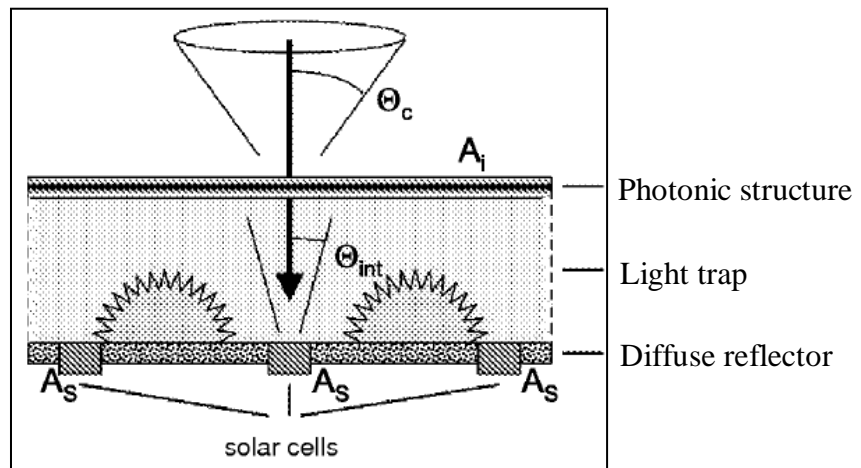
Figure 2.24. Design of second light trap [65]
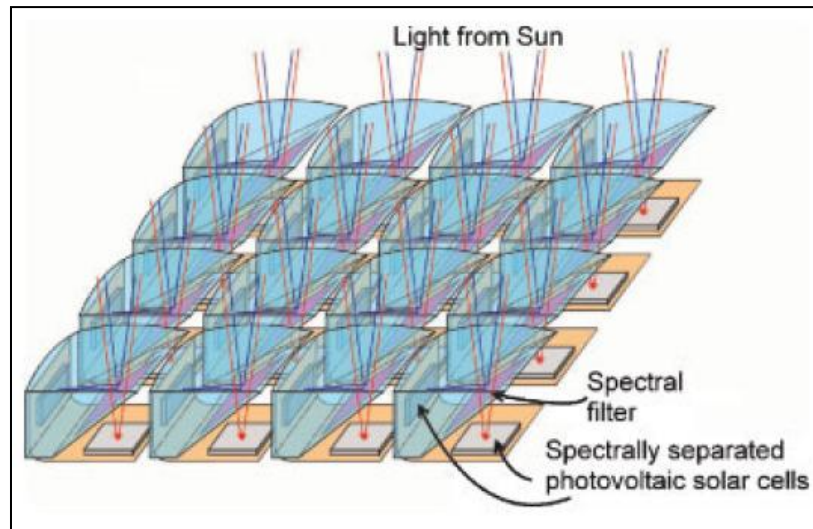
Figure 2.25. Schematic of solar system architecture: optical and solar elements [66]

Ulbrich *et al.* ([67], 2008) developed a directional light selective and trapping filter. It should be applied on top of Lambertian surface crystalline silicon cell. They assumed that the light will ideally be filtered according to its incidence angle and energy level. They investigated the impact of angularly dependent transmittance of the incident solar spectrum on the photovoltaic conversion efficiency to evaluate the advantages and disadvantages of angle selective structures. They considered normal incidence and compared the cell efficiency of three different types of solar cells; a planar cell, a cell with Lambertian surface and a cell with Lambertian surface and selective filter as shown in Figure 2.26. They investigated the gain and loss in the annual energy yield depending on the filter characteristics, irradiance and tracking mode. Three cell thicknesses of 1 μm, 10 μm and 100 μm were used in simulation with solar spectrum for two different locations. They also assumed that all direct circumsolar light incidents under angle of less than 2.5^{o} is normal incident light and considered as the threshold angle of the selective filter. Thus the whole incident spectrum is transmitted into the solar cell. Ulbrich *et al.* found their simulation results that the optimum filter has threshold angle of 2.5° and threshold energies in the range of 1.8–2.0 eV, depending on the local spectrum. This filter brings about an increase of 32.5% in the annual gain for a tracked 1 μm thick crystalline silicon solar cell. The effect decreases with cell thickness to an increase of 9% for a 100 μm thick cell. Also one-axis polar tracking implies an improvement of up to 10%. In case of no tracking at all, large angle range under which the cell faces the sun leads to larger losses that increase with small threshold angles and larger energies. They suggested two feasible filter designs, Rugate filter and inverted opal structure. Their simulations proved that these non-ideal structures still involve a significant increase of up to 5% (Rugate filter) and 7.5% (inverted opal layer) in the annual gain.

Yoon *et al.* ([68], 2006) used an infrared reflecting (IRR) coverglass on multijunction III-V solar cells. The purpose of such a filter is to remove IR wavelengths that are converted into photogenerated current by the smallest bandgap material in the 3-junction PV cell, which is usually in the bottom of the cell. They claim that this large-wavelengths generated current will be transformed into heat in the PV cell since it exceeds the produced current from the rest of the PV cell materials. Accordingly, the efficiency of the

PV cell can be enhanced by reflecting the IR part of the spectrum as a trade-off between the temperature and the photonic current reduction. The 3-junction GaInP/GaAs/Ge PV cell is used in their study, where the Ge subcell produces nearly 2x of the other two subcells. Ge subcell responds to wavelengths up to 1800 nm of the solar spectrum, where the excess current is produced from wavelengths larger than 1250 nm. However, an optimized cutoff wavelength should be designed. They used available data in their calculations to validate their proposed design of such a filter. They found that a good cutoff wavelength for Ge subcell is 1300 nm with a 2.2% power increase after accounting for the slight current reduction due to lower temperature.
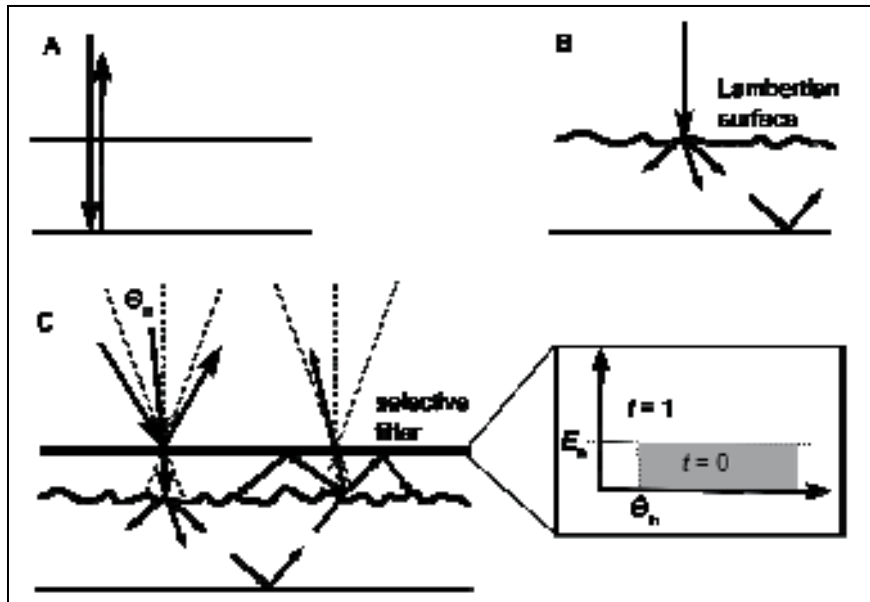
Figure 2.26. Three different Si cells studied, A) Planer cell, B) Si cell with Lambertian surface, C) Si cell with Lambertian and angular filter [67]

Beauchamp and Hart ([69], 1995) proposed a UV/IR reflecting cover for solar cells applications. They proposed a multilayer coat to transmit only the spectral region that the PV cell responds to. The main reason of proposing such a filter is to enhance the efficiency of the PV cell by reducing its temperature through reflecting some portions of the solar spectrum that are outside the cell bandgap response.

2.2.5. Active filtering of solar spectrum

In the previous section, samples of the passive optical filtering efforts are discussed. Passive filtering means that whatever the conditions are (panel temperature, day time, location, and weather conditions), the same filtering process is carried out. In this section, the efforts of using active filtering processes will be discussed. Unfortunately, few studies were found in the literature that reported active or smart optical devices for PV applications. These studies were focused on application rather than efficiency enhancement.

Anjaneyulu and Yoon ([70], 1985) designed an optical shutter using liquid crystal (LC) cells to control the solar energy. The main purpose of their study was to study the usability and the controllability of the liquid crystal cells in the solar applications without focusing on the produced electricity. They fabricated large number of testing cells using the three most commonly used types of liquid crystal cells: dynamic scattering, twisted nematic and guest-host. In their investigation, they found that phase change guest-host (PCGH) cell type with black dye as the guest material is better to fabricate large size LC-cell. They fabricated a 12.5 cm length, 12.5 cm width, and 6 µm thick LC-window using PCGH-LC mixture. Their experimental results of controlling the transmittance of the PCGH-cell are shown in Figure 2.27. They found that this LC-window has large transmission controllability up to more than 99% accuracy in the 575 to 675 nm spectral region. They concluded that thickness variation of the liquid crystal cell is major problem in fabricating a large size window.
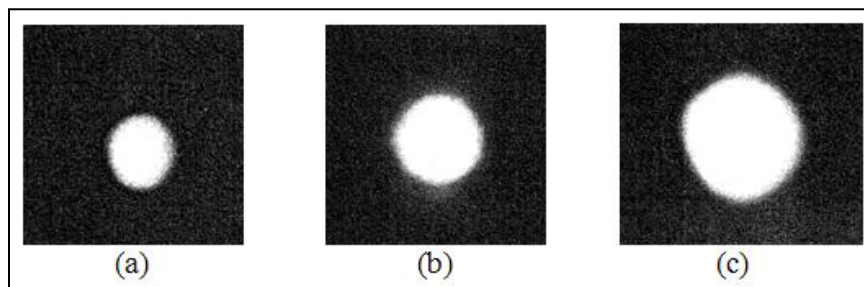
Figure 2.27. Transmitted beam through 9µm thick Nπ twist PCGH-cell: a) No voltage, b) 5 Vrms, c) 15 Vrms [70]

Chen and Lo ([71], 2009) integrated a translucent hydrogenated amorphous silicon (a-Si:H) solar cell with a twisted nematic liquid crystal cell (TN-LC) incorporated with a sub-wavelength metal grating polarization beam splitter. They have attached the TN-LC cell to the bottom of the solar cell as shown in Figure 2.28. As shown, the controllability of reflecting the light back to the PV cell is by switching TN-LC on and off. Their main input is through the novel idea of integrating the sub-wavelength metal grating polarization beam splitter in the TN-LC cell instead the conventional polarizer. This new polarizing technique is of higher light transmission efficiency and is not affected by the ultraviolet waves as the conventional polarizer sheets do. Figure 2.29 shows a comparison between the transmittance characteristics of the stand alone PV cell incorporated with the conventional and novel TN-LC cell.
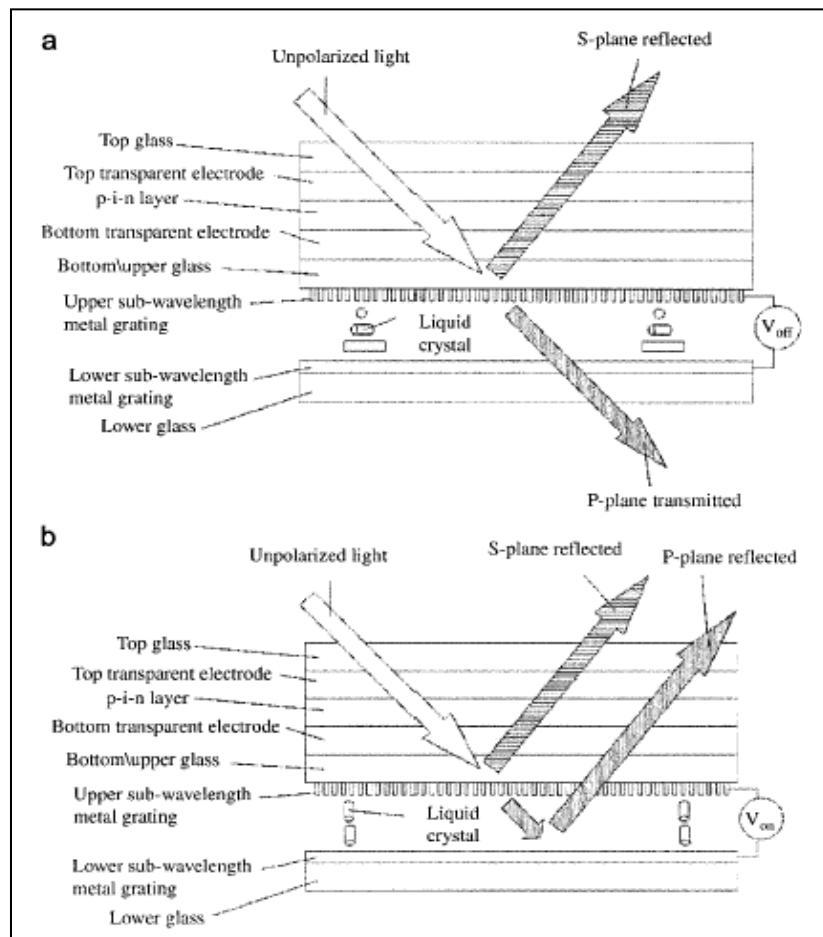
Figure 2.28. Schematic of passing and reflecting of the unpolarized light in two controlling states: a) off state, b) on state [71]

Their novel TN-LC cell is better in reflecting the light back at large wavelengths while it transmits the small wavelengths (ultraviolet wavelengths) compared to the conventional TN-LC cell. They also studied the performance of the PV cell integrated with the conventional and the novel TN-LC cells. In both cases, as shown in Figure 2.30, the output power is enhanced. However, the enhancement using their novel design is more than the conventional one. They found that the efficiency of the stand alone PV cell is 2.074%, while it is 2.087% and 2.089% for the PV cell integrated with the conventional TN-LC cell for the off and on states respectively. For the PV cell integrated with novel TN-LC, the off and on state efficiencies are 2.283% and 2.491% respectively, which represents the highest values. They have concluded that this proposed device represents an ideal solution to all applications that require adjustable brightness PV cells.
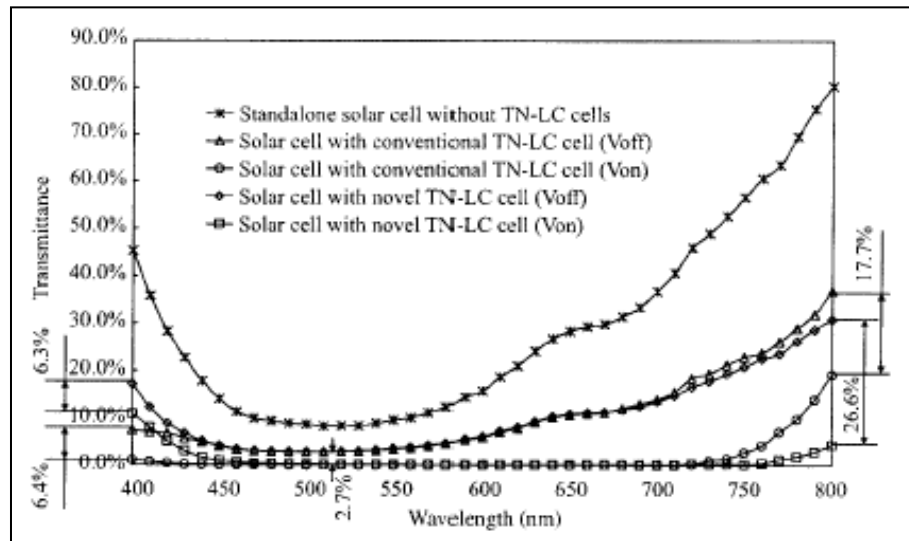
Figure 2.29. Transmittance of light through a-Si:H PV cell with and without conventional or novel TN-LC [71]

Huang *et al.* ([72], 2012) developed a photovoltaic electrochromic (PV-EC) device for photovoltaic and green applications such as self powered smart glass. They used a semi-transparent silicon thin-film solar cell (Si-TFSC) substrate, an electrochromic solution, and a transparent non-conductive substrate. The electrochromic solution is disposed between the non-conductive substrate and the Si-TFSC substrate as shown in Figure 2.31. When the device is illuminated by sunlight, portion of the generated current will be

converted into ionic current to change the shade of the PV-EC device and the remaining will power the connected load. They studied the effect of the potential produced by the cell on the shading of the electrochromic glass, where the more potential is applied, the more shading is obtained and vice-versa. This self shading-bleaching device is a good application for green buildings technology.
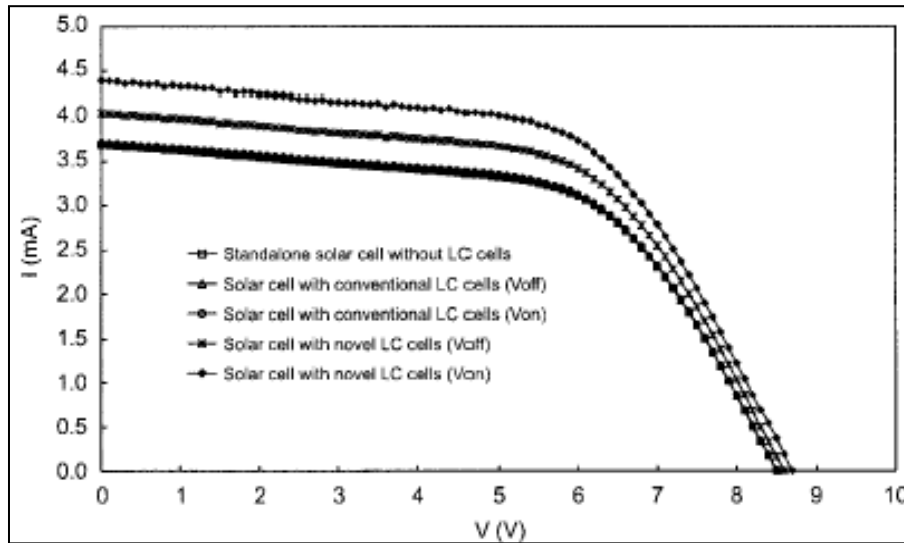
Figure 2.30. IV-curve of the PV cell integrated with different TN-LC cells [71]
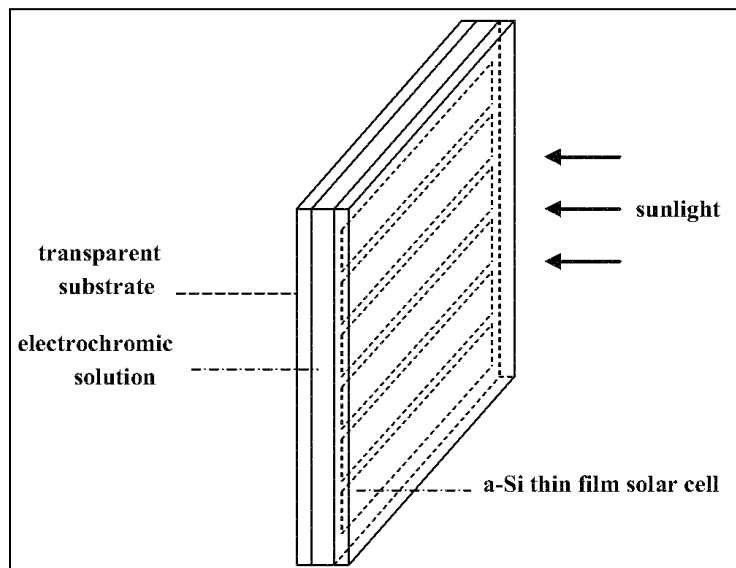
(a)
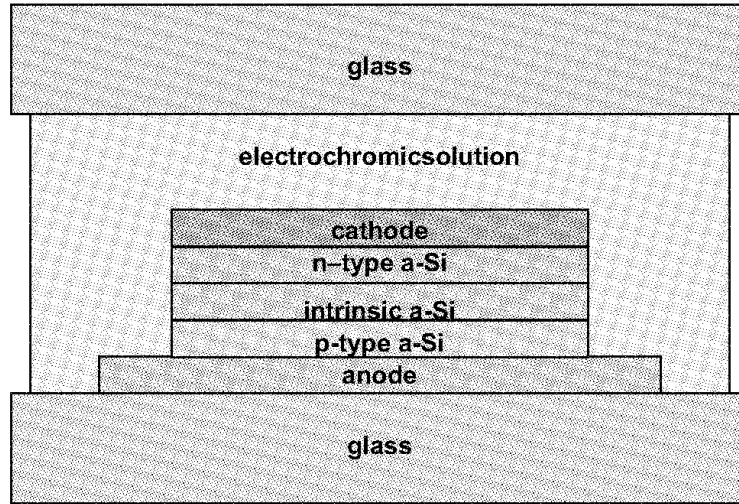
(b)

Figure 2.31. (a) Schematic prespective view of the solution type PV-EC device, (b) A schematic cross-sectional view of the solution type PV-EC device [72]

2.3. Optimization in the photovoltaics

The optimization efforts of the research community address a number of different fields in the photovoltaic energy area. Some researchers interested in optimizing the semiconductor material growth and the cell design ([73], 2008), ([74], 2009). Other researchers have used optimal numerical methods as the neural network and the artificial genetic algorithms for modeling the PV modules and to extract their parameters ([18], 2006), ([75], 2008), ([76], 2005). Some optimization efforts were conducted in order to increase the PV cells efficiency as optimizing light trapping filters, tilt angles, and sun tracking systems ([77], 2003), ([60], 2008), ([78], 2009), ([79], 2009). Only a sample of the optimization efforts that are within the scope of this research will be discussed.

Zaho *et al.* ([80], 2010) used autoregressive and moving average (ARMA) method to model two indices, the radiation loss and the amended clearness. Both indices are used to predict the radiation and the optimal tilt angle of the PV panels. They used the records of one year of solar radiation to investigate the importance of using the optimal tilt angle and to calculate this value. They concluded that, since the radiation value is the only

parameter used to build the model, the results are not accurate as using other complicated methods such as intelligent network. In addition, they found that since the solar radiation is location dependent; long term data is needed in order to develop more accurate model. Their experimental results showed that tilting the PV panel angle to a specific optimal value increases the received energy which increases its output energy. The proposed model can also be used to predict average distribution of solar radiation in a specific period of time and can give acceptable results. They reported that more accurate predictions can be made if more data is given.

Park and Yu ([81], 2004) suggested that the optimal voltage for maximum power point tracking system (MPPT) can be obtained by only the solar cell temperature. Their idea is to use the optimal voltage as indication to the optimal output power. The optimal voltage is not remarkably affected by the amount of the irradiance but by the cells temperatures. Therefore, the maximum output power will be tracked if the input voltage to the inverter is the optimum. Using a voltage-type converter can maintain the desired input voltage. Accordingly, determining the optimal voltage from the cells temperature and simultaneously controlling the converter input voltage to be at its optimal value, the maximum power point can be tracked without failure. They introduced experimental measurements to show the dependency of the output voltage on the cells temperature as shown in Figure 2.32. Furthermore, they introduced an empirical formula to calculate the optimal output voltage as a function of the cells temperature and other experimental parameters. The values of these parameters are irradiance dependent. They provided three field data measurements: sunny day, cloudy day, and rainy day. In their experimental apparatus, they used a multi-crystalline Si that is of 18% efficiency cells and commercial module of 14% efficiency. They have found that the conversion efficiency between the PV panel and the converter of the proposed control scheme was much better than the power comparison MPPT control. In addition, they found that the output voltage of PV panel was extremely stable when the optimal voltage for MPPT is obtained by only solar cell temperature.
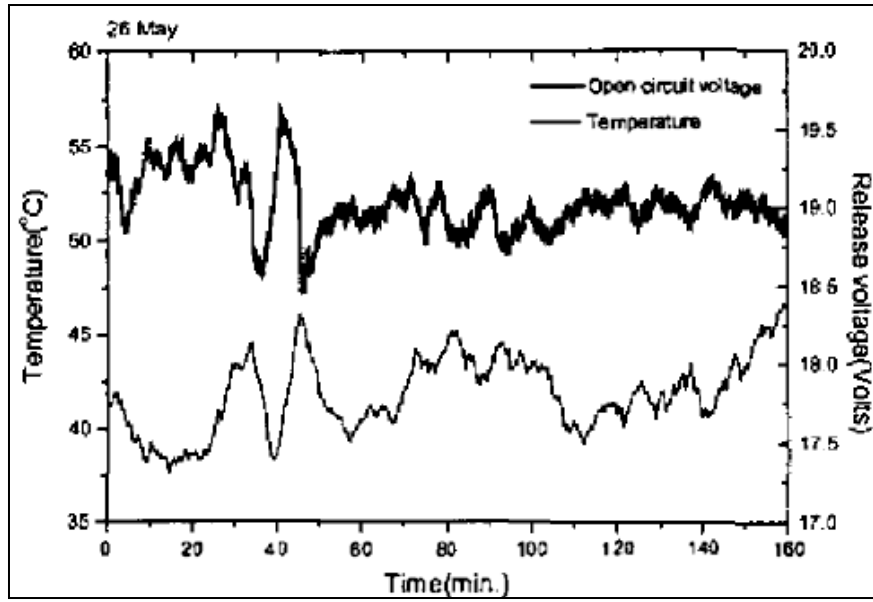
Figure 2.32. Relation between open-circuit voltage and cell temperature [81]

Xuan *et al.* ([82], 2011) presented a method in order to design and analyze the performance of the solar thermophotovoltaic (STPV) device. STPV is a light-electricity conversion system consists of solar concentrator, emitter, filter, and cooling system. Compared with the conventional PV cells, STPV utilizes the adjusted spectral light by the emitter which emits light correspondent to the bandgap of the solar cells by controlling the emitter's temperature and installing a spectral filter. They worked on optimizing the emitter spectrum in order to reflect the unused part of radiation. They designed two filters: periodic and non-periodic microstructure band-pass filters. The filter is positioned between the emitter and the PV cells. They used the genetic algorithm to optimize the non-periodic microstructure filter. Figure 2.33 shows the reflectivity of both the optimized and the periodic filter structures. They have concluded that the spectral filter plays an important role in recycling the radiation energy. They found that the optimized non-periodic filter has better performance than the periodic filter. In addition, they observed that increasing the series resistance and the cells temperature exerts negative effects on the electrical output power and the system efficiency. They recommended using high performance cooling system to maintain the cells temperature below 50 ℃.

47
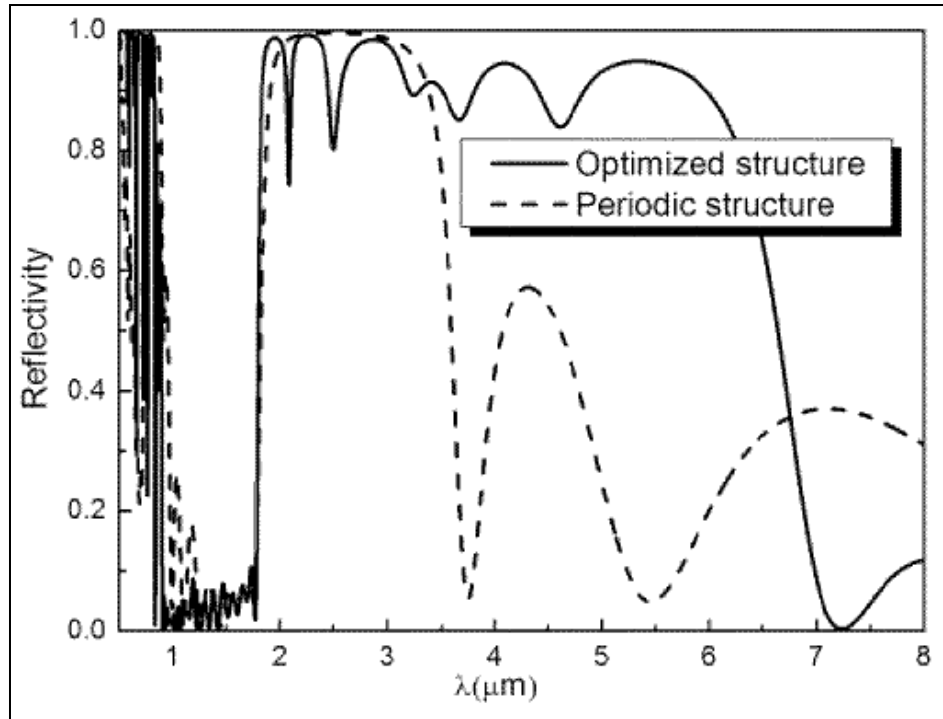
Figure 2.33. Comparison of the reflectivity of the two filters [82]

2.4. Conclusion

The literature review demonstrated that there are several approaches to enhance PVs efficiencies. However, each of them has its own shortcomings. Some of these limitations are: complexity, lack of the physical implementation, high cost, and drawbacks (i.e. increases the panel temperature) that waste the gains. Despite of the intensive studies that were reported on thermal and thermoelectrical modeling of PV cells and modules, there are no proposed thermal models that consider the individual wavelength perspectives. Such models introduce a thorough grasp and better understanding of the optical behavior of the PV modules. This accordingly enables better assessment for optical filtering applications especially if integrated with PV modules. Additionally, no studies are found in the literature focus on enhancing the PV module efficiency using active methodologies such as light filtering and trapping.

48

CHAPTER 3.

PROBLEM STATEMENT

The problem statement and the motivation are introduced in this chapter. The concept of active filtering is presented as one of the promising solutions to the proposed problem and as a new contribution to the photovoltaic research community. The functional operation of such a filter is also discussed.

3.1. Research motivation

The photovoltaic (PV) module temperature is a function of the incident radiant power density, the output electrical power, the thermal properties of the materials composing the module, and the heat transfer exchange with the surroundings.

The incident solar irradiance is the main input power to the module. Portions of the irradiance spectrum that are associated with long wavelengths do not contribute to electricity production due to their low energy levels. However, light with such wavelengths either reflects, passes through, or is absorbed as heat into the module layers. This heat increases the solar cell temperature as well. The photo-current increases slightly with increasing operating temperature due to band gap shrinkage. However, this gain is not sufficient to compensate for the drop in open-circuit voltage and PV cell fill factor [83]. Accordingly, the optical properties of the PV module affect the input power which directly impacts its temperature and output power.

Higher temperature of the PV module leads to cyclic stresses at the upper and the lower surfaces of the cell. This may cause cracks at the center part of the cell surface. These cracks reduce the cell open-circuit voltage, the short-circuit current, and accordingly the fill factor. In addition these cracks cause fatigue failure that reduces the cell lifecycle [84]. The effect of temperature on the PV module efficiency varies with cell material. For

a crystalline silicon (Si) cell, the open-circuit voltage drops by 2 mV / K and output power decreases by 0.4% / K – 0.5% / K of temperature increase, from a base of 298 K [85-87]. For amorphous Si, the decrease is approximately 0.1% / K [88]. Table 3.1 [23] summarizes the loss percentage in the efficiency of any PV system as a result of different operational parameters and conditions reported by several researchers [23]. It can be observed from column 2 of Table 3.1 that the temperature causes a significant efficiency reduction.

Table 3.1. Percentage of losses in PV systems due to different parameters [23]

Source of loss								
Reflection (%)	Temperature (%)	Inverter (%)	Low irradiance (%)	Shading (%)	Soiling (%)	Ohmic (%)	Mismatch (%)	MPPT (%)
–	3.0	7.8	–	7.1	–	–	3.8	–
–	8.0–17.0	10.0–16.0	–	–	3.5–5.0	1.0–1.5	0.15–0.17	2.0–5.0
–	–	15.0	–	–	–	2.5	2.0	–
–	–	–	–	–	–	–	–	15.0
–	–	–	–	35.0	10.0	–	–	–
3.1	7.6	4.0	0.9	0.3	–	1.2	5.7	–
–	3.3	5.3	–	3.5	–	0.24	–	–
–	3.8	17.5	4.6	11	–	1.2	5.7	–
–	2.8	13.2	–	1.7	–	2.1	9.8	4.5
–	2.2	6.9	–	4.1	–	–	5.1	–
–	4.0	8.0	–	7.0	–	–	6	–
–	3.3	5.3	–	3.5	–	–	–	–
–	–	–	–	–	4.0	1.2	0.2	0.6
–	–	10.0	–	–	3.0	–	5.0	–
2	4	15	7		1.5	1.0	1.0	2

In conclusion, changes in temperature considerably alter the PV cell performance and lifecycle. Therefore, there is a great need to reduce the temperature increase that is taking place in the PV modules which enhances both the efficiency and lifecycle.

Different approaches can be used to reduce the PV module temperature [23]. These approaches are active cooling systems such as air conditioning, assisted PV systems such as air-to-air heat exchangers, passive systems such as optical coatings and phase change materials which remove the heat by absorption [23].

Despite of its advantages, controlling the PV module temperature using active cooling systems increases the complexity of the solar system as well as its maintenance cost. Such a hybrid photovoltaic thermal (PVT) system requires additional output power from the PV module. However, the reduction in the temperature increases the output power more than the cooling pumps power consumption. The consumed power could be gained if other cooling methods are used such as the solar spectrum filtering. The hybrid PVT system is generally used for small scale solar power systems such as powering houses where hot water can be utilized. Nevertheless, the complexity and the high cost make the active cooling is not the preferred solution for large PV powering fields. The assisted PV system approach usually requires some power; however, is not as the same as active cooling, and also requires less maintenance. Phase change materials remove heat from the PV modules by changing its physical state by absorbing the heat from the module. Solar systems with phase change materials require additional maintenance and high initial investment cost as well. The passive systems might not reduce the temperature as other methods do, but it requires much lower initial investment cost and it is also maintenance free. In addition, passive systems as optical filters are reliable to be used for large scale PV energy field applications.

As mentioned above, the main input power to the PV module is the solar irradiance. The incident solar spectrum consists of vast range of wavelengths that contain high and low energy levels. The PV material does not usually respond to photons associated with large wavelengths (infrared light) and accordingly, it will not absorb them. The energy level of these photons is usually lower than the PV material bandgap energy. Therefore, they either escape the module or most probably are absorbed by other layers within the module and convert into heat. The photons associated with small wavelengths (ultraviolet light) are usually of higher energy levels than the bandgap of the PV material. The excess energy of these photons will be converted into heat.

Consequently, removing part of the solar irradiance reduces the heat and accordingly the module temperature. In Chapter two, several attempts of filtering efforts reported in the literature have been discussed. All of these efforts were focusing on designing and

developing passive filters (coatings) and light traps in order to increase the module efficiency. The optical filters were designed to passively filter the light according to wavelengths and angle of incidence. Although these passive filters enhance the output power at a specific time period, they ignore the effect of irradiance and temperature changes during the day course on the module performance. Accordingly, part of the light might be lost due to continuously changing incident angles which reduces the output power. Additionally, these optical coats are not capable of blocking the sun light if temperature reaches critical point that may end the module lifecycle. Furthermore, most of the reported designs are focused on a specific threshold wavelength, which is usually in the infrared (IR) region, and ignoring the ultraviolet (UV) light. Therefore, an active or dynamic filter would be a good solution for the passive filter limitations.

Designing an optical filter, whether passive or active, for PV applications will be a challenge due to the optical behavior of the PV module. It is not intuitive to determine the cutoff wavelengths to split or block some portions of the solar spectrum. The different optical properties (reflection and absorption) of the PV module layers and the light internal reflections between them affect the overall light reflection and absorption of the module. Light reflection and absorption of the PV module have to be a function of wavelengths for better designs. This implies that obtaining the optical properties of the module layers as a function of wavelengths is also a challenging issue. Therefore, there is a great need for an optical model that is able to predict the overall optical properties of the module using the ones of its layers.

In addition, a mathematical thermoelectrical model that is capable of considering the different factors that affect the module temperature is important for better temperature and module performance predictions.

In conclusion, developing, designing, and implementing an active optical filter for photovoltaic applications using a wavelength-based thermoelectrical model is crucial. This will not only enhance the PV module efficiency, but also will add a novel

contribution in the field of solar energy by taking the advantage of the progress achieved in other fields (control, optics, and filtering).

3.2. The concept of active optical filtering

As discussed above, the passive optical filters have some limitations which are mainly blocking some light wavelengths that generate electrons and also lack of adaptive behavior to accommodate the meteorological changes. In addition, a fixed cutoff wavelength filter is not capable of blocking more light when it is necessary to enhance the lifecycle of the PV module especially for space applications. Applying an active optical filter reduces these limitations. The concept of the active optical filtering is simple. An ideal active optical filter should remove portions of the incident solar spectrum based on the module temperature. The cutoff wavelengths are from IR and UV regions. The higher the module temperature is, the larger the UV cutoff wavelength and the smaller IR cutoff wavelength. The cutoff wavelengths are optimally calculated, and filtering decisions should be made such that the output power is maximized. An optional filtering action can be used for total light blocking once the temperature exceeds the yielding point of the PV material which may lead to plastic deformation that might destroy the module. The optical filter can either be attached to the cover of the module as shown in Figure 3.1, or can be used as the cover to reduce optical losses. An approximate schematic for the proposed conceptual active filtering system integrated with the PV module is shown in Figure 3.2.

Most of the manufactured PV cells are fabricated with a reflection layer at the bottom of the cell to reflect light back to the top of the cell in order to enhance the light absorption and also to increase the light path within the cell to improve its efficiency. In the cases where such a reflection layer does not exist, using an active optical filter might add some value to the output power if it is used as fully blocking or fully transmitting filter based on the module temperature.
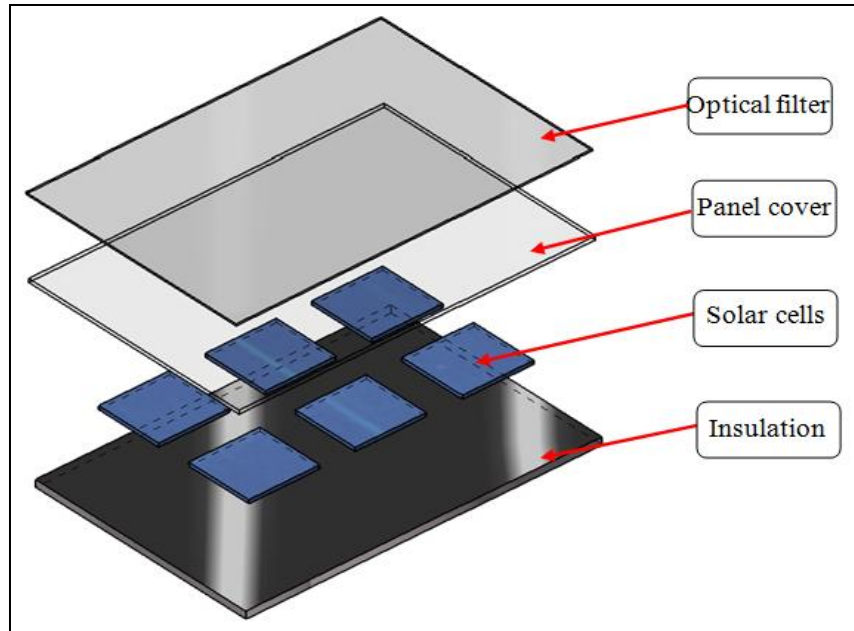
Figure 3.1. The optical filter integrated with the PV module
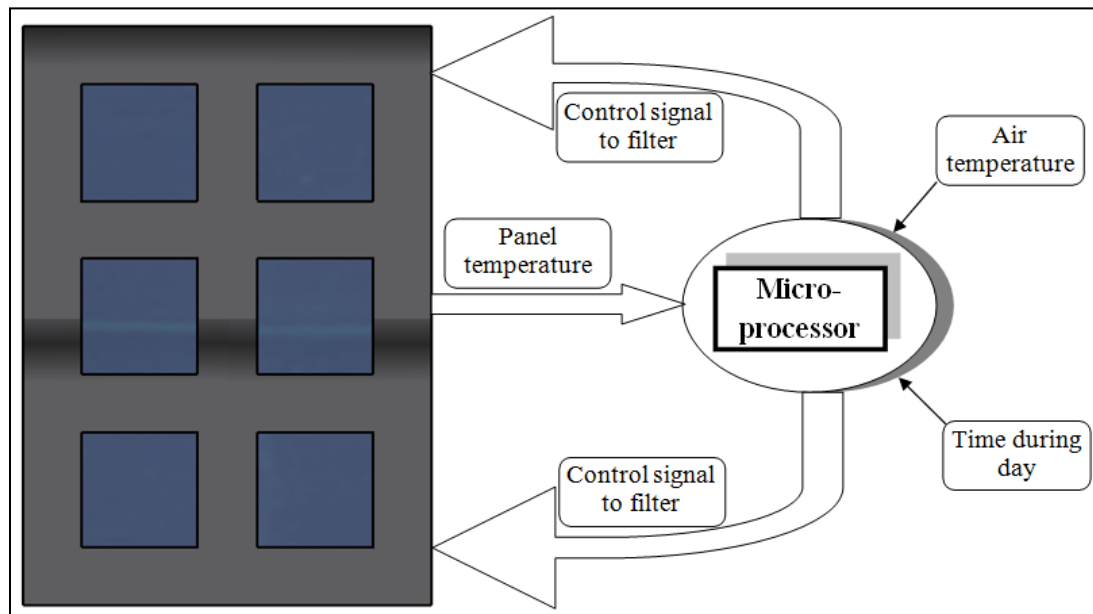
Figure 3.2. Schematic diagram of the active filtering system

54

CHAPTER 4.

WAVELENGTH BASED THERMOELECTRICAL MODEL

4.1. Introduction

The majority of the thermal and thermoelectrical models that predict the photovoltaic (PV) module temperature, output power, and the interaction between them have two major drawbacks. First, the calculated input power in these models relies on the assumption that the generated current is proportional to the total power density of the incident solar irradiance neglecting the wavelength-specific effects. It is well known that the PV cell responds to a specific wavelength range of the solar irradiance to generate electricity. This range depends on the PV material. Therefore, only this portion of the solar irradiance should be considered to calculate the input power to the PV material. Second, these models use a constant absorption coefficient for all wavelengths ignoring the different optical properties of the different module layers and the internal light reflections between these layers. This potentially affects the model input and output power predictions.

At each wavelength some energy is reflected, some is absorbed in the PV cells (contributing to electricity production), some is absorbed in other module materials, and some is transmitted through the module. A model capable of predicting this wavelength-specific behavior will generally allow better assessment of the module performance especially when it is combined with various subsystems such as optical filters.

In this chapter, a detailed derivation of a mathematical thermoelectrical model is introduced. This model is developed to consider the wavelength-specific effects, allowing for improved temperature and module performance predictions. All terms of the model are discussed. An optical model to calculate the overall light reflection and absorption of a PV module is also proposed.

4.2. Model Derivation

The PV module temperature is a function of the incident radiant power density, the output electrical power, the thermal properties of the materials composing the module, and the heat transfer exchange with surroundings. The PV model proposed herein is based on consideration of energy exchange [30], [58], [59]. All of the heat transfer modes will be considered; i.e., conduction, convection, and radiation. However, the heat conducted from the module to the structural framework is considered negligible due to the small area of contact points [30]. The electrical power produced by the module is also considered. The main heat transfer paths and energy flow to and from the module are shown in Figure 4.1.
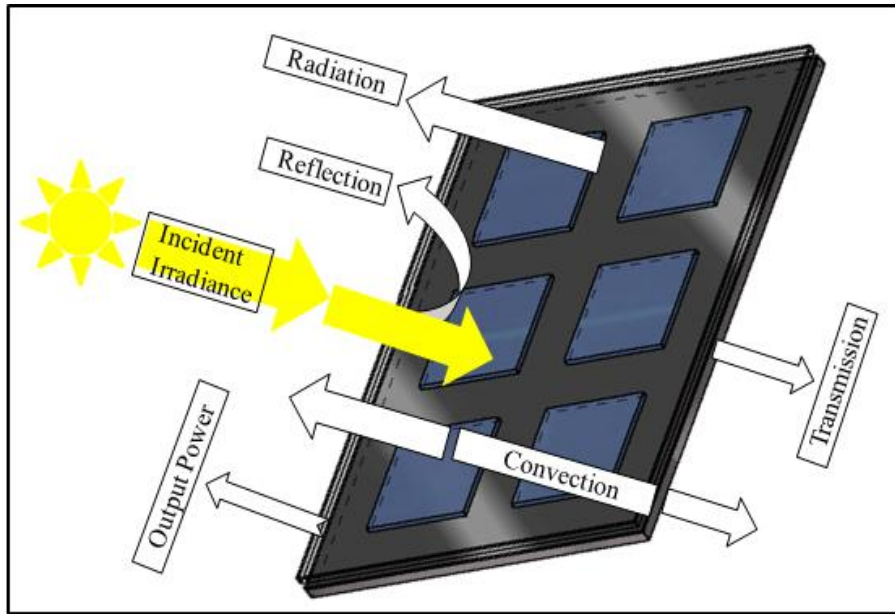
Figure 4.1. Heat transfer and energy exchange in the PV module

The rate of change in the module temperature is a function of the incident light which is referred to it as shortwave radiation q_{sw}, longwave radiation q_{lw}, heat convection to the surroundings q_{conv}, and output power P_{out} [30]. This can be expressed as

$$C_{module} \, \frac{dT_m}{dt} = q_{sw} - q_{lw} - q_{conv} - P_{out}. \qquad (4.1)$$

Table 4.1 contains the definitions of all symbols used herein. The terms given in Equation (4.1) are discussed in the following sections.

Table 4.1. Nomenclature

Symbol	Definition
C_{module}	module heat capacity (J/K)
T_m	module temperature (K)
q_{sw}	shortwave radiation absorbed by module (W)
q_{lw}	longwave radiation (W)
q_{conv}	heat convection to the surroundings (W)
P_{out}	output power (W)
A	area of module (m2)
d_m	depth of material in module (m)
A	area of module (m2)
λ_1	starting wavelength (nm)
λ_2	ending wavelength (nm)
α	absorption coefficient
F_{rr}	solar spectral irradiance (W/(m2nm))
λ	wavelength (nm)
α_{s1}	absorption coefficient of cell, cover, insulation stack
α_{s2}	absorption coefficient of cover, air, insulation stack
M	number of cells in module
A_j	area of the p-n junction (m^2)
σ	Stefan–Boltzmann const. (5.669×10^8 W/($m^2 K^4$))
$\beta_{surface}$	tilt angle measured with the horizontal (degrees)
ε_{sky}	emissivity of sky (0.95)
T_{sky}	effective sky temperature (K)
ε_{gro}	emissivity of surface of ground (0.95)
T_{gro}	ground temperature (K)

Table 4.1 (continued)

Symbol	Definition
ΔT	constant (20 K)
ε_m	emissivity of PV module (0.9)
h_c	convection coefficient (W/(m^{2}K))
T_{amb}	ambient temperature (K)
$h_{c,forced}$	forced convection coefficient (W/(m^{2}K))
$h_{c,free}$	free convection coefficient (W/(m^{2}K))
WS	wind speed (m/s)
I	load current (A)
V	load voltage (V)
I_{ph}	photonic current (A)
I_0	saturation current (A)
R_s	series resistance (Ω)
R_{sh}	shunt resistance (Ω)
K	Boltzmann const. (1.38×10^{-23} J/K)
n	quality factor depending on the technology (1–2)
q	charge of electron (1.6×10^{-19} C)
ϕ_{rr}	photonic flux (1/(m^{2}nms))
α_c	absorption coefficient of PV cell
h	Planck's const. (6.626×10^{-34} Js)
c	light speed (3×10^8 m/s)
E	photon energy (J)
I_{0r}	reference saturation current (A)
T_r	reference temperature (K)
E_g	bandgap energy (eV)
I_{sc}	short-circuit current (A)
V_{oc}	open-circuit voltage (V)
R_L	load resistance (Ω)
C_{FF}	fill factor

Table 4.1 (continued)

Symbol	Definition
P_{max}	maximum output power (W)
V_n	normalized open-circuit voltage
$P_{max,n}$	new maximum output power (W)
C_{FFn}	new fill factor
R_{ch}	characteristics resistance (Ω)
C_m	specific heat capacity of material (J/(kgK))
d_m	depth of material in module (m)
ρ_m	density of material (kg/m)
A_m	area of material (m^2)
t	time (s)
S_t	probability at time step t
Φ_{ij}	state transition matrix
R_x	reflection of layer x
A_x	absorption of layer x
N	index of the bottom layer of the module

The temperature throughout the module is assumed to be homogenous. This assumption is justified in Chapter 5.

4.2.1. Shortwave Radiation

Shortwave radiation is the input power to the PV module through its front surface. The input power is a function of the power density of the global solar irradiance that is absorbed in the module layers. Mathematically, this can be represented as

$$q_{sw} = A \int_{\lambda_1}^{\lambda_2} \alpha(\lambda) F_{rr}(\lambda) d\lambda. \tag{4.2}$$

The value of F_{rr} depends on the sun position (time), the module location, and the sky conditions (clear, cloudy, or overcast). The absorption coefficient α, which is a function of wavelength, depends on the optical properties of the module layers. The value of α specifies the fraction of the incident irradiance associated with a specific wavelength that is absorbed by the module.

Generally, PV modules contain three major layers: cover, cell, and insulation material. The insulation layer represents another source of input power to the module since it absorbs light. The input power given in Equation (4.2) can be divided into two parts. The first part represents the power that is absorbed by the area where the PV cells are present. The stack of layers that contains cover, cell, and insulation has absorption coefficient α_{s1}. The second part represents the power that is absorbed by the area where the PV cells are not present. The stack of layers that contains cover, air, and insulation has absorption coefficient α_{s2}. Accordingly, the shortwave radiation given in Equation (4.2) becomes

$$
\begin{aligned}
q_{sw} = &\left(\int_{\lambda_1}^{\lambda_2} \alpha_{s1}(\lambda) F_{rr}(\lambda) d\lambda \right) (MA_j) \\
&+ \left(\int_{\lambda_1}^{\lambda_2} \alpha_{s2}(\lambda) F_{rr}(\lambda) d\lambda \right) (A - MA_j).
\end{aligned}
\tag{4.3}
$$

The absorption coefficients are determined by considering the optical properties of the module layers and the interfaces between them.

The range $\lambda_1 - \lambda_2$ includes the wavelengths that hold the majority of the solar irradiance energy. Only some of these wavelengths excite electrons. For example, the range of wavelengths that generate electricity from silicon PV cells is 350–1110 nm, while the remaining wavelengths do not. These wavelengths may be absorbed by other layers in the module and this would be represented by the absorption coefficients of the layers for those wavelengths.

The novelty of the proposed method used to calculate the input power is breaking the overall module absorption coefficient α into sub-absorption coefficients that are layers dependent and yet functions of wavelength. This method differs from the most reported approaches in the literature [30], [89] that use α as constant for the whole module, neglecting the different optical properties of the module layers. The proposed method can be extended to any number of layers without losing the generality.

4.2.2. Longwave Radiation

The heat exchange between the PV module, the ground, and the sky is given as [30]

$$q_{lw} = -\sigma A \left(\frac{1 + \cos(\beta_{surface})}{2} \varepsilon_{sky} T_{sky}^4 \right.$$
$$\left. + \frac{1 - \cos(\beta_{surface})}{2} \varepsilon_{gro} T_{gro}^4 - \varepsilon_m T_m^4 \right) \tag{4.4}$$

The ground temperature is assumed to be the same as the ambient temperature because the testing position is close to ground. The tilt angle $\beta_{surface}$ is measured for each experiment. The sky temperature T_{sky} is different for different sky conditions [30]. For clear sky condition, sky temperature can be calculated using

$$T_{sky} = T_{amb} - \Delta T \tag{4.5}$$

where ΔT is constant and equals 20 K [30]. For overcast condition, the sky temperature equals the ambient temperature [30].

4.2.3. Convection heat transfer

The heat convection that takes place between the PV module and the ambient air can be calculated using [30]

$$q_{conv} = h_c A (T_m - T_{amb}). \tag{4.6}$$

The coefficient of heat convection h_c is calculated from the coefficients of free and forced convective heat transfer as [90]

$$h_c = \sqrt[3]{h_{c,free}{}^3 + (h_{c,forced}(WS))^3}. \tag{4.7}$$

Jones *et al.* [30] and Armestrong *et al.* [59] discussed different approaches to find the coefficients of convection heat transfer. The coefficient of free heat transfer $h_{c,free}$ of the PV module can be found using the empirical formula [30]

$$h_{c,free} = \epsilon (T_m - T_{amb})^{1/3}. \tag{4.8}$$

The coefficient of free heat transfer given in Equation (4.8) accounts for the heat lost from the back side of the module.

The coefficient of forced heat transfer $h_{c,forced}$ depends on wind speed. Armestrong *et al.* [59] presented several linear relations to calculate $h_{c,forced}$ as function of wind speed. Jones *et al.* [30] provided a wide range of constant values for the forced heat transfer from 1.91 to 9.1 W/(m²K) for different wind speed ranges. Finally, Kemmoku *et al.* [91] optimized the coefficient of forced heat transfer such that the predicted temperatures fit the experimentally measured ones.

It is found that using a constant $h_{c,forced}$ over a specific time results in a large error. This can be attributed to the fact that wind speed unpredictably fluctuates on a short time scale (i.e., within seconds) which critically affects the heat transfer process. Therefore, using a formula to calculate $h_{c,forced}$ reflects the wind speed dynamic changes.

For outdoor experiments, Armestrong *et al.* [59] discussed three formulas (Test, Sturrock, and Sharples) that could be used to calculate $h_{c,forced}$ as a function of wind speed. Testing procedure and conditions help to select the most convenient formula that predicts temperature values close to the experimental measurements. Since in most cases the PV module is tilted, and the wind speed is measured at a location beside the module (windward), Sharples-windward empirical formula given as

$$h_{c,forced} = 3.3 \left(\frac{J}{m^3 K}\right) WS + 6.5 \left(\frac{W}{m^2 K}\right) \tag{4.9}$$

is expected to predict accurate values for $h_{c,forced}$.

4.2.4. Output Power

As discussed in Chapters two and three, the output power of the PV cell is highly affected by its temperature. The relation between the thermal and the electrical aspects of the PV cell is interactive. The output power of M series connected PV cells is given as

$$P_{out} = MVI \tag{4.10}$$

The load-current I can be derived from the single-diode equivalent model [26] as

$$I = I_{ph} - I_0 \left(\exp\left(\frac{q(V + IR_s)}{nKT_m}\right) - 1 \right) - \frac{V + IR_s}{R_p}. \tag{4.11}$$

The shunt resistance R_p is assumed to be sufficiently large that the third term of Equation (4.11) is negligible. The voltage V across a load resistance R_L equals $R_L I$, therefore, Equation (4.11) becomes

$$I = I_{ph} - I_0 \left(\exp\left(\frac{q(R_L + R_s)I}{nKT_m}\right) - 1 \right). \tag{4.12}$$

The photonic current can be found using [92]

$$I_{ph} = qA_j \int_{\lambda_1}^{\lambda_2} \phi_{rr}(\lambda)\, \alpha_c(\lambda)\, IQE(\lambda)\, d\lambda \,. \tag{4.13}$$

The number of photons traveling in the same wavelength can be calculated using

$$\phi_{rr}(\lambda) = F_{rr}(\lambda)/E(\lambda) \tag{4.14}$$

where F_{rr} is the solar irradiance and E is the photonic energy which is calculated as [93]

$$E(\lambda) = hc/\lambda. \tag{4.15}$$

The reverse saturation current changes dramatically with PV cell temperature. Therefore, a model is required to calculate the reverse saturation current as a function of temperature. The formula is given as [94]

$$I_0 = I_{0r}(T_m/T_r)^3 exp\big[qE_g(1/T_r - 1/T_m)/(Kn)\big] \,. \tag{4.16}$$

The reference saturation current I_{0r} should be determined under reference conditions. These conditions are: temperature, open-circuit voltage, and short-circuit current. The reference saturation current I_{0r} can be approximated using [94]

$$I_{0r} = I_{sc}/[\exp(qV_{oc}/(MKnT_r)) - 1]. \tag{4.17}$$

The open-circuit voltage V_{oc} and the short-circuit current I_{sc} that are used in Equation (4.17) should also be measured or calculated at the reference temperature.

In the case of maximum power point tracking, the maximum output power can be found by numerically solving Equation (4.11) for the current that produces the maximum output

64

power. Alternatively, empirical relations can be utilized. The maximum output power can be found using

$$P_{max} = C_{FF} V_{oc} I_{sc} \qquad (4.18)$$

It is assumed that the effect of the series resistance on the short-circuit current is negligible, i.e. $I_{sc} \approx I_{ph}$. The open-circuit voltage V_{oc} can then be expressed as

$$V_{oc} = \frac{nKT_m}{q} \ln\left(\frac{I_{ph}}{I_0} + 1\right). \qquad (4.19)$$

The fill factor of the PV cell is function of its temperature, mainly due to the changes in the open-circuit voltage as given in Equation (4.19). A commonly used empirical formula to calculate the fill factor is presented in [95] and given as

$$C_{FF} = \frac{V_n - \ln(V_n + 0.72)}{V_n + 1} \qquad (4.20)$$

where V_n is the normalized open-circuit voltage that can be calculated using

$$V_n = \frac{q}{nKT_m} V_{oc}. \qquad (4.21)$$

The effect of the series resistance on the fill factor can be estimated using the following method [95]. The new maximum power will be the maximum power in absence of the series resistance minus the power lost into the series resistance as

$$P_{max,n} \approx C_{FF} V_{oc} I_{sc} - I_{sc}^2 R_s = P_{max}\left(1 - I_{sc} R_s / V_{oc}\right) \qquad (4.22)$$

or

$$P_{max,n} = P_{max}(1 - R_s / R_{ch}) \qquad (4.23)$$

where $R_{ch} = V_{oc}/I_{sc}$. Substituting Equation (4.18) in Equation (4.23) leads to

$$
\begin{aligned}
P_{max,n} &= V_{oc}I_{sc}C_{FF}(1 - R_s/R_{ch}) \\
&= V_{oc}I_{sc}C_{FFn}
\end{aligned}
\tag{4.24}
$$

where

$$
C_{FFn} = C_{FF}(1 - R_s/R_{ch}).
\tag{4.25}
$$

Thus, the output power can be used for various loading conditions including resistive and maximum power point loadings.

4.2.5. Heat Capacity

The heat capacity of PV module is the sum of heat capacities of the individual layers that are composing the module. For each component made of a specific material signified by m, the heat capacity of the module is given as

$$
C_{module} = \sum C_m \rho_m d_m A_m.
\tag{4.26}
$$

4.2.6. Model Integration

The thermoelectrical model of a PV module can be integrated by substituting Equations (4.3), (4.4), (4.7), (4.10), and (4.26) in Equation (4.1) as

$$C_{module} \frac{dT_m}{dt} = \left(\left(\int_{\lambda_1}^{\lambda_2} \alpha_c(\lambda) F_{rr}(\lambda) d\lambda \right) (MA_j) \right.$$

$$+ \left(\int_{\lambda_1}^{\lambda_2} \alpha_i(\lambda) F_{rr}(\lambda) d\lambda \right) (A - MA_j) \right)$$

$$- \sigma A \left(-\frac{1 + \cos(\beta_{surface})}{2} \varepsilon_{sky} T_{sky}^4 \right.$$

$$\left. - \frac{1 - \cos(\beta_{surface})}{2} \varepsilon_{gro} T_{gro}^4 + \varepsilon_m T_m^4 \right)$$

$$- \left(\sqrt[3]{h_{c,free}^3 + h_{c,forced}^3} \right) A(T_m - T_{amb}) - MVI \ . \tag{4.27}$$

This model is nonlinear and can be solved numerically. For example, the Euler method can be implemented to calculate the module temperature at every time step

$$T_m(t + t_{step}) = T_m(t) + t_{step} \frac{dT_m}{dt} \tag{4.28}$$

4.3. Optical Model for PV modules

The absorption coefficients of different combinations of the PV module layers considerably affect the input and output power calculations for the thermoelectrical model. The optical properties of the PV module determine the absorption of light through the module layers. Therefore, the optical properties of the PV module depend on its layers and their materials. Measuring the optical properties of these layers and identifying the interfaces between them is critical to understand the behavior of light within the module.

The conventional method that is often used to find the absorption coefficient of the PV module is to multiply the absorption coefficient of the PV cell and the cover optical efficiency. Most researchers [30], [89] have used constant values for both of these

parameters. It is well known that the optical properties of the silicon wafer and the cover are functions of wavelengths [96]. Therefore, it is important for a high-fidelity to treat the absorption coefficients of PV module layers as functions of wavelength. However, the simple multiplication of these wavelength-specific optical properties might not be accurate to find the net light absorption in the PV cells. This can be attributed to the internal reflections that take place at the interfaces between the module layers. These reflections can significantly affect the overall light absorption of the module layers.

In this research, an optical methodology is used to calculate the overall light absorption and reflection of the module layers. This methodology considers the light reflections at the interfaces between the module layers assuming that the light is propagating through the module in one dimension.

Once photons hit the module, some will be absorbed, and some will escape. The location at which a photon may be thought to exist is called light pocket (or state). A photon may exist in one of the following light pockets: top going down (TD), top going up (TU), absorbed into the layer (AB), bottom going down (BD), or bottom going up (BU) as shown in Figure 4.2. The same pattern repeats for each layer except for the top and bottom air layers where A, B, C, and D represent the light pockets in these two layers.
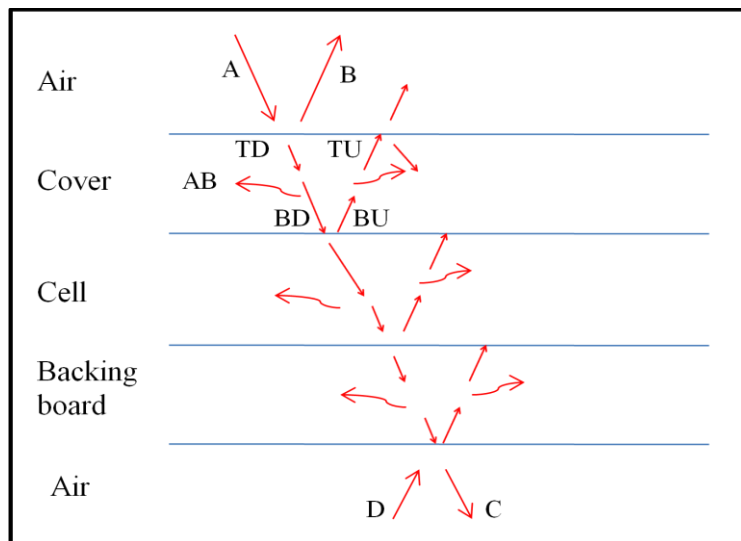
Figure 4.2. Light pockets in the PV module

A Markov chain is used to describe the probability of finding a photon at a specific state in the module layers depending on their optical properties (absorption and reflection). The basic concept depends on the probability of finding a photon in a future state from its current state. Mathematically, this can be expressed as

$$S_{t+1} = \Phi S_t \qquad (4.29)$$

where Φ is the state transition matrix that contains the conditional probabilities of a photon transitioning from one state to another. The transition matrix size equals the number of light pockets in the module. For example, in the stack of layers shown in Figure 4.2, there are 19 light pockets, hence Φ is 19×19. Using Figure 4.2, Equation (4.29) is expanded as

$$S_{A,t+1} = 0 \qquad (4.30)$$

$$S_{B,t+1} = S_{B,t} + R_1 S_{A,t} + (1 - R_1)S_{1,TU,t} \qquad (4.31)$$

$$S_{x,TD,t+1} = \begin{cases} (1 - R_x)S_{(x-1),BD,t} + R_x S_{x,TU,t}, & x > 1 \\ (1 - R_x)S_{A,t} + R_x S_{x,TU,t}, & x = 1 \end{cases} \qquad (4.32)$$

$$S_{x,TU,t+1} = (1 - A_x)S_{x,BU,t} \qquad (4.33)$$

$$S_{x,AB,t+1} = S_{x,AB,t} + A_x S_{x,TD,t} + A_x S_{x,BU,t} \qquad (4.34)$$

$$S_{x,BD,t+1} = (1 - A_x)S_{x,AB,t} \qquad (4.35)$$

$$S_{x,BU,t+1} = \begin{cases} R_x S_{x,BD,t} + (1 - R_x)S_{(x+1),TU,t}, & x < N \\ R_x S_{x,BD,t} + (1 - R_x)S_{C,t}, & x = N \end{cases} \qquad (4.36)$$

$$S_{C,t+1} = S_{C,t} + R_N S_{D,t} + (1 - R_N)S_{N,BD,t} \qquad (4.37)$$

$$S_{D,t+1} = 0 \qquad\qquad (4.38)$$

The subscripts can be expressed as in the example $S_{x,TD,t}$ which refers to the probability of a photon being in the state (light pocket) top going down in layer x at the step t. The entries of the state transition matrix Φ are dependent on the surface reflectance R_x between layers x and $x-1$ and on the absorption A_x of layer x.

The initial states vector is $S_0 = [1 \quad 0 \quad ... \quad 0]^T$, where a photon initially strikes the module at its surface traveling down. The final state vector S_∞ represents the fraction of photons that remain in a given pocket. Photons can ultimately be reflected from the module ($S_{B,\infty}$), absorbed in one of the layers ($S_{x,AB,\infty}$), or transmitted through the module ($S_{C,\infty}$). As an example, the contents of the S vector during the Markov chain's evolution for 30 steps for a photon with 600-nm wavelength striking the acrylic-covered PV module are plotted in Figure 4.3. It can be observed that the steady-state for all states is reached after approximately 5 steps. All states decayed to zero after this number of steps except two states. The first state (Pocket 10) corresponds to photons being absorbed in the PV cell. The second state (Pocket 2) corresponds to photons being reflected from the module. This behavior depends on the optical properties of the layers which are inputs to the optical model. The reflection and absorption of each layer in the module are required as a function of wavelength.

The optical model proposed herein can be used to find the overall light absorption coefficients of the different layer combinations throughout the module, i.e., α_{s1} and α_{s2}, as functions of wavelengths as it will be discussed in the next chapter.
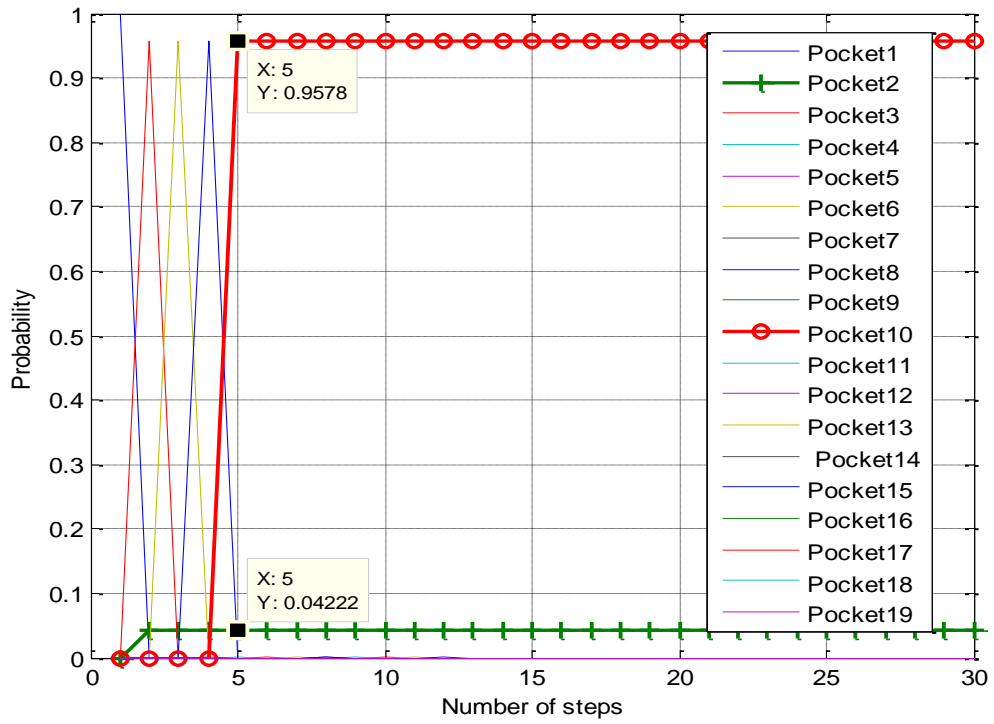
Figure 4.3. Final light pocket occupancy probability for 600 nm.

CHAPTER 5.

EXPERIMENTAL PARAMETERIZATION AND MODEL VERIFICATION

5.1. Introduction

The parameterization procedure of a computational model is crucial to determine its parameters and hence allows using it to simulate various conditions. A characterization procedure allows the model to predict the performance of a PV module under various meteorological conditions and to use the model for other PV materials. To validate the model proposed in Chapter four, each term presented in Equation (4.26) should be characterized for any photovoltaic (PV) module. The experimental parameterization advances the use of the model to predict the temperature and the output power of a given PV module at various locations and meteorological conditions (solar irradiance, ambient temperature, and wind speed).

In this chapter, a method to characterize the proposed thermoelectrical model is presented. The experiments that are used to parameterize and validate the model are described. A comparison between the experimental and the simulated results is discussed. Different PV module covers are tested.

5.2. Model Parameterization

In this research, two photovoltaic modules are built to characterize and to validate the model. Each of the modules consists of three layers: cover (acrylic or glass), PV cells (monocrystalline silicon), and insulation board (polystyrene) as shown in Figure 5.1. The experimental setup used to collect data for model characterization and validation is shown in Figure 5.2. The data acquisition system, which is shown in Figure 5.2, is designed and built to serve the goals of this research. It is basically designed to log the temperature measurements using four thermocouple inputs, and also to obtain the characterization curve (IV-curve) of the PV module continuously at a specific time rate

that can be changed. This would allow tracing the IV-curve of the module at different temperatures to monitor its performance. In addition, this system is capable of calculating the maximum power point from the IV-curve, which can be used to calculate the optimal load for the module, and also shows the effect of temperature on the module performance. The acquisition system will be discussed later in more details.
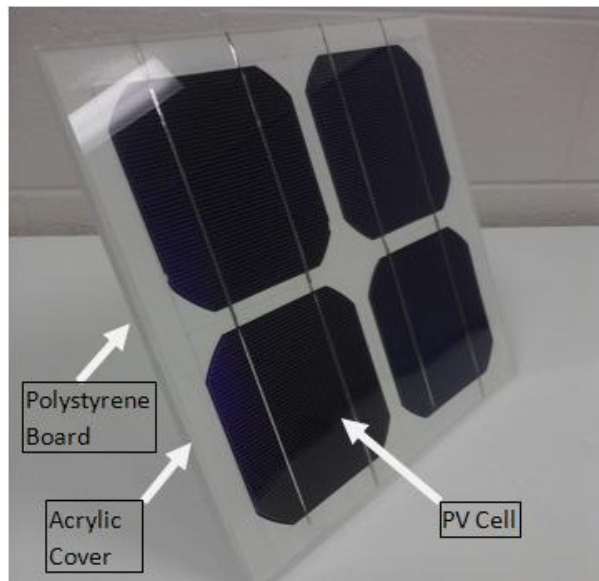
Figure 5.1. Lab-built monocrystalline Si PV module
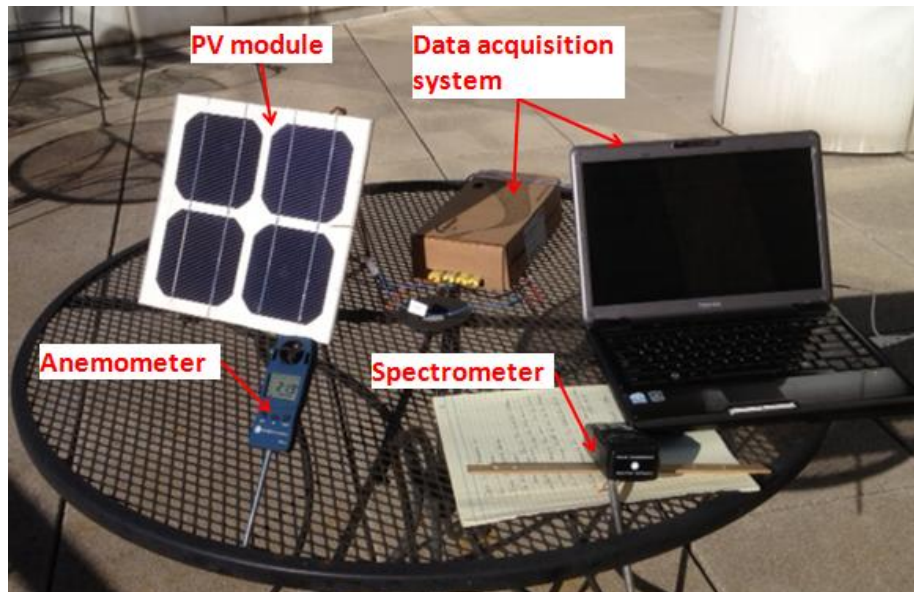
Figure 5.2. Experimental setup

73

5.2.1. Module optical properties

The optical model proposed in Chapter four requires the optical properties of the PV module layers to be defined as functions of wavelength. These properties can be obtained using experiments and optical models. In this section, light reflection and absorption of the module layers stacked into different combinations will be discussed. All symbols used in this section are defined in Table 5.1

Table 5.1. Nomenclature

Symbol	Definition
AR_t	antireflection coat thickness (nm)
$\lambda_\circ$	maximum irradiance wavelength (600 nm)
n_{ar}	refraction index of the AR coat
n_{si}	refraction index of silicon
n_i	refractive index of the layer i. i =1,2,3,..
R_{pp}	p-polarized reflection
R_{sp}	s-polarized reflection
r_{ij}	Amplitude reflectance
R_{av}	average reflection
R	reflection
T_{total}	total transmission
θ	incident angle
H	light power density (W/m^2)

The PV cell is coated with an antireflection (AR) coat. It is assumed that the AR coat is a single-layer thin film. If a light beam is incident on a thin-film coat, some of it will be reflected at the front surface, some will be reflected at the rear surface, and the remainder will be transmitted to the following medium. For thin films, the material absorption and the light scattering can be ignored [97]. Therefore, the light reflection at the interface between the cover and the PV cell depends on the behavior of the AR coat. The AR coat

light transmission depends on light angle of incidence, coat thickness, number of AR layers, and refraction indexes of AR layers and the materials surrounding them.

The optimal thickness of a single AR coat can be calculated using [61]

$$AR_t = \lambda_o/(4n_{ar}) \tag{5.1}$$

where λ_o is the wavelength at which the irradiance is maximum, which is 600 nm, and the AR is assumed to have this thickness. For optimal thickness, the optimal n_{ar} is found for the value of n_{pv} at 600 nm wavelength. Accordingly, the optimal refraction index of the AR coat can be calculated using [61]

$$n_{ar} = \sqrt{n_c n_{pv}} \ . \tag{5.2}$$

To calculate the reflection of AR coat, the angles of refractions into the materials surrounding the coat are required. As shown in Figure 5.3, these angles are θ_1, θ_2, and θ_3. For the case of normal incidence, $\theta_1 = 0$.
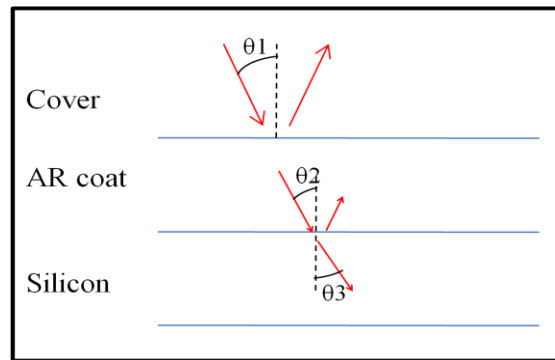
Figure 5.3. Refraction angles through PV cell

In this work, only normal incident is considered to calculate the reflection of the AR coat. However, θ_1 can be any value between $0°$ and $180°$. In this case ($\theta_1 > 0$), the light refraction angles inside the AR coat and the layer below can be calculated using [97]

$$\theta_2 = \arcsin\left(\frac{n_1(\lambda)\sin\theta_1}{n_2(\lambda)}\right) \tag{5.3}$$

and

$$\theta_3 = \arcsin\left(\frac{n_1(\lambda)\sin\theta_1}{n_3(\lambda)}\right). \tag{5.4}$$

The single interface amplitude reflectance for the parallel (P) and the normal (s) polarizations are given as [97]

$$r_{(i)(j)p} = \frac{n_j\cos\theta_1 - n_i\cos\theta_2}{n_j\cos\theta_1 + n_i\cos\theta_2} \tag{5.5}$$

$$r_{(i)(j)p} = \frac{n_{j+1}\cos\theta_2 - n_j\cos\theta_3}{n_{i+1}\cos\theta_2 + n_j\cos\theta_3} \tag{5.6}$$

$$r_{(i)(j)s} = \frac{n_i\cos\theta_1 - n_j\cos\theta_2}{n_i\cos\theta_1 + n_j\cos\theta_2} \tag{5.7}$$

$$r_{(i)(j)s} = \frac{n_j\cos\theta_2 - n_{j+1}\cos\theta_3}{n_j\cos\theta_2 + n_{i+1}\cos\theta_3}. \tag{5.8}$$

The subscripts $r_{(i)(j)s}$ and $r_{(i)(j)p}$ are the amplitude reflectances for the s-polarized and p-polarized light, respectively, at the interface between layers i and j. Layer i is the cover, layer j is the AR coat, and layer $j+1$ is the PV cell.

The reflection of the AR coat considering both interfaces (top and bottom) for both phase differences between the reflected waves are [97]

$$R_{pp} = \frac{r_{(i)(j)p}^2 + r_{(j)(j+1)p}^2 + 2r_{(i)(j)p}r_{(j)(j+1)p}\cos(2\beta)}{1 + r_{(i)(j)p}^2 r_{(j)(j+1)p}^2 + 2r_{(i)(j)p}r_{(j)(j+1)p}\cos(2\beta)} \tag{5.9}$$

$$R_{sp} = \frac{r_{(i)(j)s}^2 + r_{(j)(j+1)s}^2 + 2r_{(i)(j)s}r_{(j)(j+1)s}\cos(2\beta)}{1 + r_{(i)(j)s}^2 r_{(j)(j+1)s}^2 + 2r_{(i)(j)s}r_{(j)(j+1)s}\cos(2\beta)} \qquad (5.10)$$

The variable β is the phase difference in the external medium between waves reflected from the first and second surfaces of the AR coat. It is given as [97]

$$\beta = \frac{2\pi}{\lambda} n_2(\lambda)\, h \cos\theta_2 \; . \qquad (5.11)$$

Accordingly, the average reflection is [97]

$$R_{av} = \frac{R_{pp} + R_{sp}}{2} \; . \qquad (5.12)$$

To calculate the reflection of the AR coat, the refraction indexes of the surrounding mediums are required. The PV modules are usually covered with special low iron glass that has a refraction index equals 1.5 [92]. The refraction index of acrylic is nearly constant over the desired wavelength range (300–1100 nm) and equals to 1.49 [98]. It can be observed that the refraction indexes are almost similar for both covers. The refraction index of silicon is function of wavelength as shown in Figure 5.4 [96]. At the optimal wavelength (600 nm), the optimal refraction index and optimal thickness of the AR coat using the refraction index of the glass are found equal 2.4226 and 61.917 nm, respectively. Assuming optimal thickness, for normal incident light, the reflection of the AR coat is shown in Figure 5.5 as function of wavelength.

The reflection of the cover layer should also be obtained as function of wavelength. The refraction index of acrylic is almost constant over the desired wavelength range due to nearly constant light transmission over this range which is experimentally measured as shown in Figure 5.6. The data shown in Figure 5.6 represent the overall light transmission of the sheet. However, the surface reflection is not the complement of the total transmission. This is due to the internal reflections that occur between top and bottom surfaces of the acrylic sheet.
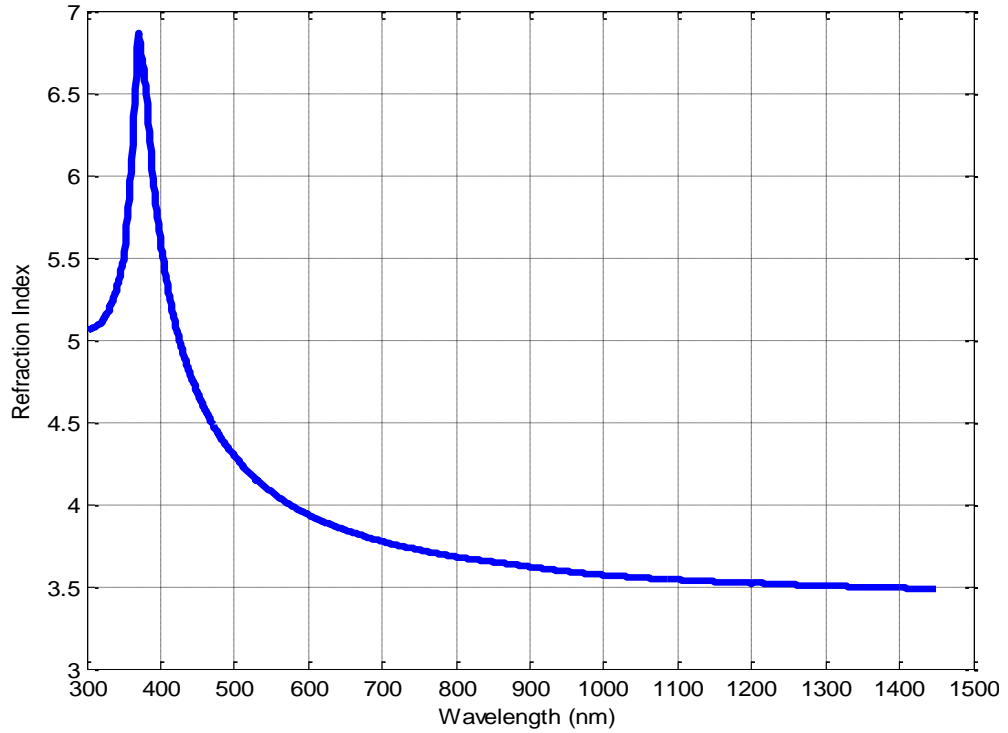
Figure 5.4. Refraction index of silicon
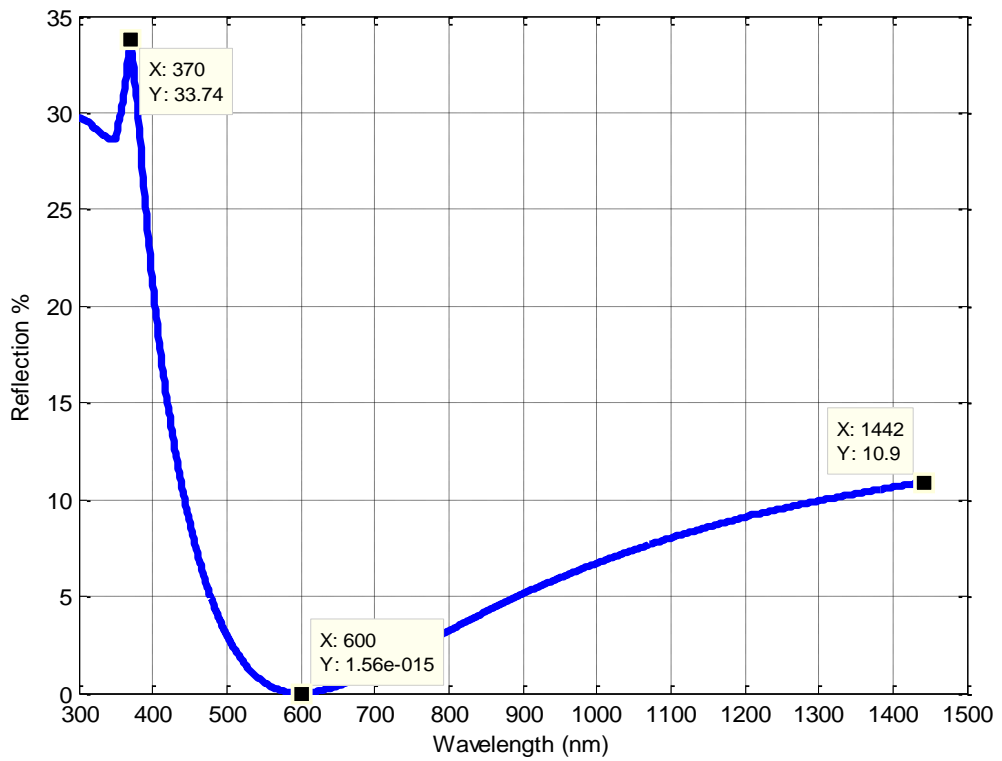
Figure 5.5. Reflection of AR coat between silicon and acrylic/glass
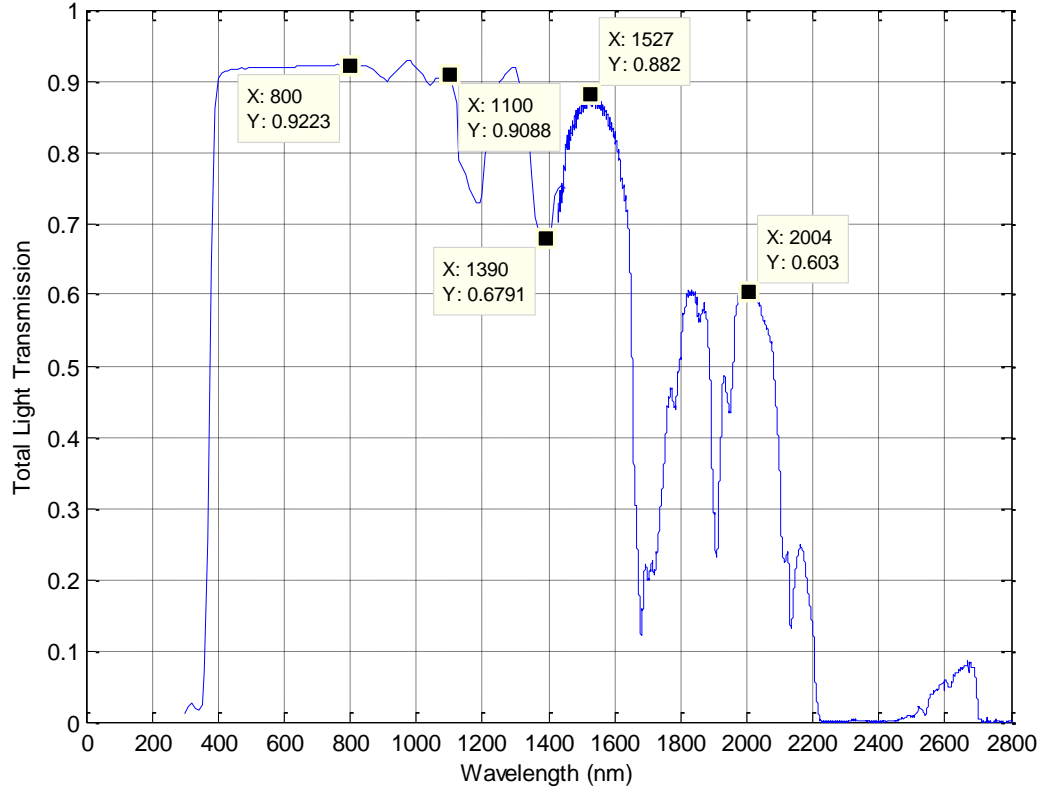
Figure 5.6. Total light transmission of 3.2-mm thick acrylic sheet

The same optical model that is proposed in Chapter 4 can be used to obtain the acrylic surface reflection. Assuming that both surfaces of the acrylic sheet have the same reflection, it is found that the total light transmission can mathematically be represented as

$$T_{total} = (1 - R)^2 \sum_{i=0}^{\infty} R^{2i} \qquad (5.13)$$

The geometric series given in Equation (5.13) can be expressed as

$$T_{total} = \frac{1 - R}{1 + R} \qquad (5.14)$$

Accordingly, the surface reflection of the acrylic sheet is

$$R = \frac{1 - T_{total}}{1 + T_{total}}. \tag{5.15}$$

The same concept can be followed to obtain the light reflection of the glass cover. In this research, a 3.2-mm thick low-iron glass that is commercially known as Solarphire [99] is used. The light transmission of this glass is shown in Figure 5.7.
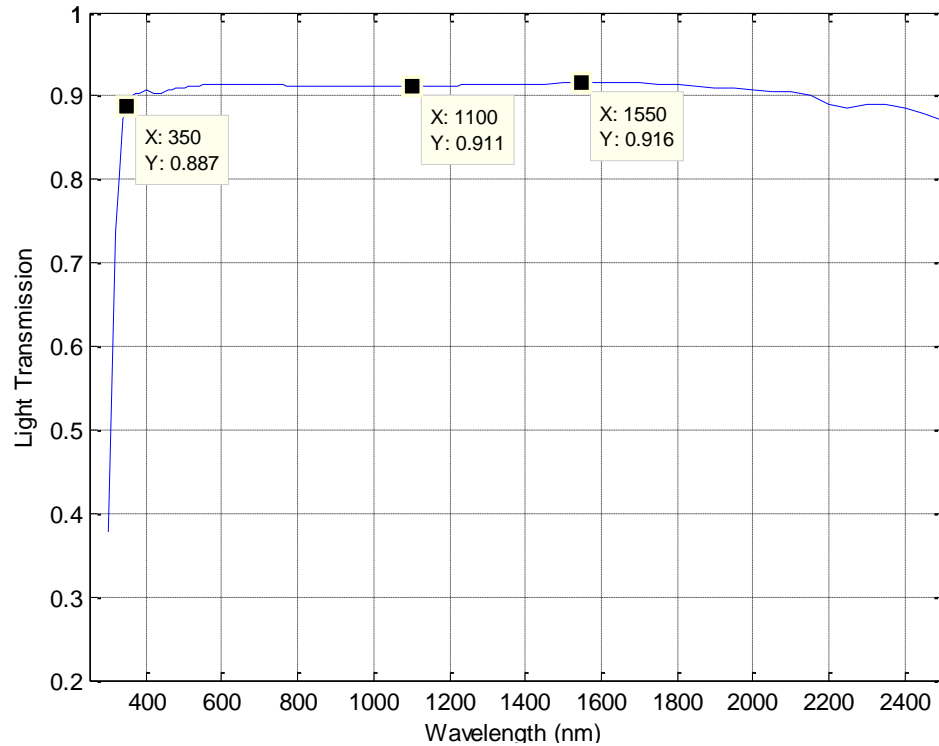
Figure 5.7. Total light transmission of 3.2-mm thick Solarphire PV glass

The polystyrene board is tested to find its light transmission, reflection and absorption when it is covered only with acrylic. It is assumed that the cover does not absorb light, therefore, it either transmit or reflect light. A solar simulator is constructed to generate 1 sun (1000 W/m^2) of light to serve the goals of this research as shown in Figure 5.8. The irradiance is distributed over 14 in by 14 in area with accuracy of $\pm$50 W/m^2. According to Guvench *et al.* [100], the combination of metal-halide and quartz halogen light sources generates an artificial light that has a spectrum close to the standard solar spectrum. A spectrometer is fixed in a spot that does not block any light.

The testing procedure is performed as follows. First, a Lambertian-surface black board is placed at the floor of the simulator assuming that no light will be reflected back from it. The light noise from surroundings is measured. Second, the acrylic-covered polystyrene board is positioned at a specific distance from the light source where 1000 W/m^2 is approximately received. Third, the light reflected from this assembly is measured. This measurement includes the noise from surroundings which is already measured, so it should be subtracted. Fourth, the spectrometer is attached to the back side of the assembly at a point that is perfectly aligned with the point at which the reflected light is measured. This setup measures the transmitted light. It is found that the assembly of the board covered with acrylic transmits about 4.1%, reflects about 29.3%, and absorbs 66.6% of light which converts into heat. It is assumed that these numbers are close to the case of using glass cover due to the similarity of light transmissions in the desired wavelength range.
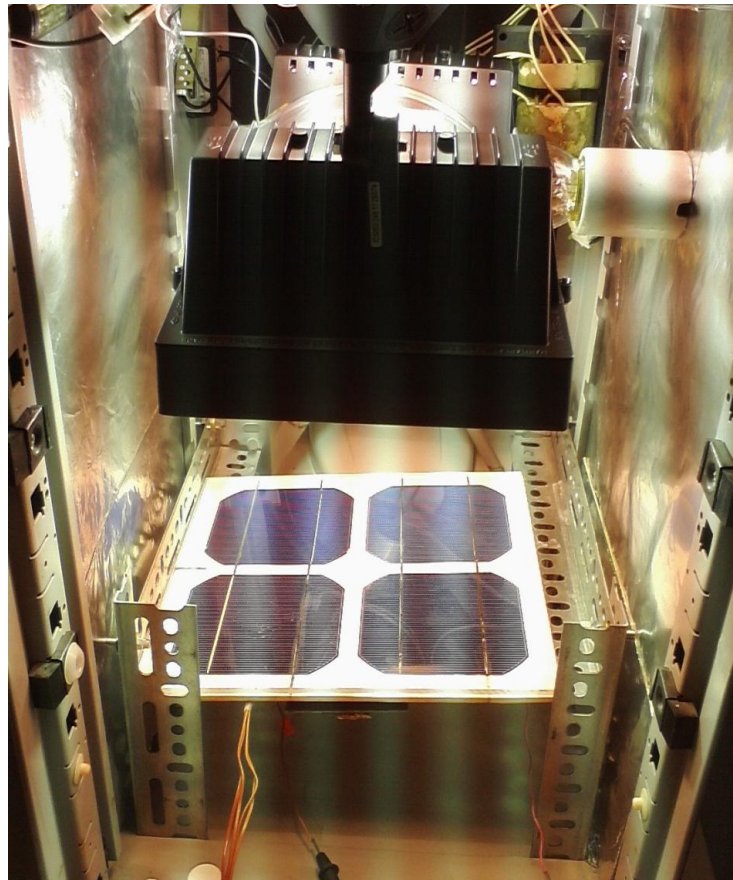
Figure 5.8. Large area solar simulator

The same experimental setup is used to measure the light absorption of the polystyrene that is covered by the PV cell. It is found that the PV cell does not pass light through. This implies that it is fabricated to reflect all light that hits its bottom in order to increase its efficiency by increasing the light path.

Using the proposed experimental and predicted data, the overall light absorption coefficients of the different layer combinations can now be found as given below using the methodology discussed in Chapter four.

5.2.2. Input power

The input power term requires the absorption coefficients $\alpha_{s1}(\lambda)$ and $\alpha_{s2}(\lambda)$. These parameters can be obtained using the proposed optical methodology. The overall absorption coefficient of the silicon PV cell that is sandwiched between acrylic cover and polystyrene board is shown in Figure 5.9. The overall absorption coefficient of the polystyrene insulation board covered with acrylic is shown in Figure 5.10. In the case of glass cover, the absorption coefficients $\alpha_{s1}(\lambda)$ and $\alpha_{s2}(\lambda)$ are shown in Figures 5.11 and 5.12 respectively. The value of $\alpha_{s1}(\lambda)$ and $\alpha_{s2}(\lambda)$.per each wavelength represents the fraction of photons propagate with this wavelength that will be absorbed in that stack of layers. Since it is assumed that the covers do not absorb light, and the PV cell is assumed to have a reflection coat at its back surface; all the light that hits the three layers stack will be absorbed in the PV cell by a fraction that is specified by $\alpha_{s1}(\lambda)$. In case of the stack where the PV cell layer does not present, the fraction defined by $\alpha_{s2}(\lambda)$ represents the light absorbed by the polystyrene board.

5.2.3. Output power

The terminologies used herein to distinguish between the PV modules built to serve the goals of this research are module 1 (M1) which is usually covered with glass and module 2 (M2) which is usually covered with acrylic. Both covers can be switched between the modules. The output power model requires four unknown quantities that are properties of the PV module under test. These quantities are photonic current I_{ph}, reverse saturation

current I_0, series resistance R_s, and quality factor n. As presented in [101], I_0 can be calculated from the reference saturation current I_{0r} that can be calculated at reference conditions. At the reference conditions, both currents are identical. The least square error method is used to find the optimal values of the unknown quantities.

At least four data points should be used to solve the nonlinear output current equation for the unknown quantities. To obtain these points, the PV modules are loaded with two different resistive loads (0.35-Ω, and 1.08-Ω). Each of PV modules is exposed to sun light (1065 W/m^2, at 3:30 pm on 04/06/2012, Lexington, Kentucky) until its temperature reached the steady state (343 K).
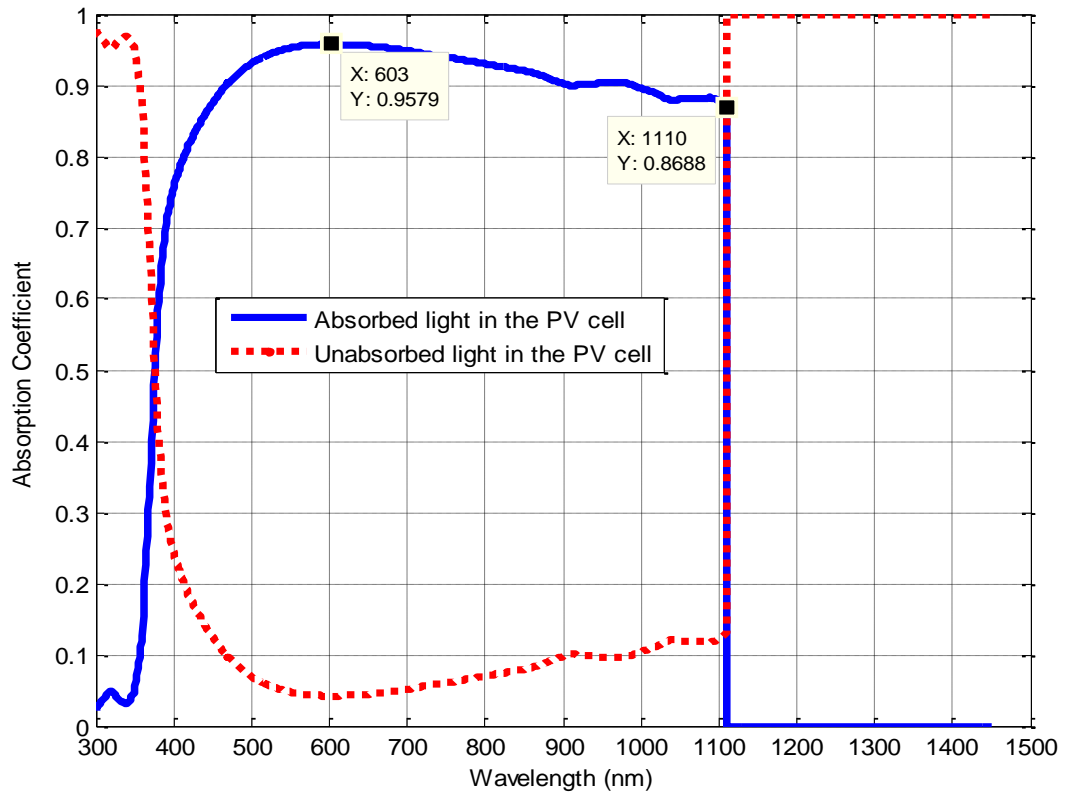
Figure 5.9. Absorption coefficient of acrylic-covered Si PV cell
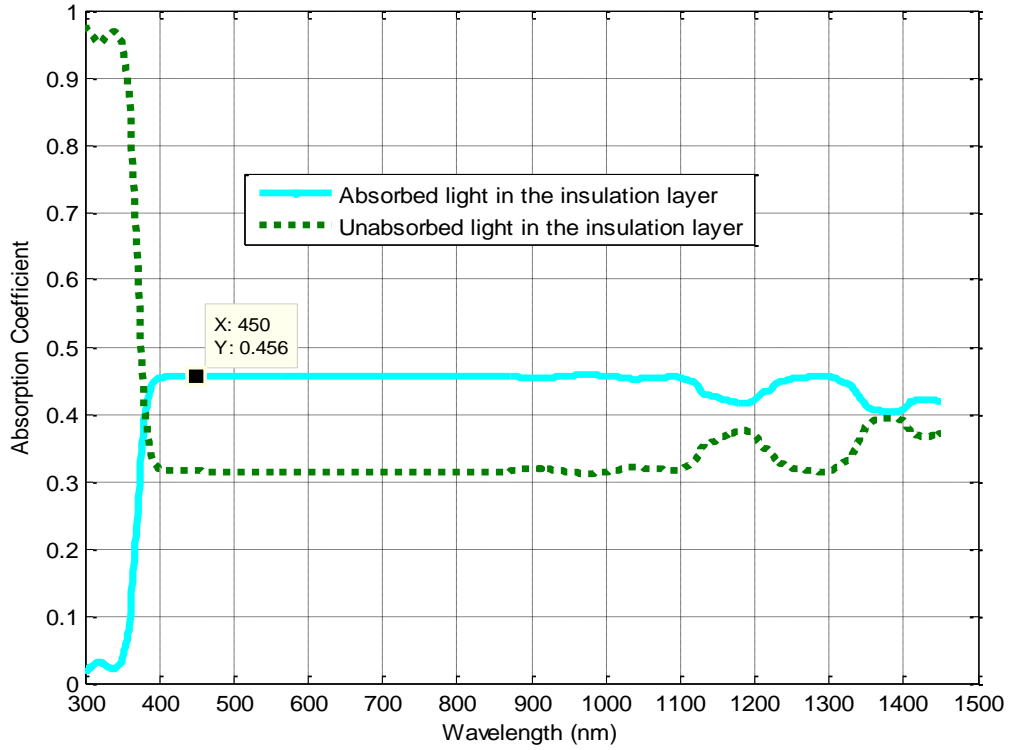
Figure 5.10. Absorption coefficient of acrylic-covered polystyrene material
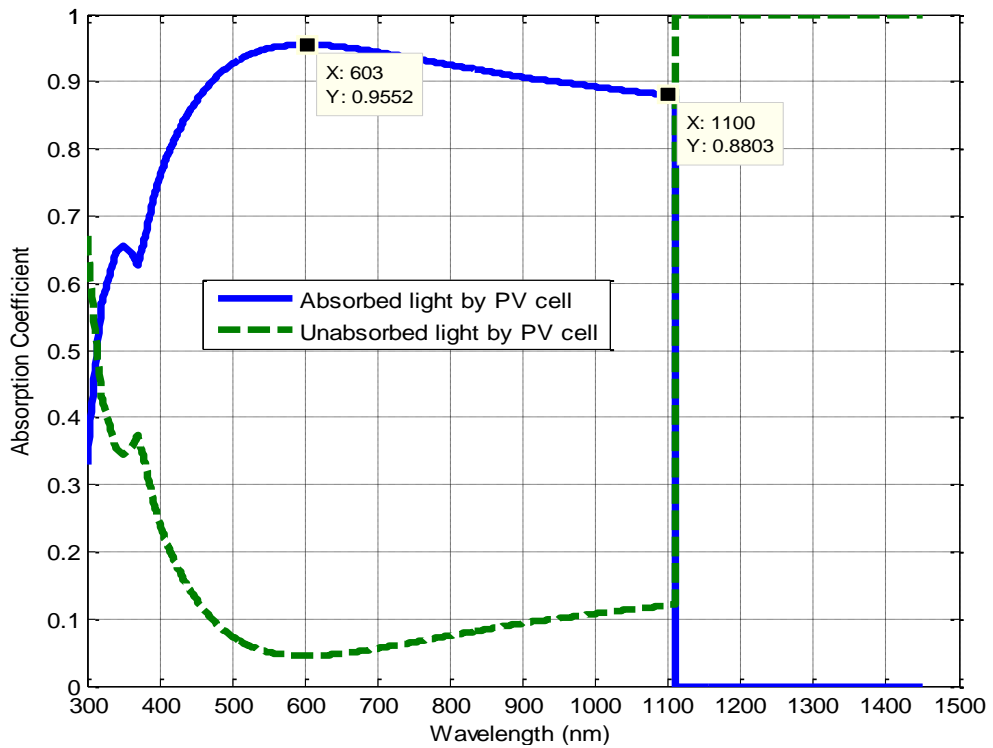
Figure 5.11. Absorption coefficient of glass-covered Si PV cell

84
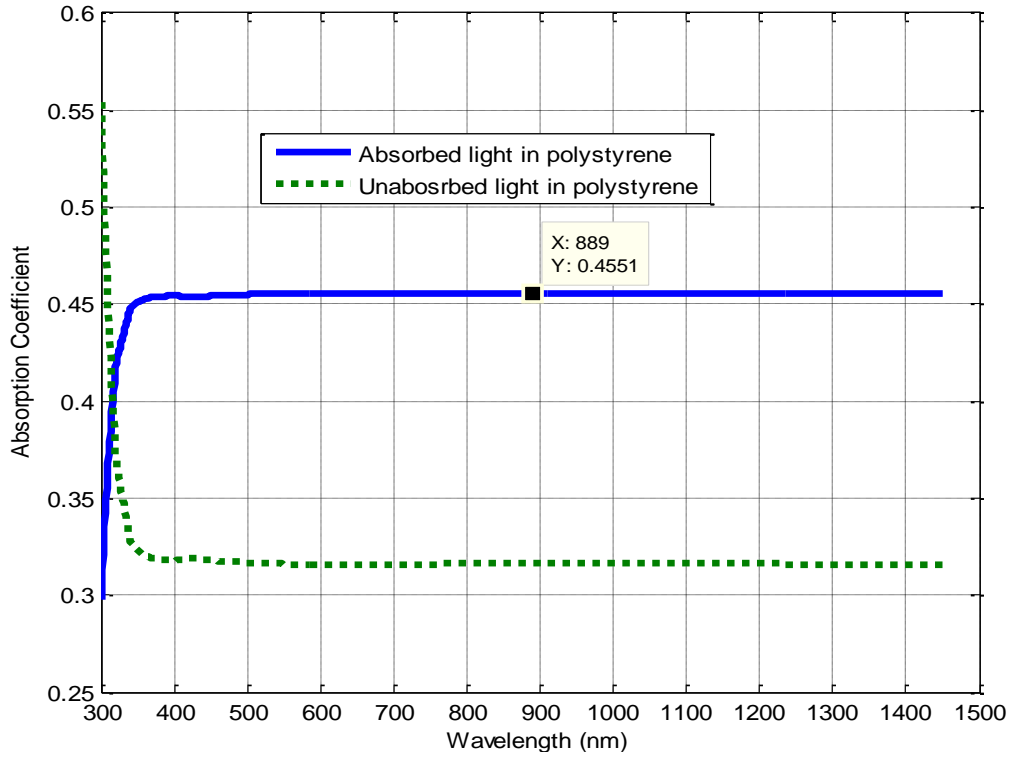
Figure 5.12. Absorption coefficient of glass-covered polystyrene material

The open-circuit voltage and short-circuit current of the modules are measured. The current and voltage are also measured individually for each load at the same temperature (343 K). The data points are collected for both modules in two cases, loaded and unloaded, and are given in Table 5.2. Matlab optimization algorithms and the least square error method are used to find the optimal values of these parameters. The optimal values of the unknown quantities that satisfy the data points are found and given in Table 5.2.

The internal quantum efficiency (IQE) is function of wavelength [92]. In this work, the IQE is presented as an averaged constant value [63], [66]. The IQE value can be tuned until the calculated I_{ph} match the optimal I_{ph} that is based on the experimental measurements. It is found that IQE of the glass-covered M1 is 0.74 and IQE of the acrylic-covered M2 is 0.69.

The photon flux $\phi_{rr}(\lambda)$ should be obtained for the location, date, and time of the experiment. The spectral irradiance proposed in [102] is adopted as the reference

spectrum for this work. The spectral irradiance values are obtained using SMARTS 2.9.5 [103] for 04/06/2012 as shown in Figure 5.13. Obtaining the spectral irradiance will be discussed later in more details. The solar light power density H is measured in location, where the spectrometer used for measurements is of $\pm5\%$ accuracy. The tilt angle is selected in order to get normal incident light with H is 1060 to 1070 W/m2. Accordingly, the tilt angle $\beta_{surface}$ lies in the range 60°–70°. It is found that H calculated using SAMRTS for 04/06/2012 is 1053 W/m^2, which is close to the spectrometer measurements.

Table 5.2. Experimental data and calculated unknown quantities of M1 and M2

Parameter	Glass-covered module 1	Acrylic-covered module 2
I_{sc} (A)	4.28	4.62
V_{oc} (V)	2.084	2.069
Load 1 (I, V)	3.51, 1.275	3.3, 1.198
Load 2 (I, V)	1.63, 1.76	1.58, 1.712
I_{ph} (A)	4.2806	4.6209
I_{0r} (A)	120.5×10^{-7}	7.2403×10^{-7}
R_s (Ω)	0.0377	0.0505
n	1.38	1.12
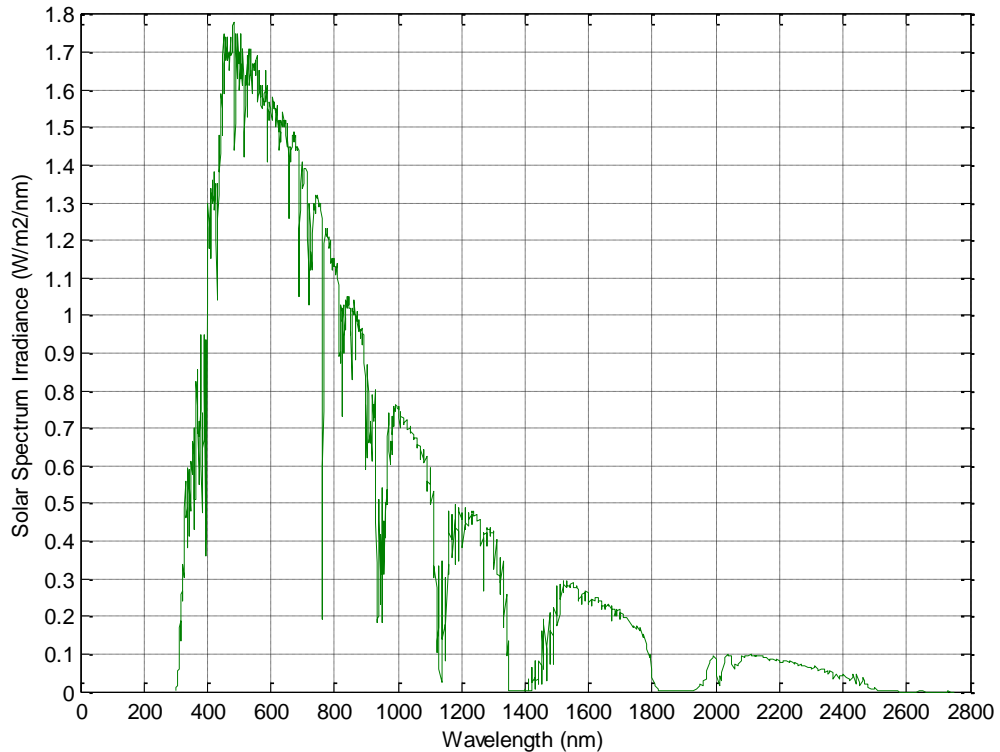
Figure 5.13. Global solar irradiance, 3:30 pm, 04/06/2012, Lexington, KY

As a result, the characteristic curves of the PV modules M2 and M1 are obtained based on the optimally derived quantities are shown in Figure 5.14 and Figure 5.15 respectively. This curve represents the data operating points of the module for any load. The current and voltage of loads 1 and 3 are used to derive the module parameters of M2 as given in Table 5.2. As shown, these data points lie on the IV-curve. In addition, to validate this curve, M2 is loaded with a 0.55-Ω resistive load. The voltage and current measured across this load at the same temperature and insulation conditions are 1.5 V and 2.72 A respectively. This loading operating point is close to the predicted loading point marked as Load 2 (2.75 A, 1.5 V) as shown in Figure 5.14. The load-current error is 1.1%. The IV curve of M1 is also validated by loading the module with 1.08-Ω. The experimentally measured current and voltage of this load at the same temperature and isolation conditions used for M2 are 1.58 A and 1.712 V. As shown in Figure 5.15, this data point is close to the loading point marked as Load 3 (1.508 A, 1.712 V) with an error in the load-current equals 4.56%.
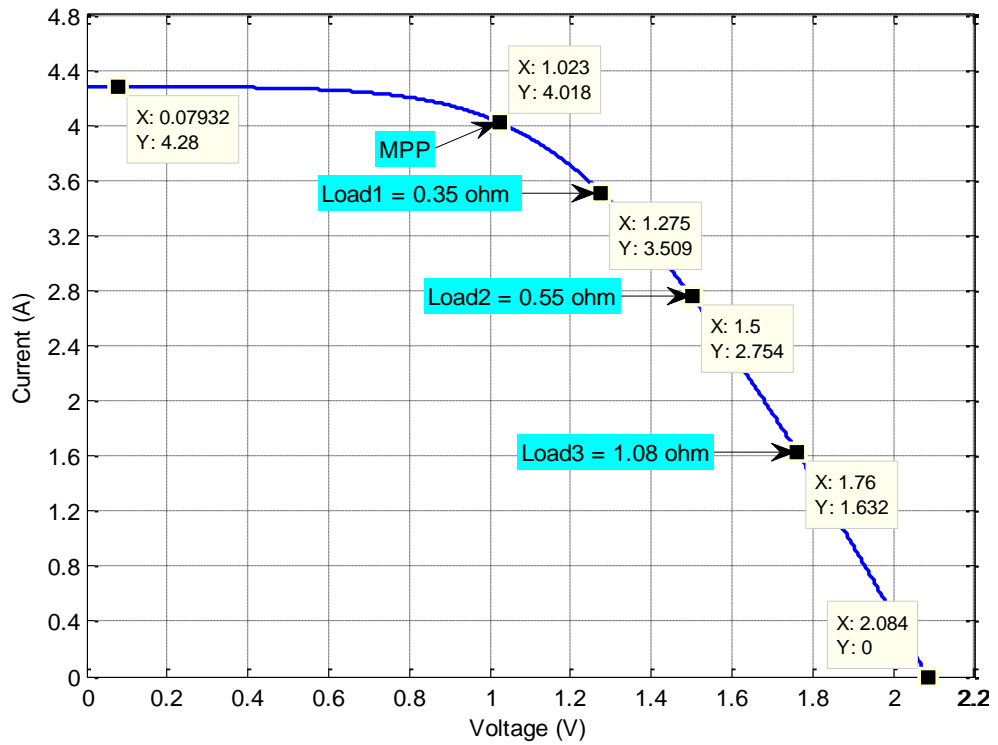
Figure 5.14. Numerically optimized IV-curve of the PV module M2.
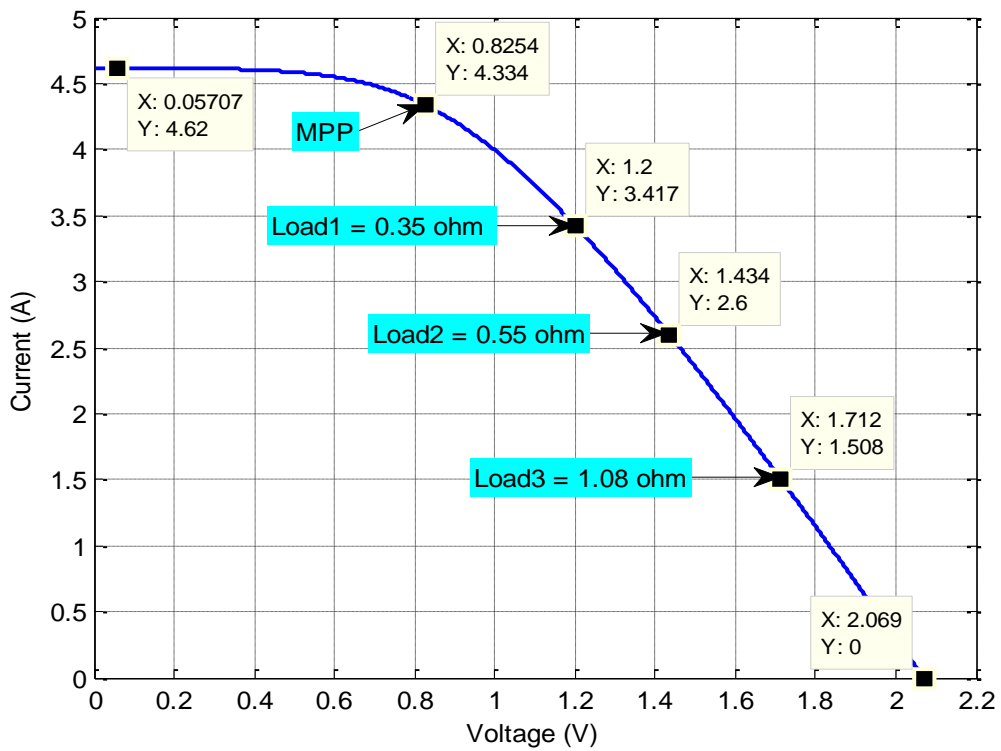
Figure 5.15. Numerically optimized IV-curve of the PV module M1.

Several sources can cause the error between the calculated and the measured data points. Some of these sources are: tolerance in the resistive load values, changes of resistive loads when they heat up, the uncounted wiring resistive loads, and the minor changes of solar isolation due to time changes when the experiments are conducted.

5.2.4. Forced heat transfer

The coefficient of forced heat transfer $h_{c,forced}$ depends on the wind speed. For outdoor experiments, as mentioned in Chapter four, Armestrong *et al.* [59] discussed three formulas (Test, Sturrock, and Sharples) that could be used to calculate $h_{c,forced}$ as function of wind speed. In this research, the PV module is tilted, and the wind speed is measured at a location beside the module (windward), Sharples-windward empirical formula given as

$$h_{c,forced} = 3.3 \left(\frac{J}{m^3 K} \right) WS + 6.5 \left(\frac{W}{m^2 K} \right) \tag{5.16}$$

is expected to predict accurate values for $h_{c,forced}$.

The temperatures of the loaded and unloaded module using the three formulas are shown in Figures 5.16 and 5.17 respectively. It can be observed that both Sharples and Test methods predict $h_{c,forced}$ such that the predicted module temperature is very close to the experimental measurement. However, Sharples is selected in this work because it provides more accurate predictions in the case of the unloaded module as shown in Figure 5.17. In addition, it corresponds with the physical arrangement of the module under consideration.
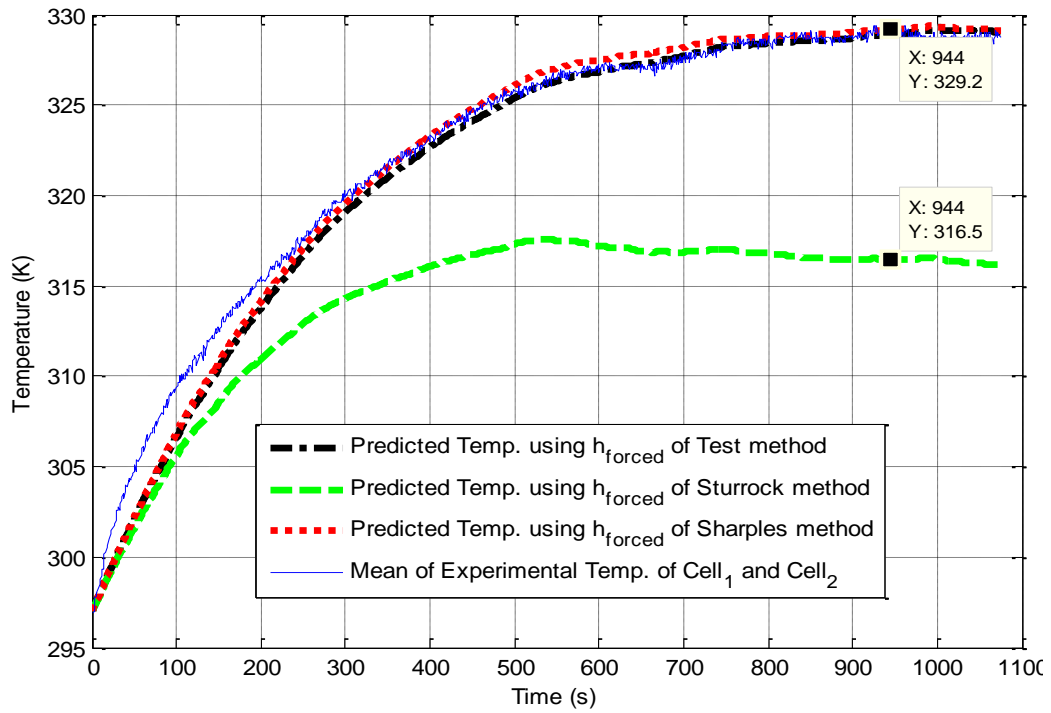
Figure 5.16. Various formulas of $h_{c,forced}$, loaded module under live one sun solar irradiance.
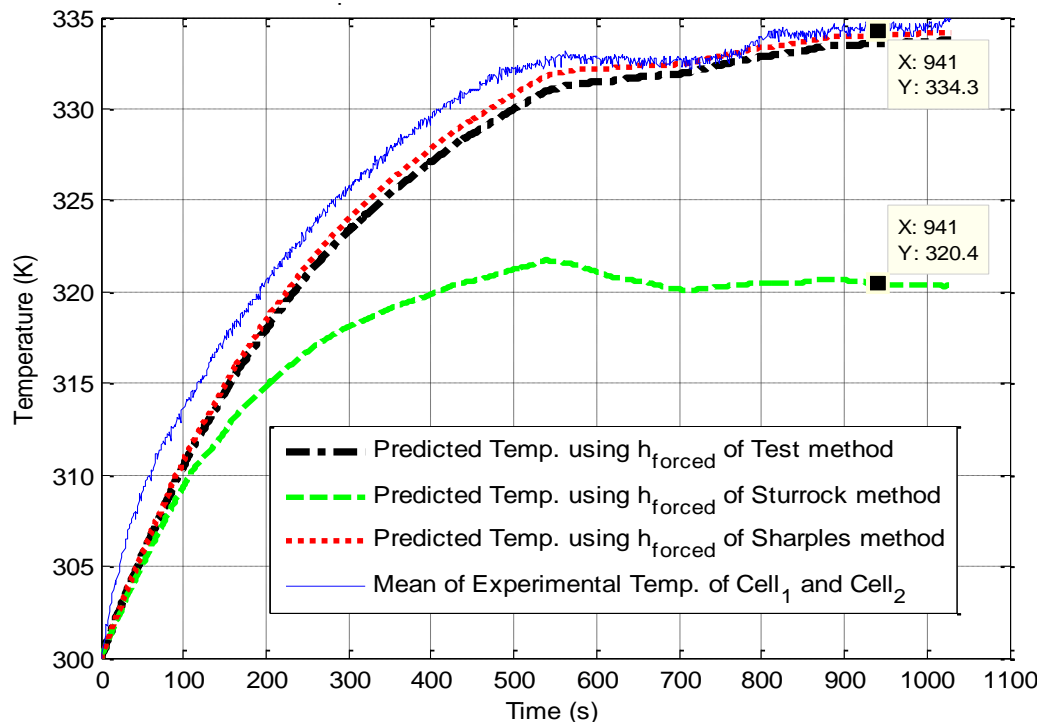
Figure 5.17. Various formulas of $h_{c,forced}$, unloaded module under live one sun solar irradiance.

90

5.3. Spectral irradiance

Solar irradiance is vital to validate the developed thermoelectrical model. As discussed in Chapter four, the main input energy to the PV module is the solar irradiance. Measuring or predicting the solar irradiance as function of wavelengths for a specific date, time, and location is important for characterizing and validating the model. There are two standards of solar spectrum defined for terrestrial use specified as ASTM G-173-3 in 1992 with an extra terrestrial solar constant that equals 1366.1 W/m^2. First is the AM1.5 Global spectrum which is designed for flat plate modules and has an integrated power of 1000 W/m^2. Second is the AM1.5 Direct (plus circumsolar) spectrum that is defined for solar concentrator work. It includes the direct beam from the sun plus the circumsolar component in disk 2.5 degrees around the sun. The direct plus circumsolar spectrum has an integrated power density of 900 W/m^2 [104]. However, a newer spectral irradiance was proposed by Gueymard in 2004 [105], which is reported as more accurate than the ASTM G-173-3 with equal extra terrestrial solar constant value. This new solar spectrum is adopted in this research.

The location of all experiments conducted in this research is Lexington, Kentucky, USA. This location has the coordinates of 34N latitude and 84W longitude, height of 305 m above sea level, and -5 hours time difference zone [106].

The spectral irradiance of this location is obtained using SMARTS 2.9.5 (Simple Model of Atmospheric Radiative Transfer of Sunshine) software developed by Gueymard at NREL (National Renewable Energy Laboratory) [107], [108]. SMARTS computes the clear sky spectral irradiances (including direct beam, circumsolar, hemispherical diffuse, and total on a tilted or horizontal receiver plane) for the specified location and the desired atmospheric conditions. The earlier version SMARTS 2.9.2 was the basis for American Society of Testing and Materials (ASTM) reference spectra (ASTM G-173 and ASTM G-177) used for photovoltaic performance testing and materials degradation studies. Using SMARTS, the global spectral irradiance for the location mentioned above is obtained for different dates and times at which experiments are conducted. For example, the spectral

irradiance on 06/15/2010, from sunrise at 5:30 am to sunset at 20:00 pm is obtained every half an hour. The spectral irradiance is obtained for the wavelengths range of 280 to 4000 nm with 0.5 nm step for 280–400 nm, 1 nm step for 400–1700 nm, and 5 nm step 1700–4000 nm. A 3-dimentional plot is created for the obtained spectral irradiances for the wavelength range 300–2700 nm versus time as shown in Figure 5.18. Out of this data, a window of wavelengths that depends on the semiconductor material is used in the simulation for input and output powers calculations. For silicon, this window is 300 nm to 1100 nm.
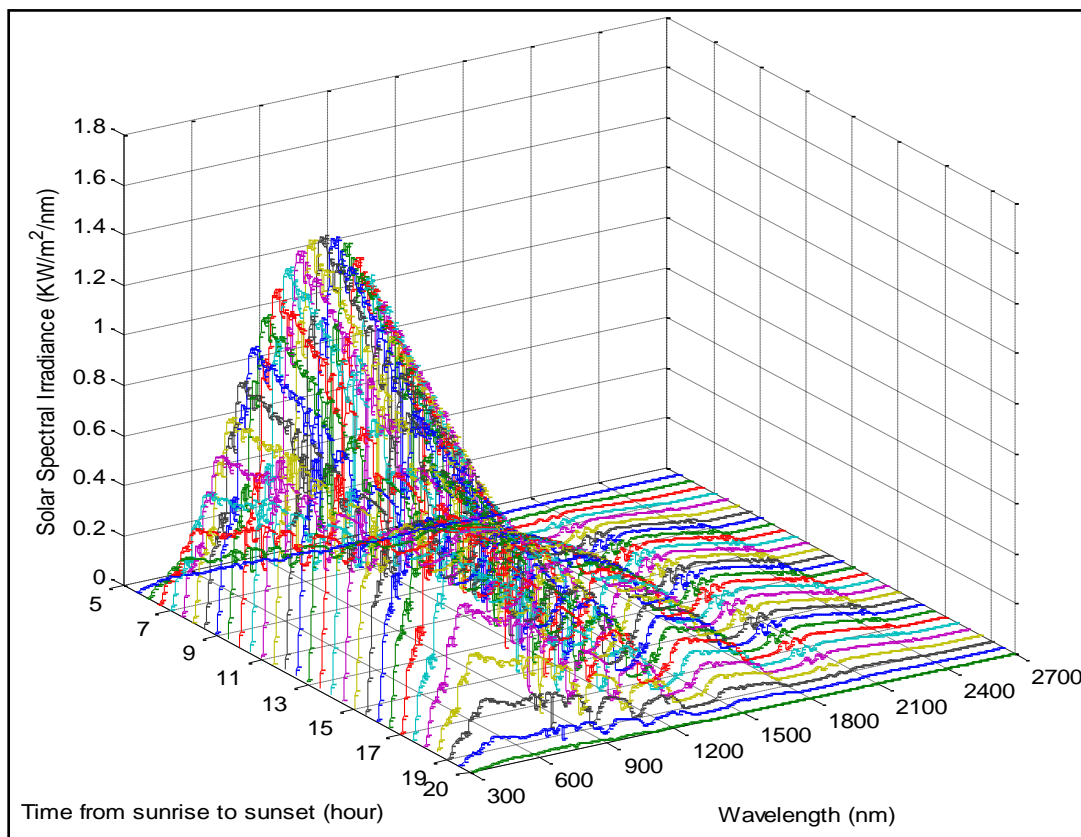
Figure 5.18. Solar spectral irradiance, Lexington, KY, on 06/15/2010

5.4. IV-curve tracer and data temperature acquisition system

As mentioned above, the temperature measurements and the IV curves are collected using the data acquisition system (DAS) shown in Figure 5.2. The hardware part of this

simple system consists of 4 thermocouple amplifier digital chips (MAX6675), a transistor, operational amplifier, current-sensor resistor (CSR), and microcontroller kit as shown in Figure 5.19. The electrical circuit layout of this system is shown in Figure 5.20.
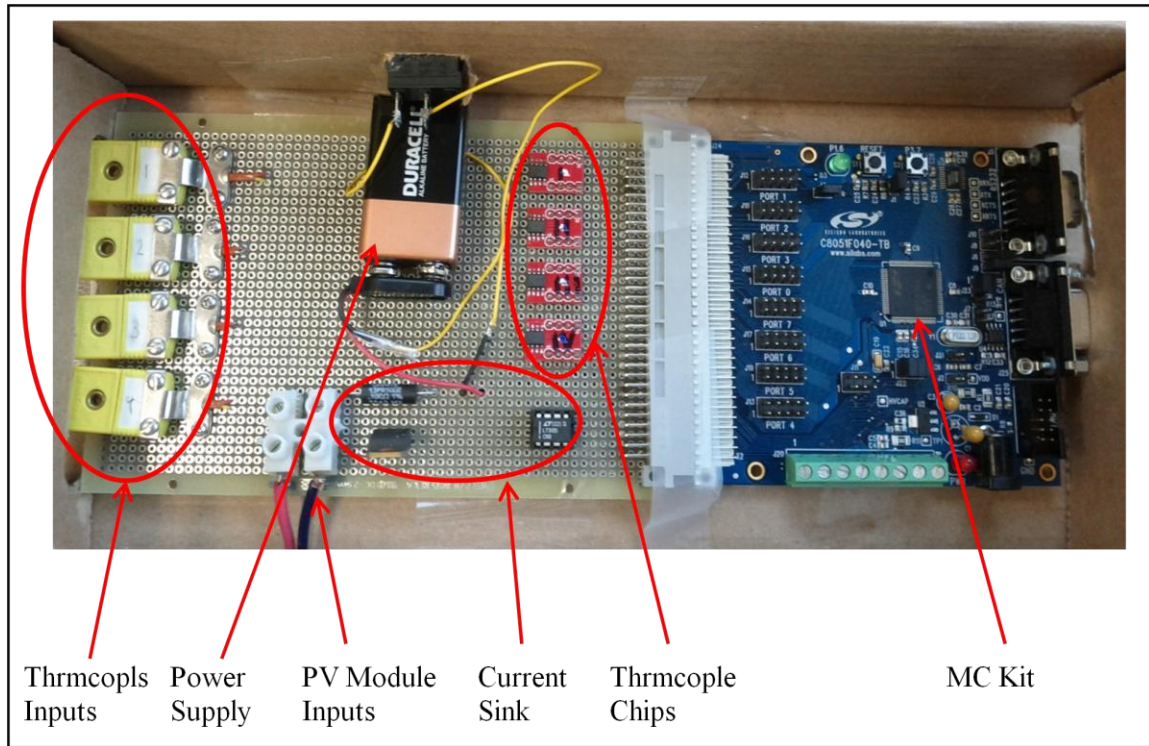
Figure 5.19. Actual data acquisition system

The temperatures are simply read by the microcontroller (MC) through the digital inputs where the thermocouple chip converts the analog voltage signal sent by the K-type thermocouples into digital. The digital signal will be read by the MC which processes this signal and converts it into temperature measurements.

The IV-curve tracer part of the DAS uses the current sink principle, where the analog signal generated by the MC is applied to the operational amplifier. The operational amplifier and the MOSFET connected to each other as shown in Figure 5.20 create current sink. The current sink works as a gate that passes no current when no signal is applied to the op-amp. Once the op-amp receives a signal from the MC, then it passes the generated current gradually through the MOSFET until it becomes fully opened gate. The

93

current passes through the current-sensor resistor creates a voltage drop across it. The voltage drop is measured by the analog input of the MC and the current is internally calculated using Ohm's low and the value of the CSR. The voltage across the PV module is measured using the analog input. Both, the calculated current and the measured voltage represent the characteristics of the module to create its IV-curve. There always be a voltage drop across the CSR, therefore, the voltage won't reach zero once the module is considered in short circuit condition. The value of this drop depends on the rated short-circuit current of the PV module and the value of the CSR. However, the current usually reaches its steady state value which is the short-circuit current at voltage value that is close to zero. This can be overcome by using smaller CSR that is able to hold large current values.
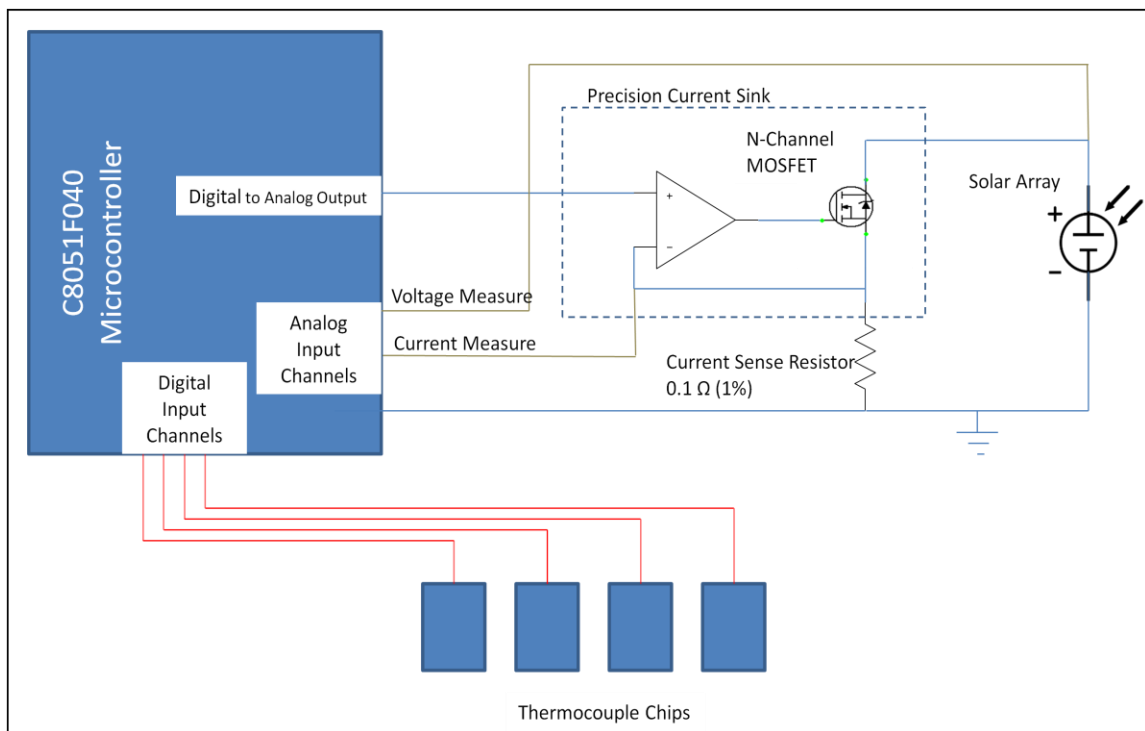
Figure 5.20. Electrical circuit layout of the data acquisition system

The IV curves of the PV Modules M1 and M2 are generated by the IV-curve tracer and compared against the numerical IV-curves as shown in Figures 5.21 and 5.22 respectively. As shown, the IV-curve tracer overestimates the current values that are

numerically obtained. The IV-curve tracer is calibrated to accurately measure the short-circuit current and the open-circuit voltage. However, the calibration is not linear to enhance the tracer capabilities of measuring the remainder of the operating points on the curve. This behavior might be caused by the fast sweeping process of the current sink which is faster than the voltage changes across the module which may lead to the error shown in the plots. This error might be reduced by slowing down the current sink through using higher time delays between the ADC and DAC. The code of the MC is modified such that the user is able to modify these values as desired.
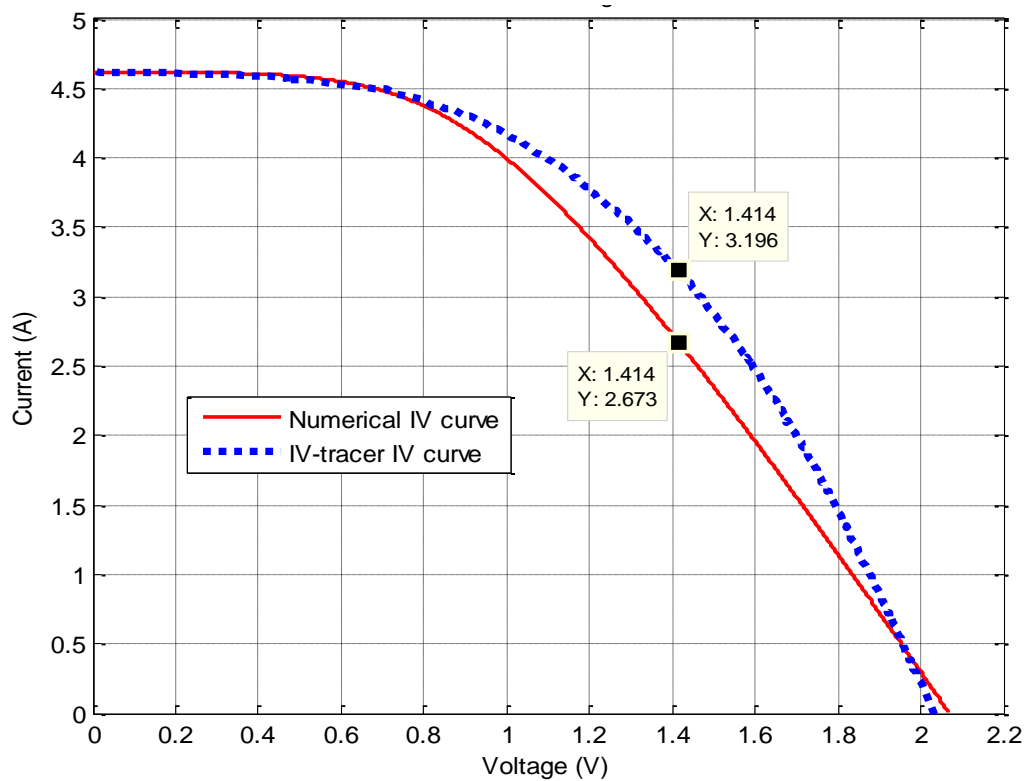
Figure 5.21. Numerical versus tracer IV curves of M1

The main menu of the DAS contains a list of options that appear when connecting it to the PC through RS323 cable. One of these options is the maintenance tools as shown in Figure 5.23. Special terminal software is required to communicate with the MC kit. In this research Termite 2.8 is used. The DAS can be developed also to be able to calculate

the series and shunt resistors from the curves. The cost of the hardware components of this system is less than $300 including the MC kit.
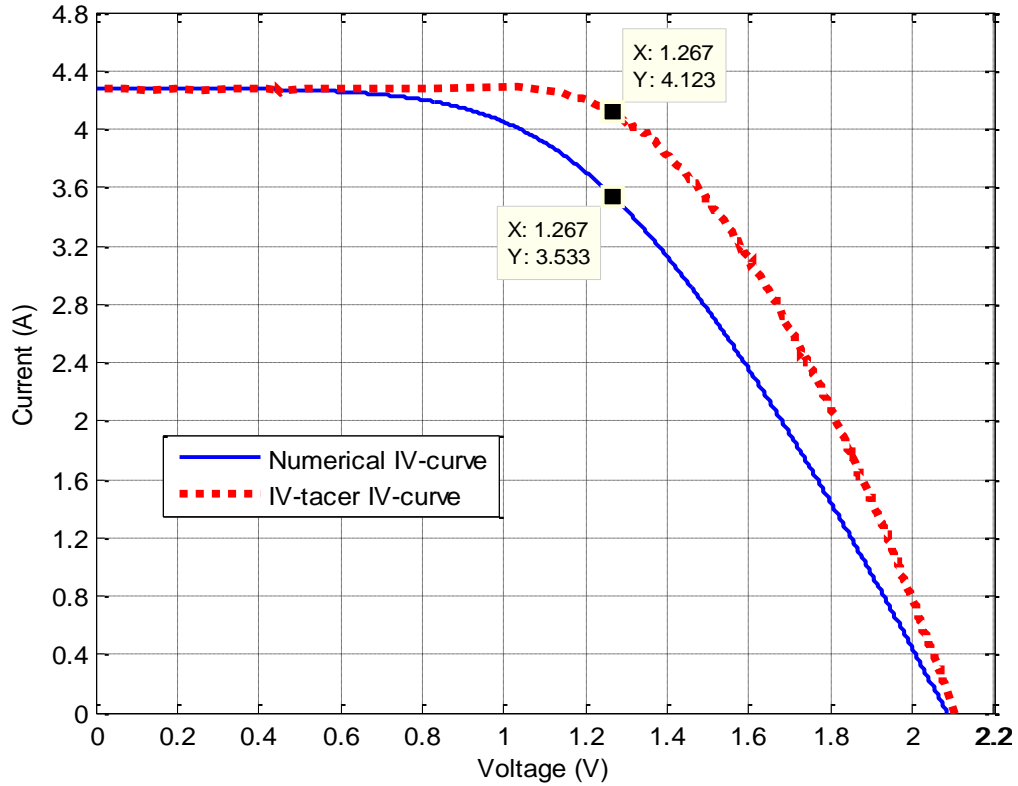
Figure 5.22. Numerical versus tracer IV curves of M2
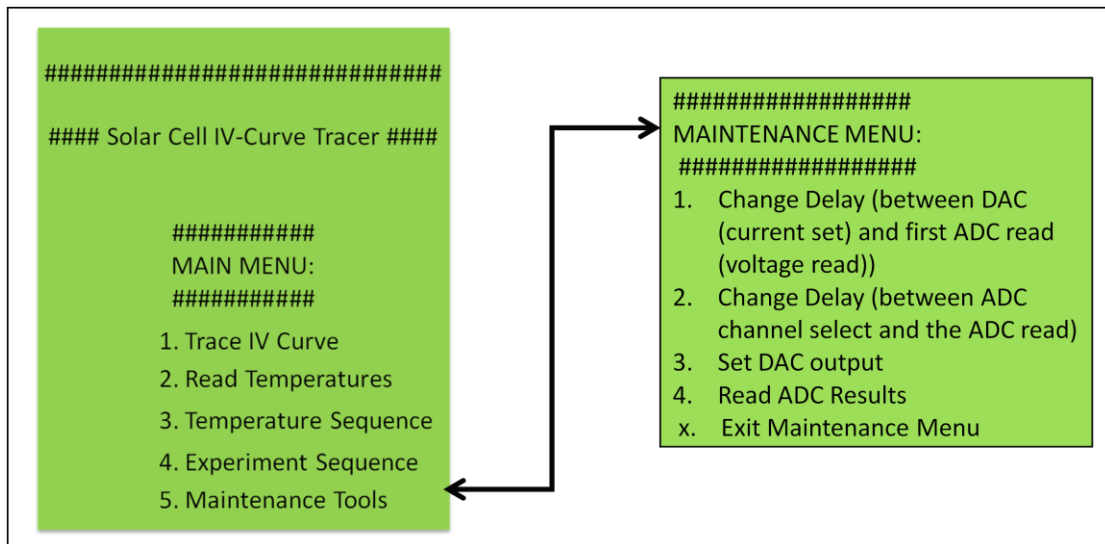
Figure 5.23. Data acquisition system communication menus

5.5. Model validation

The model is validated using the experimental setup that is shown in Figure 5.2. The ambient temperature and the wind speeds are measured at the same location. The model is validated using the data collected for the PV module M2 that is covered with acrylic. The data used to validate the model are date, time, tilt angle, and meteorological data. The meteorological data are: ambient temperature, wind speed, and solar spectrum. The ambient temperature and wind speeds are measured at the location where the experiments are conducted. These data are collected on 02/02/2012 at Lexington, Kentucky, USA. The experimental data that are used to validate the model are different from the data used to characterize it. This would indicate the robustness of the characterized model.

The temperature of the module is measured at three different locations. Two thermocouples (1 and 2) are attached to the back of two different cells. A third thermocouple is attached to the top of the insulation board in the space between the cells, as shown in Figure 5.24. The assumption of temperature homogeneity throughout these layers is justified using the experimental measurements shown in Figure 5.25. It can be observed that the temperature measurements of the PV cells are very close to the temperature measurements at the interface between the cover and the insulation board. The measurements are most similar in the steady-state. Transient dissimilarities can be attributed to the difference in the heat capacity and heat conductivity of these layers. Nonetheless, the heat transfer between the layers becomes greater with larger temperature difference, correcting the deviations that arise. The heat capacity of the module is calculated using the data given in Table 5.3. The experimentally measured electrical characteristics of the PV module are given in Table 5.4.

The model is validated for temperature and output power predictions. These validations are obtained by measuring the temperature of the module, the load-current, and the load-voltage. The model predictions of temperature are validated for transient and steady-state responses. To do this, the PV module is suddenly exposed to 1060 W/m^2 of live sunlight measured at its location. The ambient temperature and the wind speeds are also measured

at the same location. The wind speed is found to have a critical effect on the temperature of the PV module. It not only affects the coefficient of forced heat transfer, but it also affects the local ambient temperature.
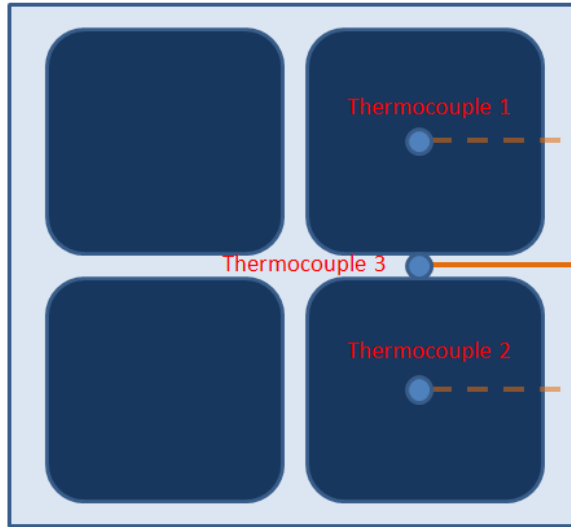
Figure 5.24. Layout of thermocouples immersed into the module
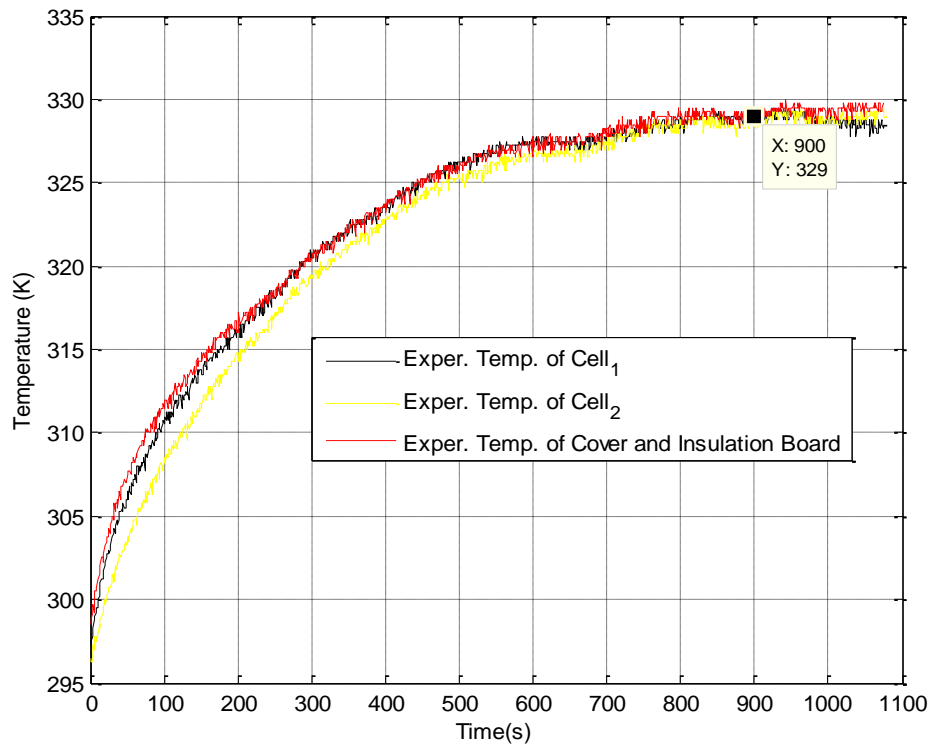
Figure 5.25. Temperature measured through the PV module layers

Table 5.3. Lab-made PV module heat capacity data

Element of module	ρ_m (kg/m^3)	C_m (J/(kgK))	d_m (m)
Monocrystalline silicon PV cells [30]	2330	677	2×10^{-4}
Acrylic cover [98]	1470	1190	3.2×10^{-3}
Polystyrene board[109]	121.7	1300	5×10^{-3}
Glass cover[99]	2510	858	3.2×10^{-3}
$C_{module,acrylic}$ (J/K)		397.6	
$C_{module,glass}$ (J/K)		474.3	

Table 5.4. Electrical characteristics of M2, acrylic-covered at 298 °K

Parameter	Value
Short-circuit current, I_{sc}	4.31 A
Open-circuit voltage, V_{oc}	2.43 V
Series resistance, R_s	0.0377-Ω
Area of cell, A_j	148.25 cm^2
Number of cells in series, M	4
Area of the PV module, A	655 cm^2
Internal quantum efficiency, IQE	0.69

Two cases are validated: the module with a 0.356-Ω resistive load and the unloaded module. The experimental and simulation temperature results for these cases are shown in Figures 5.26 and 5.27, respectively. It is observed that, in both cases, the model underestimates the module temperature in the transient response by about 2.8 K. However, this is only at the initial period of the transient response. This might be attributed to the transient internal temperature variations due to the initial lack of temperature homogeneity within the module as discussed above and shown in Figure 5.25. In the steady-state response, the model accurately predicts the module

temperature. It can also be observed that the temperature for the loaded module is lower than the temperature for the unloaded module.

Figure 5.28 shows the load-voltage as function of the module temperature. The experimental measurements of the load-voltage and the load-current at 297 K are 1.415 V and 3.99 A, respectively. At the steady-state temperature (329 K), the measurements are 1.31 V and 3.677 A, respectively, which are close to the predicted values as shown in Figure 5.28. The current is related to the voltage by the resistive load value. The drop in the load-voltage due to the temperature increase of 32 degrees is 8.07% which represents a drop of 0.25% per degree. The output power is dropped by 15.49% which represents a drop of 4.8% per degree. These numbers agree with reported values in the literature as discussed in Chapters two and three.
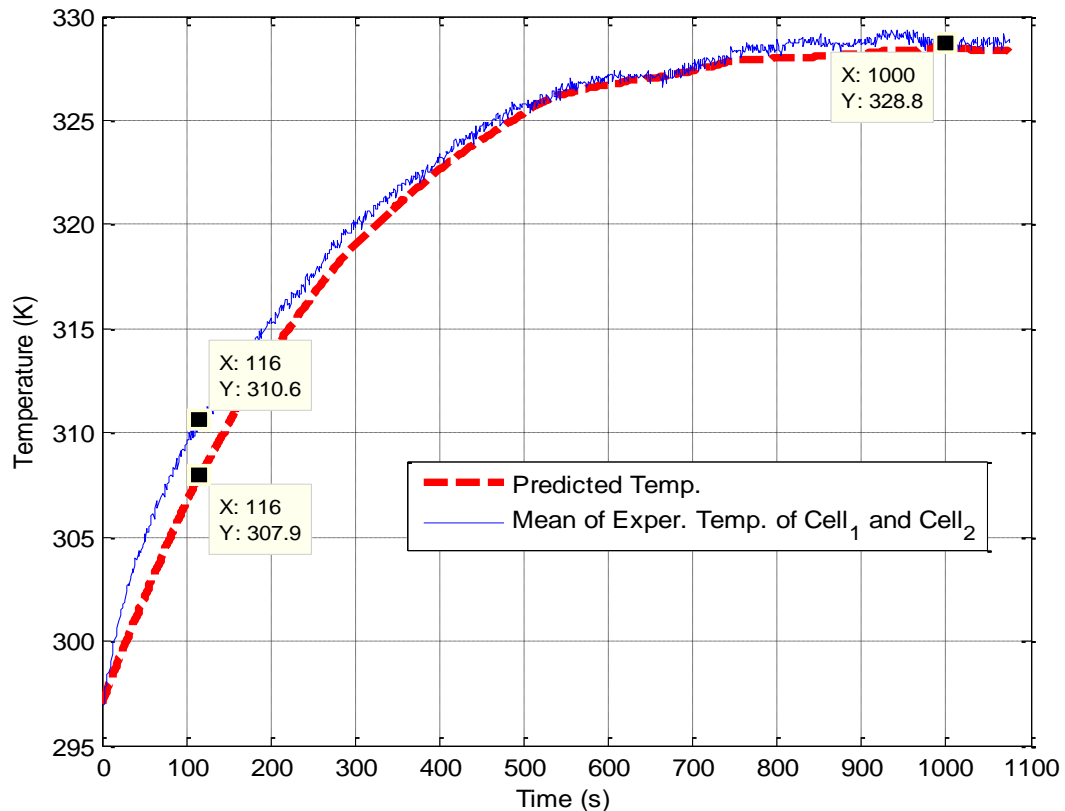
Figure 5.26. Temperatures of loaded module on 02/02/2012
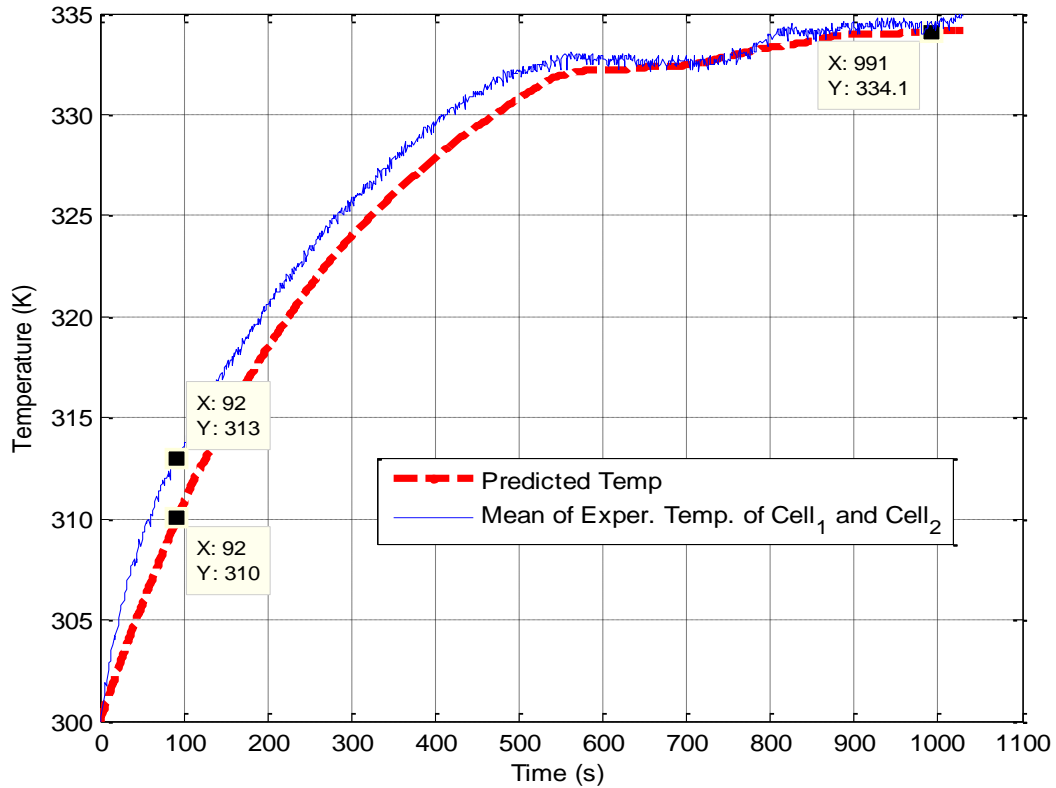
Figure 5.27. Temperatures of unloaded module on 02/02/2012

5.6. Acrylic versus glass covers

For a valid comparison between glass and acrylic covers, both should be applied to the same PV module, and should be exposed to the same meteorological conditions. Experimentally, it is hard to maintain the same meteorological conditions to compare between the glass and the acrylic covers for the same module. In such a situation, where the experimental conditions can't be consistent, the developed model can be used since it is validated. Figure 5.29 shows the predicted temperature of the loaded PV module for both covers. It is clear that the steady-state temperature of the glass-covered module is lower than the temperature of the acrylic-covered module by 0.7 K. The peak difference in temperature is about 2.2 K. Accordingly, the power produced by the glass-covered module is higher than the power produced by the acrylic-covered module as shown in Figure 5.30.
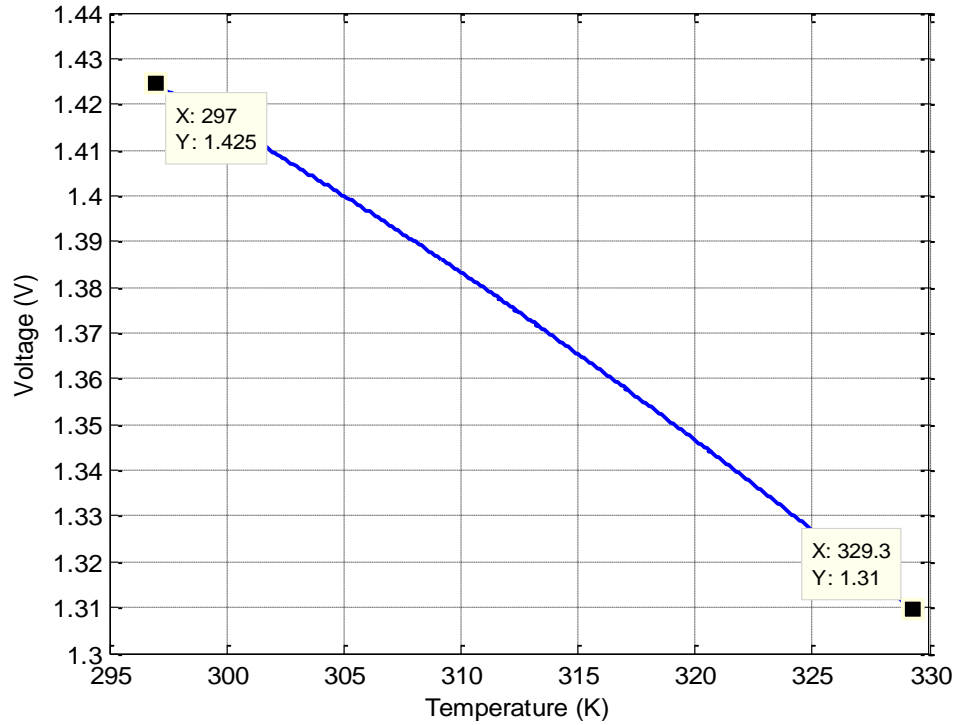
Figure 5.28. Predicted load-voltage as temperature increase.

The temperature reaches the steady-state in case of acrylic-covered module faster than the glass-covered module. This can be mainly attributed to the difference in the cover heat capacities as given in Table 5.3. The heat capacity of the glass is higher than the heat capacity of the acrylic. This means that the amount of energy required to increase the temperature of the glass by one Kelvin is higher than it is for acrylic. Therefore, more energy is required to reach the steady-state temperature for the glass-covered module than for the acrylic-covered module.
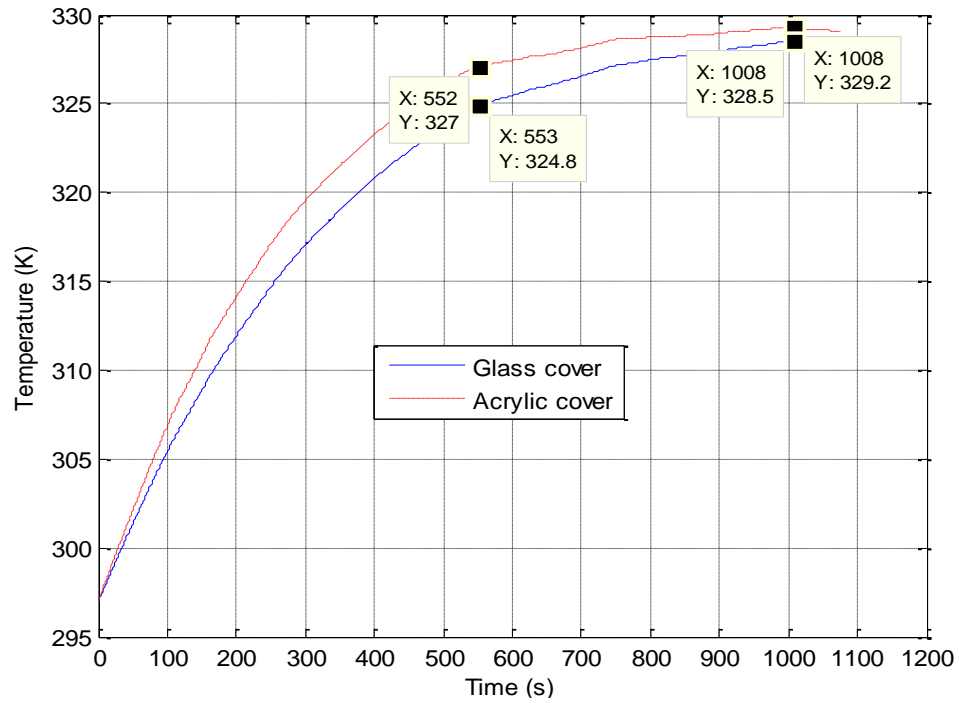
Figure 5.29. Temperature of glass versus acrylic covered loaded module
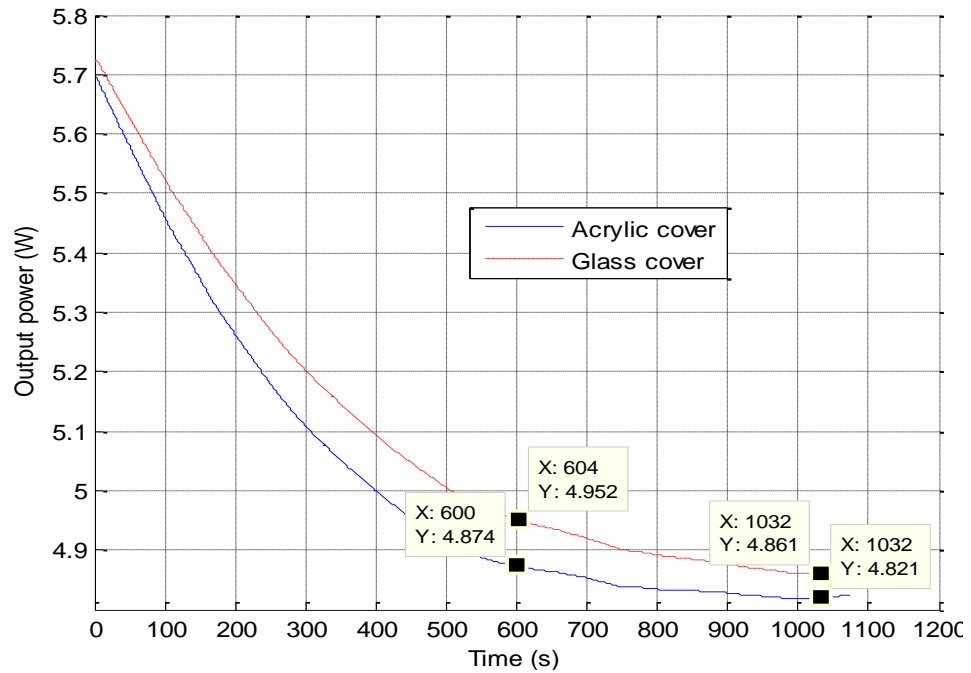
Figure 5.30. Output power of glass versus acrylic covered loaded module

103

CHAPTER 6.

OPTICAL ACTIVE FILTERING

6.1. Introduction

The main objective of this research is to enhance the efficiency of the photovoltaic (PV) module using an optimal active optical filtering process. The wavelength-based thermoelectrical model that is developed in Chapter 4 and parameterized in Chapter 5 helps to understand the light behavior within the PV module and improves the vision toward designing the desired optical filter for wavelength-based filtering purposes.

In this chapter, the electrothermal model is used to design an active optical filter in order to enhance the output power of the PV module. The optical filter actively specifies the cutoff wavelength by which a portion of the solar spectrum is blocked. This chapter comprises the discussion on (1) the effect of light filtering on the PV module performance, (2) the optimization strategies that can be used to find the optimal cutoff wavelength, (3) the results of the optimization process (4) the effects of the time period length by which the active filter is applied, and (5) the technologies that can be harnessed to physically implement the desired filter.

6.2. Light filtering effects on the PV module performance

The intervals of the incident solar spectrum that are associated with long wavelengths (infrared light) do not contribute to electricity production due to their low energy levels. Light with such wavelengths partially passes through the module layers while the remainder is either reflected or absorbed as heat into them. On the other hand, the light associated with short wavelengths (ultraviolet light) hold higher energy level than the bandgap of the PV material. The excess energy converts into heat. The absorbed heat from both, the short and the long wavelengths, increases the PV module temperature which reduces its efficiency. Therefore, blocking both; the wavelengths that generate heat

more than electricity and the ones that do not generate electricity, reduces the PV module temperature and accordingly enhances its efficiency.

The effect of light filtering on the module temperature can be learned using the developed wavelength-based model. The undesired wavelengths are simply blocked by excluding them from the calculations of the generated photonic current. The remaining wavelengths after filtering are dependent on the PV module temperature and the PV material. In other words, the cutoff wavelengths are properties of the module material and temperature. In this research, monocrystalline silicon PV cells are used. Silicon bandgap responds to wavelength range 300–1110 nm. Therefore, light associated with wavelengths longer than 1110 nm are not expected to generate current, but rather, they might dissipate in the PV module layers as heat. Accordingly, blocking these wavelengths passively (all wavelengths longer than 1110 nm) might eventually increase the output power. On the other hand, short wavelengths hold energy exceeds the required level to generate electrical current which converts into heat. It is expected that these wavelengths degrade the efficiency of the PV module more than their electrical contribution. Hence, blocking some of this light may also enhance the module efficiency.

To study the effect of light filtering, different infrared (IR) and ultraviolet (UV) light filters are applied to the PV module. The temperature of the PV module is calculated using the model. Figure 6.1 shows the predicted module temperature without filters compared to its temperature with IR filter that has 1110 nm cutoff wavelength. It can be noticed that the difference between the temperatures is negligible. The IR light with wavelengths longer than 1110 nm is absorbed only by layers other than the PV cells. The amount of input heat to the module from this portion of light is very small, so filtering it out does not have potential effect. Figure 6.2 shows the predicted module temperature without filters compared to its predicted temperature with different UV cutoff wavelength filters. It can be observed that the effect of the UV light on the module temperature is considerable compared to the IR light. The more blocked UV light, the lower is the temperature. Table 6.1 presents a comparison between different UV cutoff wavelengths and their effects on the module steady state temperature and output power.
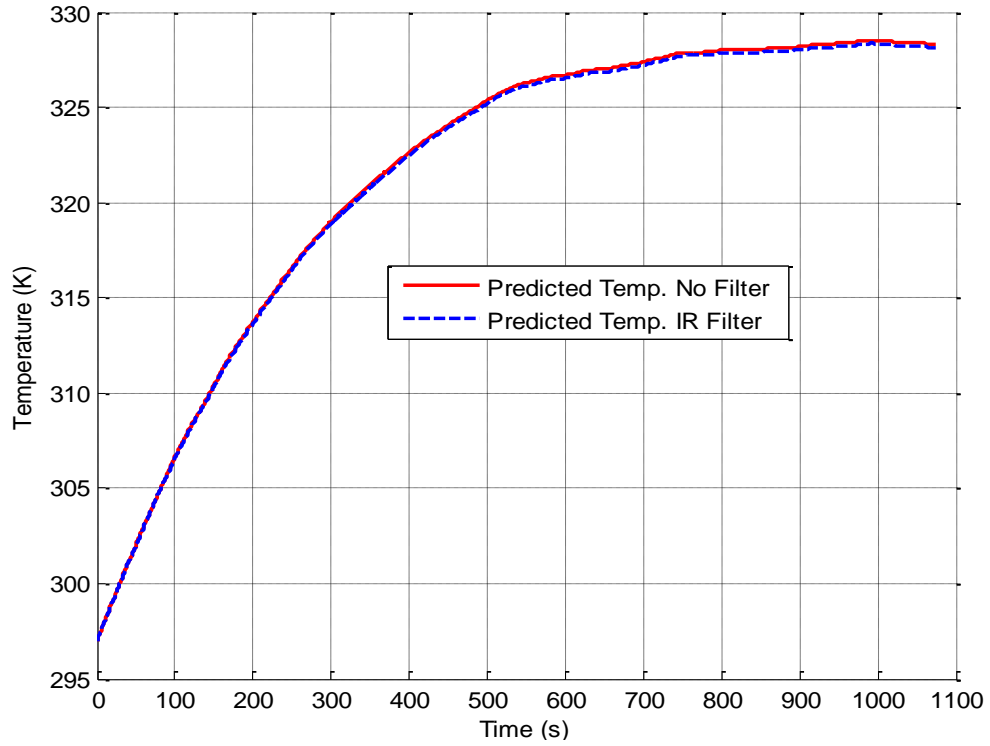
Figure 6.1. Predicted temperature of M2 with and without IR filter
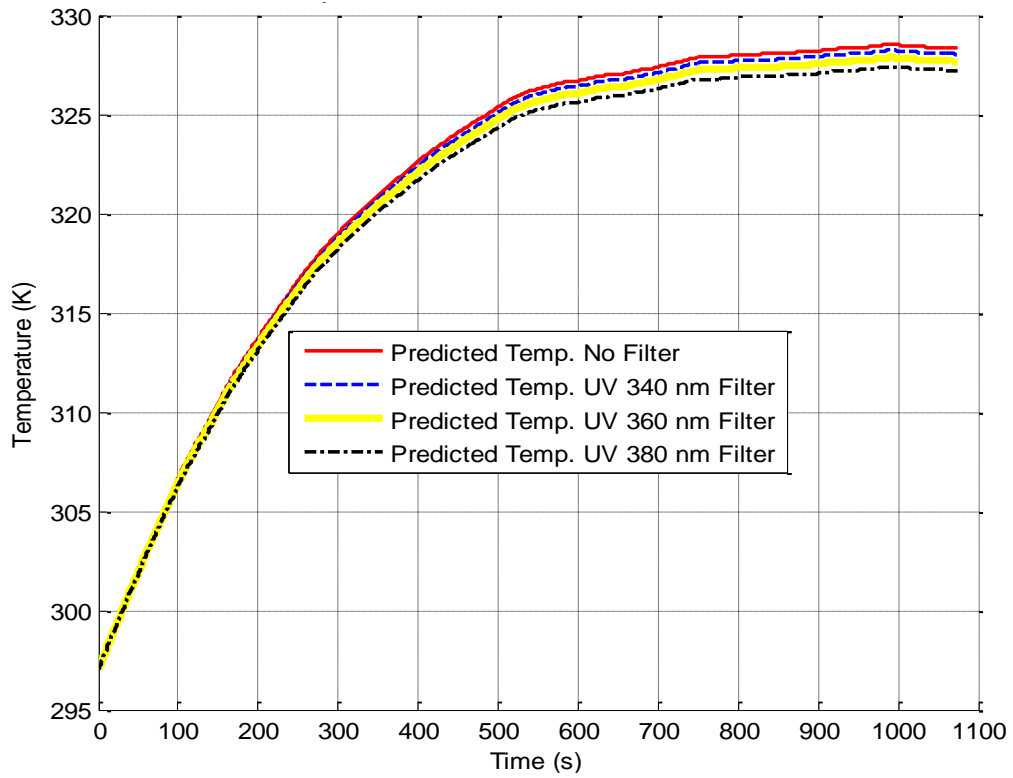
Figure 6.2. Predicted temperature of M2 with and without UV filter

Table 6.1. Effect of different UV cutoff wavelengths on the PV module

Cutoff wavelength (nm)	PV module temperature (K)	Output power (W)
300 (No filter)	328.5	4.8446
340	328.2	4.8526
360	327.8	4.8622
375	327.6	4.8659
380	327.4	4.8650

Figure 6.2 and Table 6.1 show that filtering part of the UV light that generates electricity reduces the temperature and accordingly increases the output power. The tradeoff between the photo-current generated by the blocked UV light and the excess heat is beneficial. In other words, reducing the module temperature enhances the output power more than required to compensate for the lost power due to filtering out the UV light.

Figure 6.3 presents a comparison between the module output power without filtering and the module output power with UV and IR filters that have 375 nm and 1110 nm cutoff wavelengths respectively. It can be seen that the effect of the filters gradually increases as temperature reaches the steady state as shown in Figure 6.4.

In summary, the IR filter can be passive filter with a fixed cutoff wavelength that depends on the bandgap of the PV material. The UV filter can be active with a tunable cutoff wavelength that depends mainly on the PV module temperature.
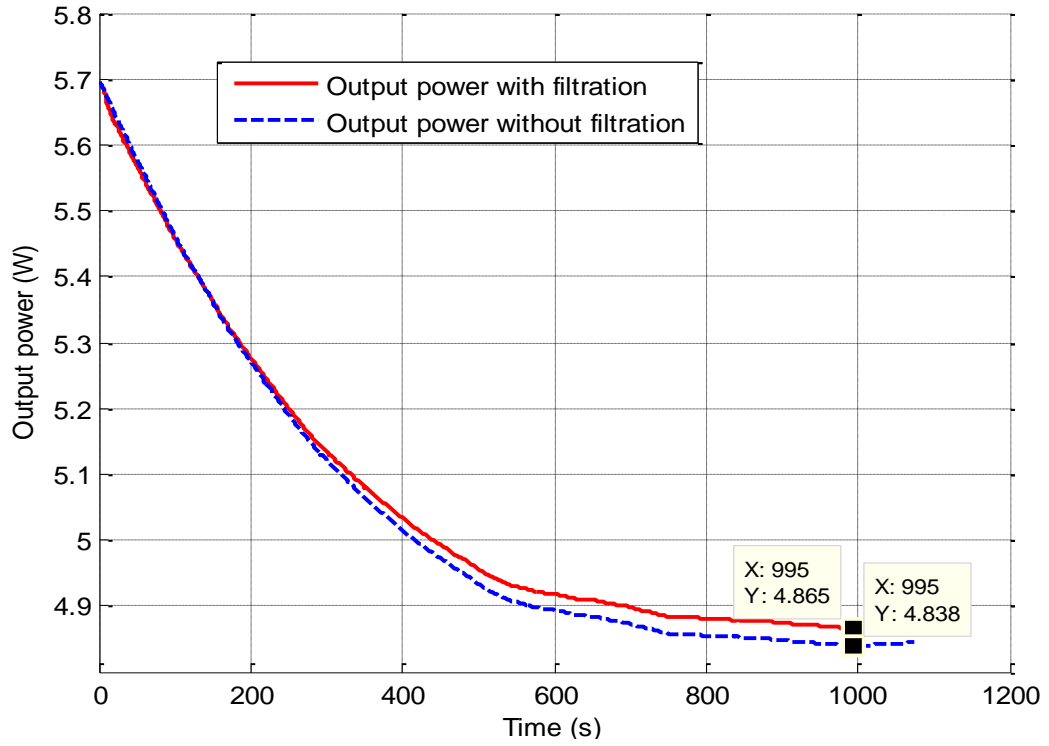
Figure 6.3. Output power of PV module with and without filtering
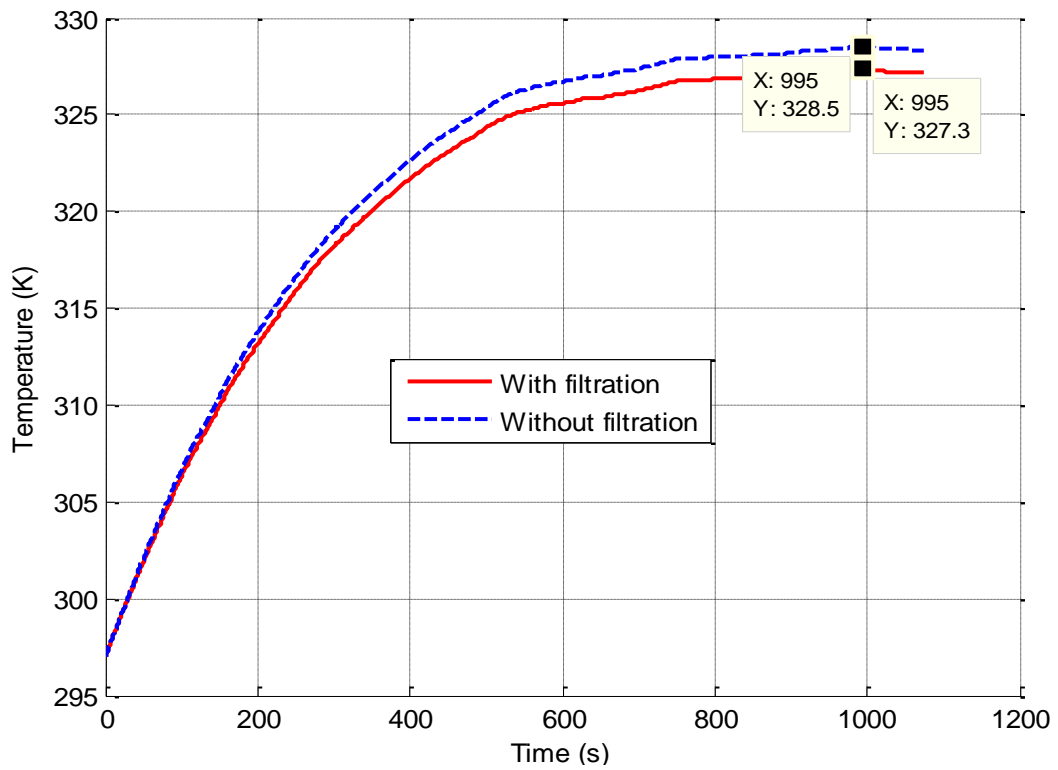
Figure 6.4. Temperature of PV module with and without filtering

108

6.3. Optimization strategy to find the optimal UV cutoff wavelength

The values of the UV cutoff wavelengths given in Table 6.1 are selected arbitrarily regardless of the module temperature. These values should be specified such that the output power is maximized. In this section, an optimization methodology is used to find the optimal cutoff wavelength in order to maximize the output power.

Several optimization methodologies are examined in order to select the most convenient method that is capable of solving this optimization problem. These methods are genetic algorithm, gradient descent, and Fibonacci search. These methods require a cost function that is function of a single or multiple variables. The cost function is minimized or maximized at the optimal value of the variable. The optimization problem of the active filter is to determine the value of the cutoff wavelength (variable) that maximizes the output power. From the model given in Equation (4.26), the output power is related to wavelength through the photonic current. The output power is also function of the module temperature and other variables as given in Equation (4.16). Therefore, the output power (cost function) can't be obtained as an explicit function of wavelength, and hence, the aforementioned optimization techniques can't directly be used to solve the active tuning optimization problem.

To overcome the limitation of the cost function, two optimization options can be used to find the optimal cutoff wavelength. The first option is space scanning, where the model given in Equation (4.26) is solved as many times as the UV cutoff wavelength increments until it reaches the IR cutoff wavelength. The output power can be collected each time the model is solved. The maximum value in the output power vector and the UV cutoff wavelength associated with this output power value represent the optimal solution for this problem. This approach is time and memory consuming and requires a potential computational power. The second option can be utilized by any of the optimization methods that are mentioned above. However, the gradient descent method is used in this work for optimization purposes since it is the simplest among them. In this option, the model is solved at each wavelength value that is calculated using the output power

gradient. Once the gradient changes its polarity form positive to negative, a maximum value for the output power is found and the wavelength value used to find it is the optimal cutoff wavelength. This approach is simple and much faster than the first option. Therefore, the gradient descent optimization method is recommended to be used. This method looks for the global maximum output power value for a specific time period. The optimization process works as shown in Figure 6.5.
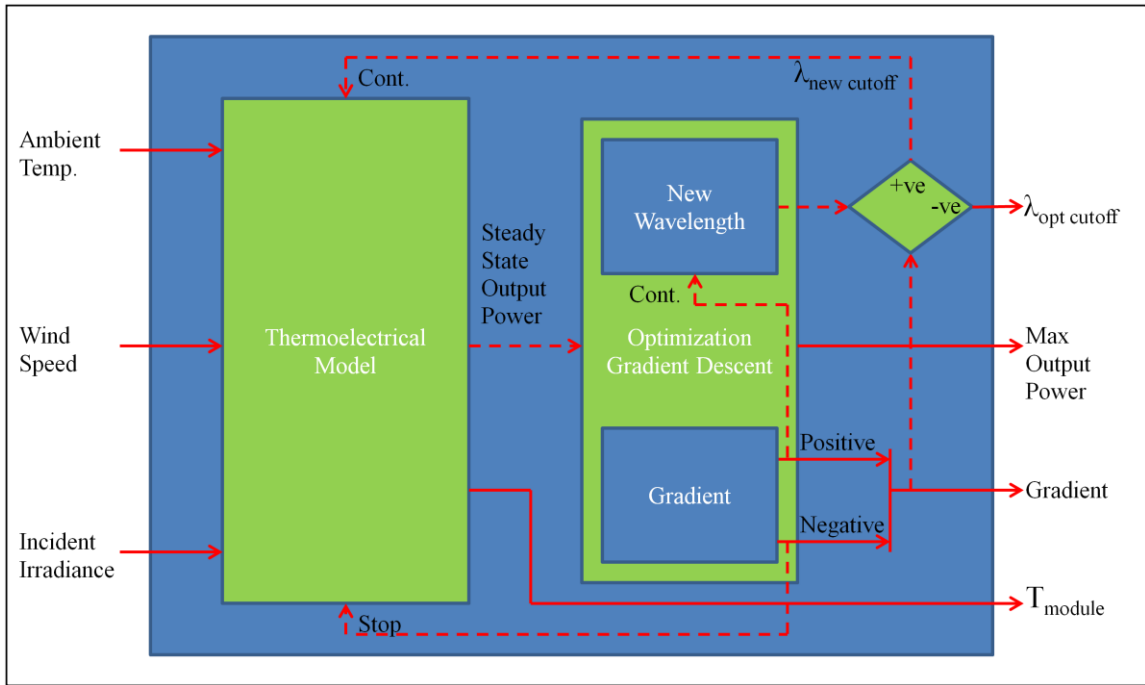
Figure 6.5. Schematic of the optimization process

Initially, the model calculates the output power for two cases, with and without UV filter where the initial cutoff wavelength is 301 nm. The steady state output power in both cases is delivered to the optimization block as shown in Figure 6.5. The steady state output powers and the cutoff wavelengths are used to calculate the gradient as

$$Gradient = \frac{dP_{ss}}{d\lambda_{cutoff}} = \frac{P_{new\ ss} - P_{old\ ss}}{\lambda_{new\ cutoff} - \lambda_{old\ cutoff}}. \qquad (6.1)$$

110

For the initial calculations of the gradient, the wavelengths 300 nm and 301 nm are used as the old and the new cutoff wavelengths respectively. Once the gradient value is calculated, the new cutoff wavelength can be calculated as

$$\lambda_{new\ cutoff} = \lambda_{old\ cutoff} + Gradient \times K \ .$$
(6.2)

Table 6.2 contains the definitions of the symbols that are used in Equations (6.1) and (6.2). The new cutoff wavelength will be used to run the model again to calculate the steady state output power. This output power value is used to calculate the new gradient using Equation (6.1) and then the new cutoff wavelength using Equation (6.2). This scenario continues as long as the gradient value is positive. When the gradient value becomes negative, a global maximum output power value is found which is $P_{old\ ss}$ and the optimal cutoff wavelength is $\lambda_{old\ cutoff}$. Once the optimal UV cutoff wavelength is specified, the filter should only pass the wavelengths longer than it and shorter than the IR (passive) cutoff wavelength.

Table 6.2. Nomenclature

Symbol	Definition
Gradient	gradient constant (W/nm)
P_{ss}	steady state output power (W)
$P_{new\ ss}$	new steady state output power (W)
$P_{old\ ss}$	old steady state output power (W)
λ_{cutoff}	cutoff wavelength (nm)
$\lambda_{old\ cutoff}$	old cutoff wavelength (nm)
$\lambda_{new\ cutoff}$	new cutoff wavelength (new)
K	descent increase factor (1 is used)

6.4. Simulation results of optimization process

The approach discussed in the previous section is used to find the optimal UV cutoff wavelength for the active filter. The experimental PV module and the meteorological data that are used in Chapter 5 are also used herein for the optimization simulation.

Figure 6.6 shows the values of the gradient and the steady state output power as a function of UV cutoff wavelengths. The output power is 4.85 W when only IR filter with cutoff wavelength 1110 nm is applied. It can be observed that the output power gradually increases as the UV cutoff wavelength increases to reach its optimal value at 372 nm where the maximum value of the output power is found using the optimization process. It can also be observed that the optimization process stopped when the gradient value changed from positive to negative.
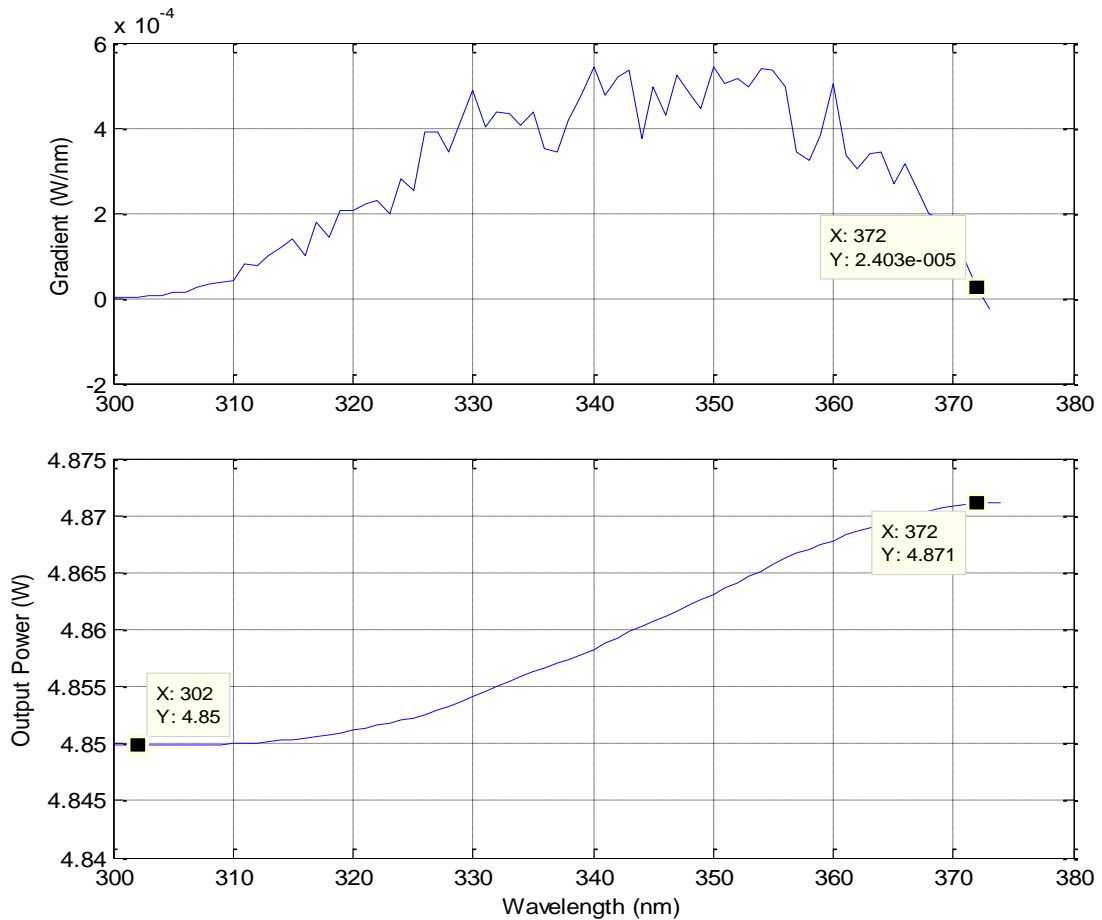
Figure 6.6. Output power of M2 and gradient values during the optimization process

The UV cutoff wavelength, as mentioned previously, changes as the module temperature changes. Figures 6.7 and 6.8 show different optimal cutoff wavelengths for lower and higher ambient temperatures at similar wind speeds and solar irradiance. It can be observed that the higher the ambient temperature (higher module temperature) is, the higher the cutoff UV wavelength and the lower the steady state output power. Table 6.3 lists different optimal cutoff wavelengths that are found for different ambient temperatures which are lower, equal, and higher than the experimentally measured temperature. All of the results are predicted for the same incident irradiance and wind speeds.
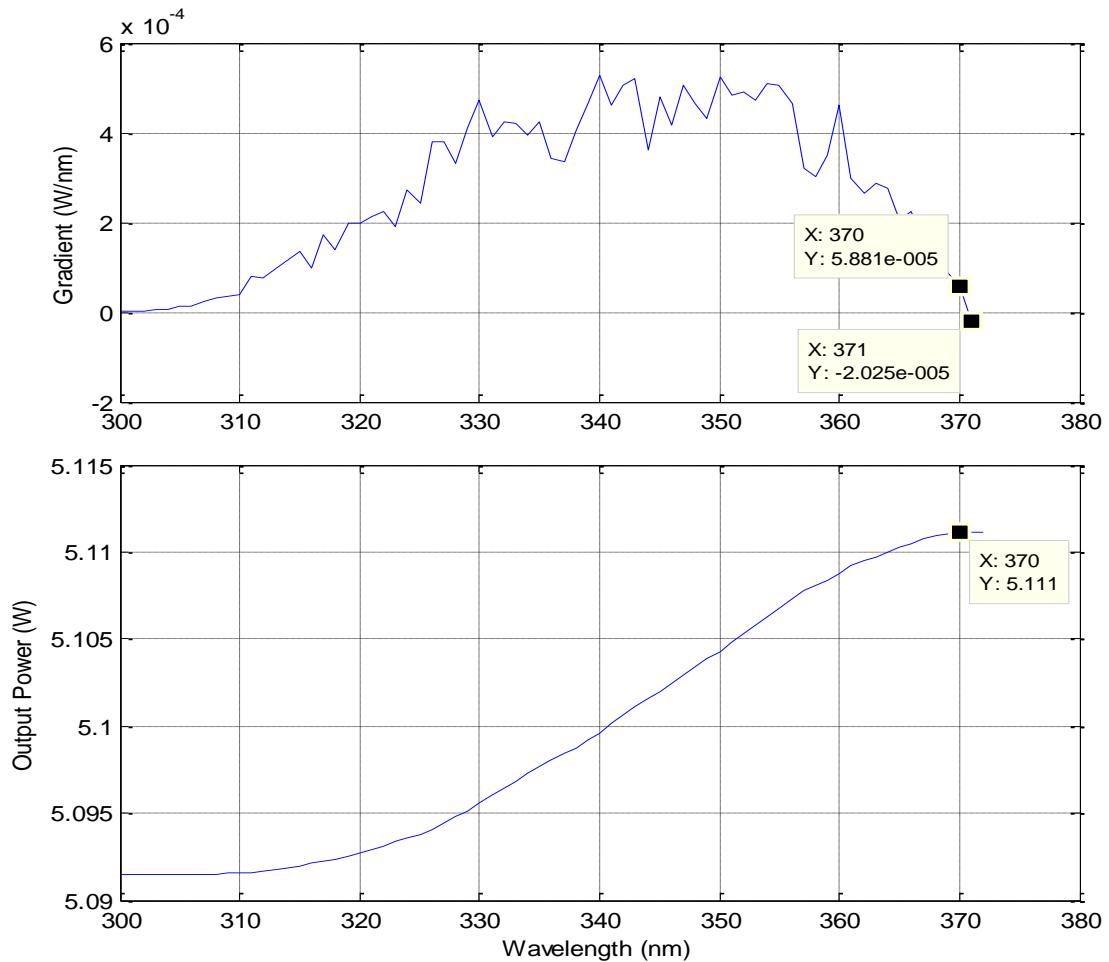
Figure 6.7. Optimal cutoff wavelength, average ambient temperature is 281
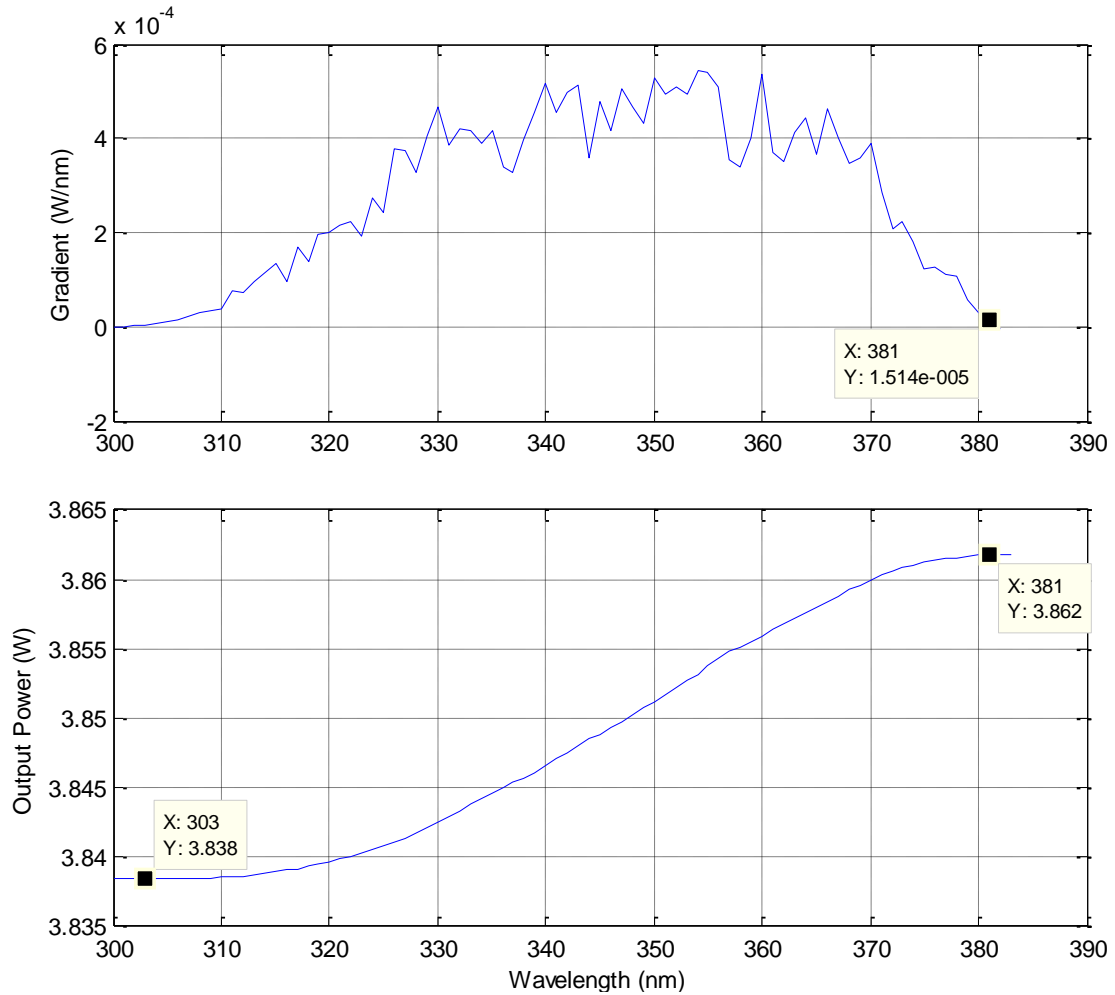
Figure 6.8. Optimal cutoff wavelength, average ambient temperature is 321 K

Table 6.3. Optimal UV cutoff wavelengths, acrylic-covered M2

Average ambient temperatures (K)	281	290	298	306	314	321
Optimal cutoff UV filter (nm)	370	372	374	376	378	381
SS Temp., IR filter (K)	320.0	328.1	336.3	344.4	352.6	360.8
SS Temp., UV, IR filters (K)	319.0	327.1	335.3	343.4	351.5	359.6
SS Output power, IR filter (W)	5.091	4.850	4.601	4.348	4.093	3.838
SS Output power, UV, IR (W)	5.111	4.871	4.623	4.371	4.116	3.862
Enhancement percentage	0.387	0.438	0.485	0.528	0.569	0.609

The optimization algorithm is able to identify the optimal cutoff wavelengths for different covers with different optical properties. This can be justified by running the optimization algorithm for other covers such as the low iron glass. The simulation is conducted for the PV module M2 covered with glass instead of acrylic. The only difference between the simulations is the optical and material properties of the cover as well as the electrical properties of this module when covered with glass. The meteorological simulation data (wind speed, ambient temperature, and incident irradiance) are similar to those used in the simulations for acrylic cover.

Figure 6.9 shows the steady state output power when different UV cutoff wavelengths are used. The maximum output power is obtained when the cutoff wavelength is 406 nm (gradient becomes negative for higher wavelength). This optimal value is different from the optimal cutoff wavelength (372 nm) that is found for similar meteorological conditions using different cover (acrylic) as shown in Figure 6.6.
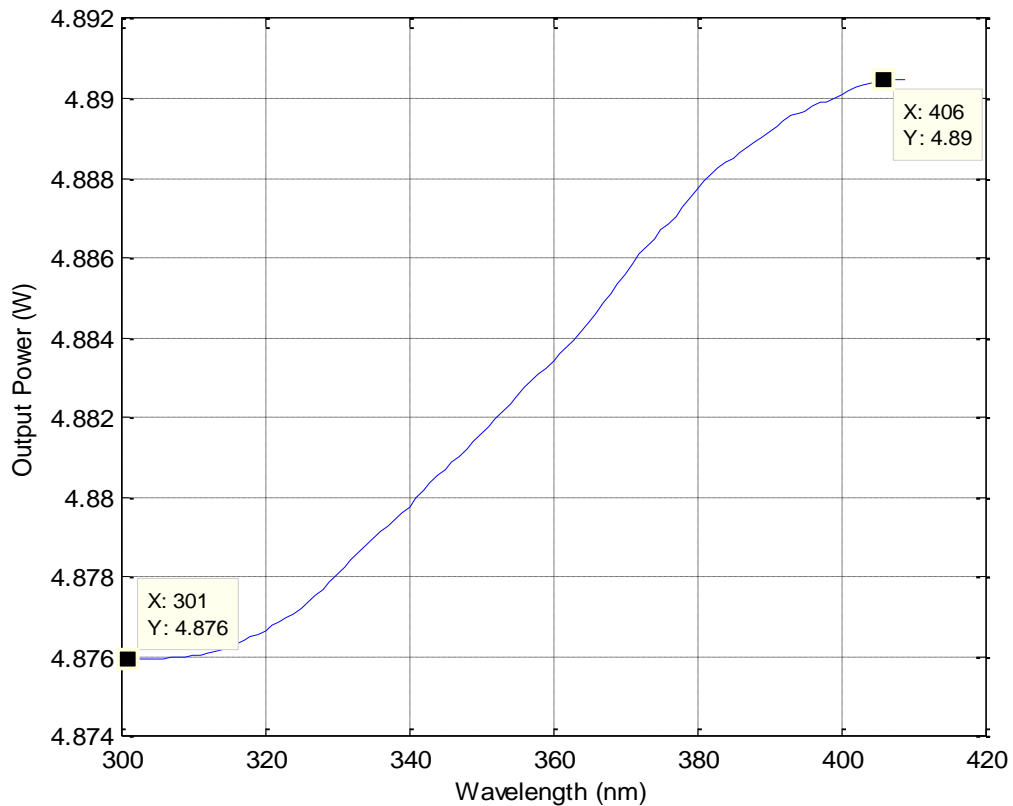
Figure 6.9. Steady state output power of glass-covered M2

115

Table 6.4 shows the simulation results for different ambient temperatures. The optimal cutoff wavelengths are different for different covers at all ambient temperatures as given in Tables 6.3 and 6.4. These results demonstrate that the optimization algorithm is capable of finding the optimal cutoff wavelength and the maximum steady state output power for different module temperatures.

Table 6.4. Optimal UV cutoff wavelengths, glass- covered M2

Average ambient temperatures (K)	281	290	298	306	314	321
Optimal Cutoff UV filter	404	409	413	417	420	424
SS Temp., IR filter	319.3	327.6	335.8	344.1	352.3	360.5
SS Temp., UV, IR filters	317.4	325.5	333.6	341.7	349.9	358.0
SS Output Power, IR filter	5.142	4.876	4.615	4.361	4.112	3.869
SS Output Power, UV, IR filters	5.155	4.890	4.631	4.377	4.129	3.886
Enhancement Percentage	0.255	0.297	0.338	0.377	0.413	0.446

6.5. Benefits of active filter over time

The results of using an optical UV active filter shown in Figures 6.3 and 6.4 are calculated using an 18 minutes real time experimental data. In other words, the experimental meteorological data used to predict the model temperature and output power are continuously collected for 18 minutes. The optimization algorithm is applied on these data and therefore the enhancement percentages of the predicted output power shown in Tables 6.3 and 6.4 are for this short period of sunlight exposure. The efficiency enhancement is expected to increase when applying the active filter for longer time of sunlight exposure.

Simulating the model for longer time periods is potentially time and memory consuming process since the optimization algorithm is running simultaneously with the model simulation. In addition, the meteorological data (solar irradiance, ambient temperature,

and wind speed) are collected every time step. The smaller the time step, the more accurate the predictions are. Therefore, the data required to run the simulation, especially the solar irradiance, are hard to be obtained for short time steps (for example, 1 second) over the entire day. However, this limitation can be conquered by collecting the meteorological data for an entire day on short time rate. The data between the actually measured data points are either can be interpolated or the simulation time step can be used as the same as data collection time rate. Therefore, to learn the trend of applying active optical filtering over an entire day, the meteorological data are collected for Lexington, Kentucky, on 06/15/2010 at the rate of 15 minutes. The ambient temperature and the wind speeds are experimentally measured by a local weather station [110]. Ambient temperature and wind speed values are assumed to be equal to their first experimentally sampled value until reaching the next sampling time. This assumption is valid since the history of the experimental data provides the average value of the measurements. The spectral irradiance is obtained using SMARTS as discussed in Chapter five.

The temperature of the module changes drastically over the entire day, therefore, the optimal cutoff UV wavelength changes to associate with the temperature variations. Accordingly, the optimization algorithm is run at the same time rate of meteorological data collection (15 minutes). The PV module temperature and output power calculations are based on tracking the maximum output power point of the module. The PV module used in the simulation is covered with acrylic (M2). The optimal cutoff wavelength is calculated for each time period (15 minutes) such that maximizing the steady state output power during that period. This optimal wavelength is then used for the entire period. The calculated optimal cutoff UV wavelengths over the entire day are shown in Figure 6.10. The predicted temperature and output power of the module without and with optical filters are shown in Figures 6.11 and 6.12, respectively. It can be observed that the calculated optimal cutoff UV wavelength changes in accordance to the temperature changes such that the output power is maximized. This agrees with the observations discussed above, where the higher the module temperature is, the higher the cutoff wavelength. It can also be observed from the predicted data, that the optical filtering has

117

the most effect on the module performance at the time when the maximum solar irradiance is received.
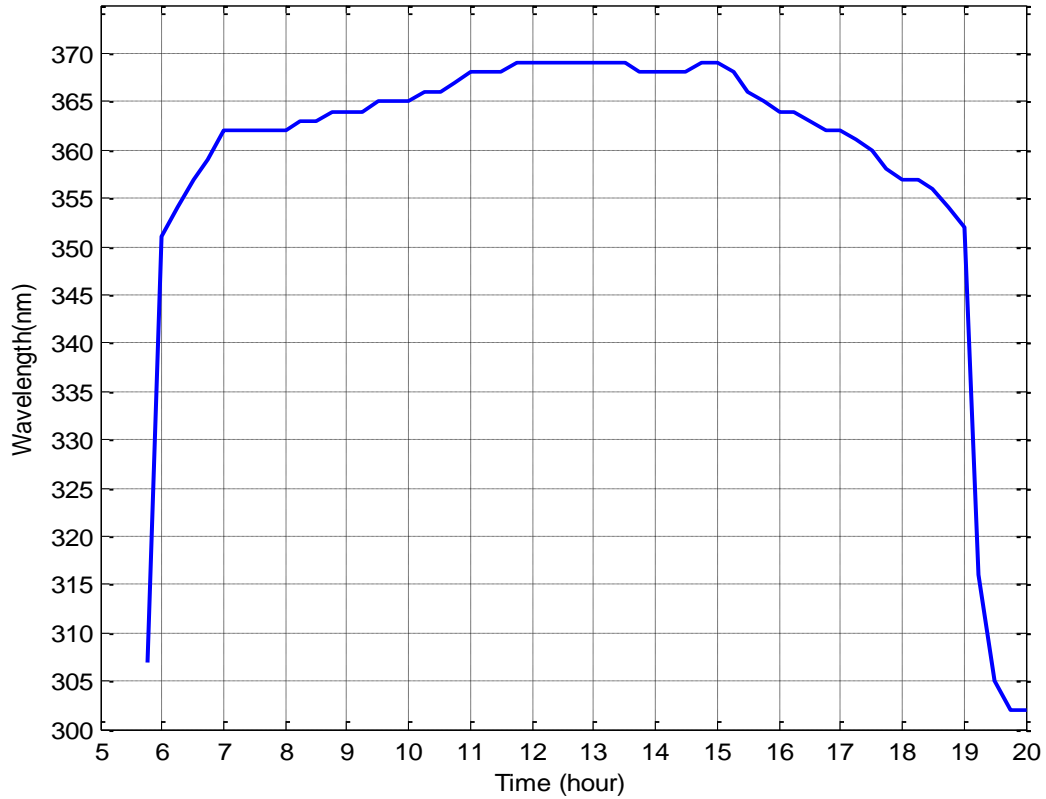
Figure 6.10. Optimal cutoff UV wavelengths over the entire day

The reduction in the module temperature due to filtering is not significant, where the maximum reduction is about 2 degrees at noon time. Accordingly, the enhancement in the output power is modest as shown in Figure 6.12. Despite that the instantaneous output power enhancement appears to be not substantial, the total output power enhancement at the end of the day is considerable. It is found that the total energy produced by the PV module at the end of the day without filtering is 2.0239×10^5 J (56.2194 W.hr) and with filtering is 2.0341×10^5 J (56.5028 W.hr).

It is found that the gained energy when using the optimal UV and passive IR optical filters is 1020 J (0.2833 W.hr). In addition, it is found that the PV module efficiency has increased from 12.13% to 12.20% with an increase by 0.58%. The efficiency calculations

118

are based on the input power with no optical filtering. The enhancement in the output power is expected to increase for higher ambient temperatures and also for larger PV modules area.

If the PV module is loaded at a point that is not the maximum output power, the optical filtering may have different effect on its performance. The following example is for the PV module loaded with a resistive load that is not associated with its maximum power point. Since the optical filtering has the most effect when the solar irradiance is maximum (noon time), the optimization algorithm is run for 72 minutes when approximately 1 sun of solar irradiance is received. The meteorological data used in the simulation are collected on 02/02/2012. For the 72 minutes time period, the angle of incidence slightly changes which can be neglected. The module temperature dynamically changes during the 72 minutes time period. Therefore, several optimal cutoff UV wavelengths can be used. The optimization algorithm is run four times during this time period, one time each 18 minutes. The predicted temperatures of the PV module without and with optical filters (UV and IR) are shown in Figure 6.13. The variations in the module temperature are associated with the variations of the wind speed. It is found based on the predicted temperature that the optimal cutoff wavelengths are 373 nm, 373 nm, 373 nm, and 374 nm, respectively. Figure 6.14 shows the predicted output power of the PV module without and with the optical filters. The variations in the output power values are associated with the variations of the module temperature. The output power over the 72 minutes increased from 2.1021×10^4 J (5.84 W.hr) without filters to 2.1134×10^4 J (5.87 W.hr) when filters are applied. Energy increased by 113 J. The efficiency of the module increased from 9.99% to 10.05% with 0.60% increase.
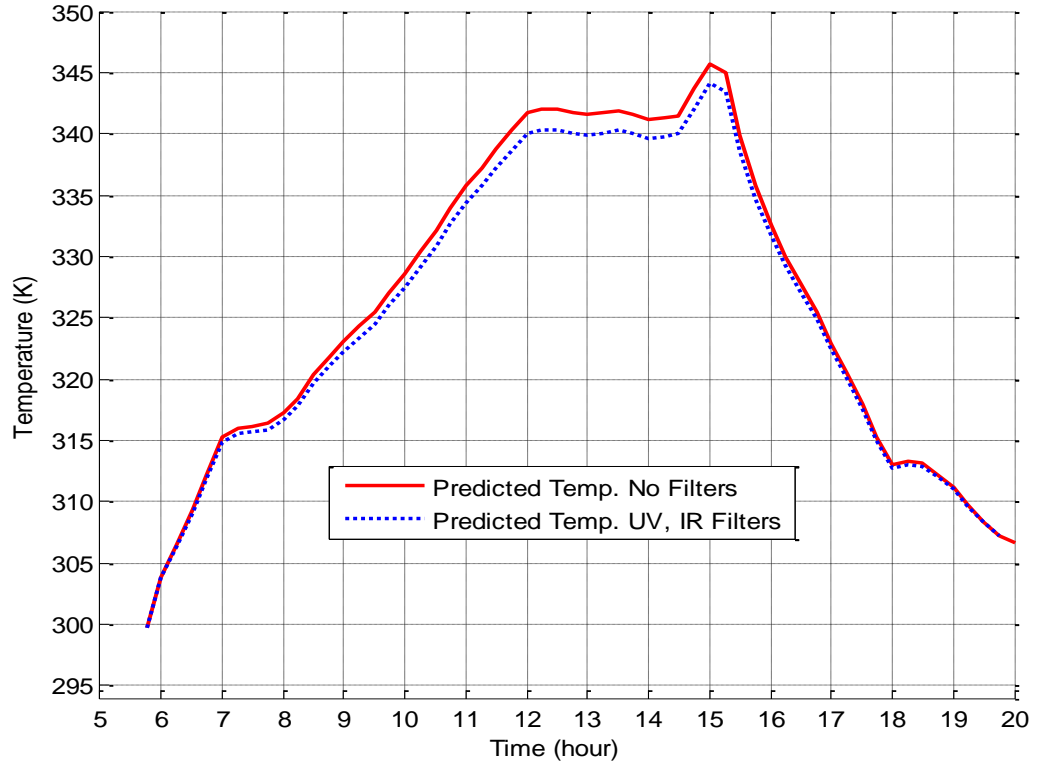
Figure 6.11. Module temperature over the entire day
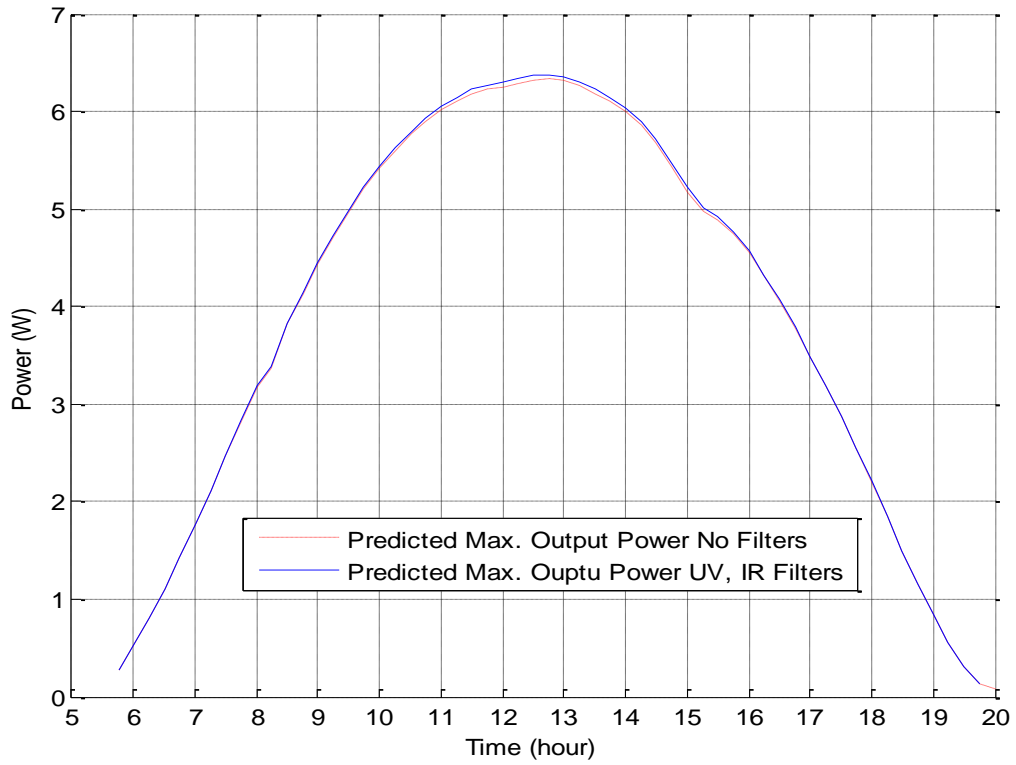
Figure 6.12. Module maximum output power over the entire day

120

As discussed above, for higher ambient temperatures, the effect of using the filters increases over time. In areas such as Arizona, Texas and sometimes in Kentucky, the summer time ambient temperature is relatively high. For example, if the ambient temperatures used in the simulation are in average close to 40 ℃, the predicted PV module temperature and output power are shown in Figures 6.15 and 6.16, respectively. The optimal cutoff wavelengths in this case are 381 nm, 378 nm 379 nm, and 379 nm.

It is found that the output power of the PV module over the 72 minutes increased from 1.8077×10^4 J (55.0214 W.hr) without filters to 1.8197×10^4 J (5.0547 W.hr) with filters. The produced energy increased by 121 J. The efficiency of the PV module increased from 8.59% to 8.65% with an increase by 0.73%.
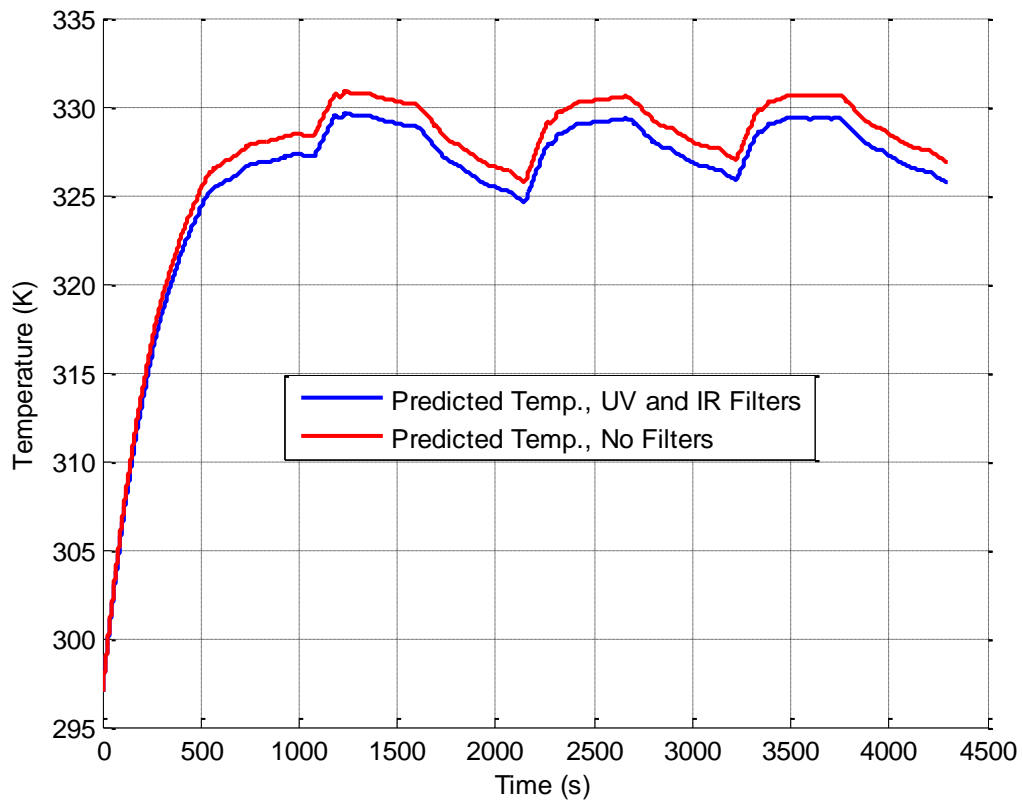
Figure 6.13. Predicted temperature of M2 for 72 minutes of 1 sun irradiance

In conclusion, higher module temperature results in higher cutoff UV wavelength. In addition, the higher the module temperature is, the higher the effect of applying the filter

on the output power. Furthermore, it can be observed that the longer the optical filter is applied, the higher its effect will be on the output power. Moreover, the effect of optical filtering is better when the loading point of the module is not the maximum output power loading point.
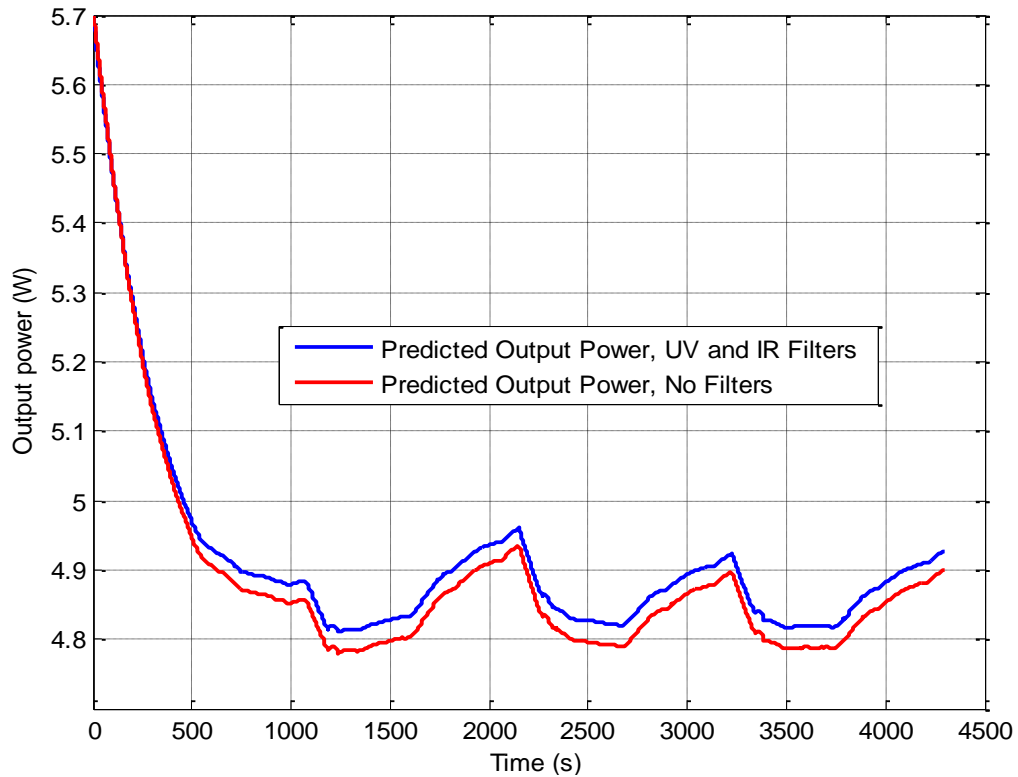
Figure 6.14. Predicted output power of M2 for 72 minutes of 1 sun irradiance

Based on the predicted results over the entire day, it can be observed that the active filtering can be applied only when it is most beneficial that is at noon time. There are several conditions by which the filter operation can be controlled. These conditions are time or incident solar spectrum (function of time), wind speed, ambient temperature, and PV module temperature. These conditions either directly or indirectly affect the module temperature. Therefore, controlling the active filter can be simplified by using only one condition that is the module temperature. In other words, the filter will be activated once the module temperature reaches a specific value (for example, room temperature). Once the module cools down below the threshold temperature, the UV light will not be blocked.
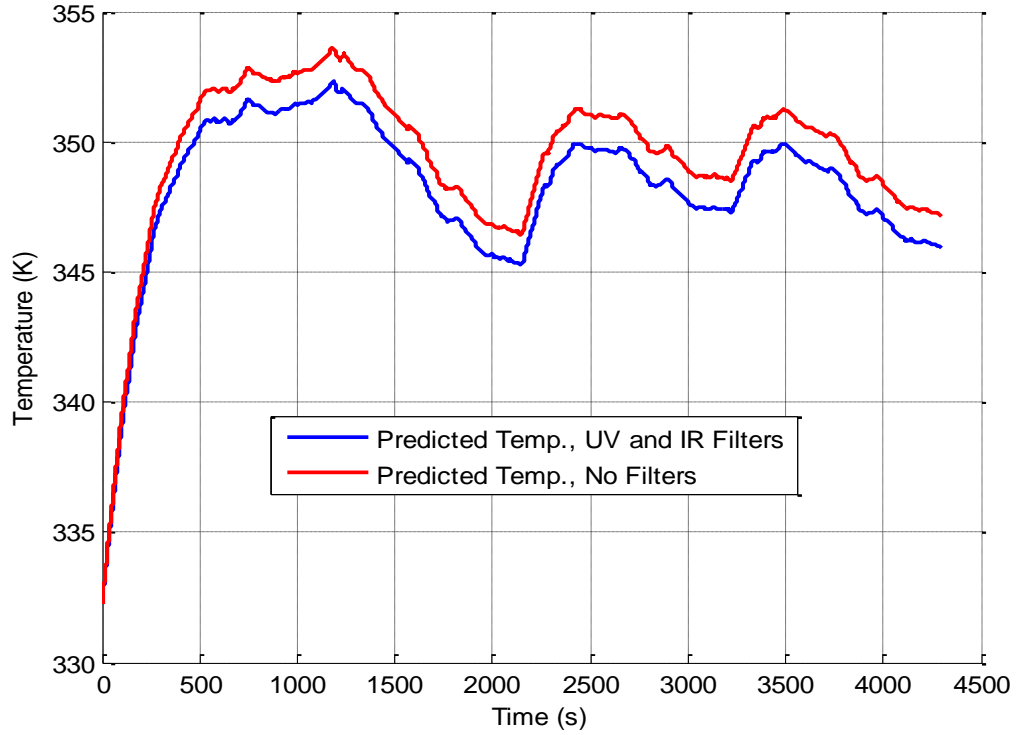
Figure 6.15. Predicted temperature of M2, higher ambient temperature
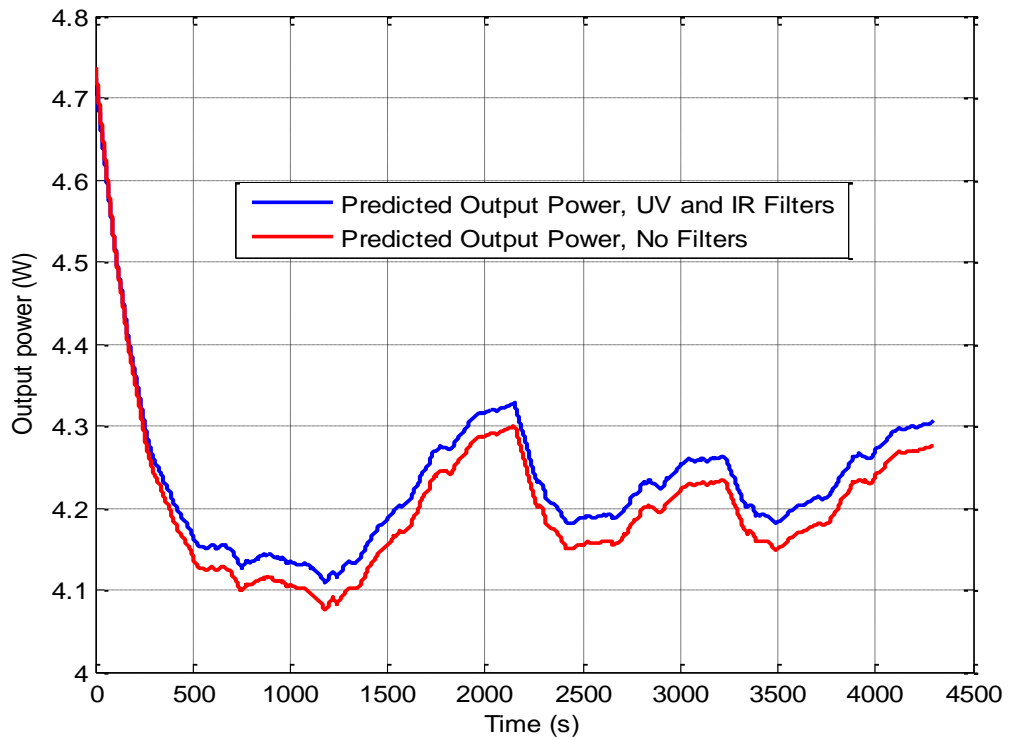
Figure 6.16. Predicted output power of M2, higher ambient temperature

6.6. Proposed physical implementation of the active UV optical filter

An ideal physical active optical filter must be able to block the IR light at the desired cutoff wavelength which is material dependent. It also must be able to actively change its UV cutoff wavelength that depends on the PV module temperature. This filter is a band-pass optical filter that passes only the desired wavelengths band. Both cutoff wavelengths (IR and UV) can be actively changed. However, the IR cutoff wavelength is fixed for a specific photovoltaic material while the UV cutoff wavelength actively changes based on the optimization process that mainly depends on the module temperature.

In this section, some of the technologies that can be harnessed to implement the proposed active filter are discussed. These technologies are used for applications other than photovoltaics. These applications are either optical devices or smart glass for construction applications.

The tunable filters that are designed for optical devices applications [111], [112] represent an ideal implementation for the desired active optical filter for PV applications. These filters are controlled (tuned) using an electrical signal that affect the orientation (polarization) of nano-sized particles such as liquid crystal (LC) droplets targeting a specific wavelength threshold. The power required to tune these particles is less than a watt and their response time is milliseconds. However, these optical filters are intended to be for small surface areas and to affect an artificial light that propagates into closed channels such as optical fibers. In addition, the available technologies of these filters affect a very narrow wavelength band (spikes). Therefore, these filters might not be a feasible solution for large area PV applications and wide wavelength bands.

Smart glass technologies are basically used for construction purposes to reduce carbon footprint effects toward green environment by saving heating and air conditioning power. This technology is used also for internal design purposes and to create private areas for occasional activities such as meeting rooms. Examples of these technologies are electrochromic glass [113], suspended particle devices (SPDs) [114], polymer dispersed

liquid crystal devices (PDLCs) [115], and micro-blinds [116]. The basic operating principle of all these devices is the applied electrical voltage that bleaches or colors the device as desired. The electrochromic glass requires the electrical signal every time changes its state from opacity to transparency or vice versa. The electrical signal is not required to maintain a particular shade or state that is reached. The normal state of the PDLC glasses is opaque since the LC droplets are randomly arranged resulting in scattering the light as it passes through. When a voltage signal is applied to the device, the electrical field generated between the device electrodes rearranges the dissolved LC droplets and converts it into transparent state. This makes the light to pass through the device with no scattering. The electrical signal is required all time to maintain translucent state. The SPDs are similar to the PDLCs in their operational concept. However, they are different in materials and response time. The micro-blinds smart glass technology is still under ongoing development. Basically, these devices are composed of rolled thin metal blinds and other substrates. If an electrical signal is applied to the device, the generated potential difference between the rolled metal layer and the transparent conductive layer causes the metal micro-blinds to stretch and block the light. Once the electrical field is removed, the device returns back to be translucent.

The differences between the smart glass technologies are listed in Table 6.5. This table represents a decision matrix by which one of these technologies can be selected for PV applications. It can be observed that the electrochromic smart glass with its high light transmission, flexible controllability, durability, and low power consumption is attractive to be integrated with PV panels.

Smart glass technology has been integrated with PV panels for self powering smart glass products. Such applications are introduced by different researchers as Huang *et al.* [72] and Dep [113] who only focused on the electrochromic smart glass technology.

The electrochromic smart glass can be used for optical filtering applications for PV panels since it overcomes the shortcomings of the optical filters that are discussed above. The advantages of the smart glass are the applicability for large area surfaces, durability,

performance stability, and designed for natural incident sunlight. The main disadvantage of using the smart glass as an active or tunable optical filter is lack of controllability over the desired wavelength range and it is also not able to block the light at a specific cutoff wavelength. When an electrical controlling signal is applied to the smart glass, the spectrum wavelengths are equally affected by the new glass transmittance as shown in Figure 6.17.

Table 6.5. Decision matrix, smart glass technologies

Technology Comparison Aspect	Electro- chromic Device	PDLC	SPD	Micor- Blinds Device
Input power (VAC)	50–100	32–75	30–120	NA
Energy consumption (W/m^2)	Peak: 2.69 Avg: 0.43	5.38	0.646	NA
Switching time	Less than 1 second	Milliseconds	Milliseconds to seconds	Milliseconds
Transparency	60–95%	75–80%	50–70%	NA
Opacity	3–10%	5–55%	1–5%	NA
Operation temperature (℃)	-20–60	-10–60	0–60	NA
Power down default	Opaque or clear	Opaque	Opaque	Clear
Intermediate state (dimmable)	Yes	No	Yes	No
Thickness (mm)	20	Glass: 8 Polycarbonate: 1.6	3	NA
Manufacturer (Supplier)	SageGlass	LTI Smart Glass	Inspechtech Aero-Services	Under developments by "Canadian National Research Council"
Cost for 12 in^2	$350	$225	$850	NA

Despite of this major limitation, electrochromic glass can be used to protect the PV panels at high ambient temperatures such as space applications. This protection is a tradeoff between the output power and the PV panel lifecycle. The extreme temperatures

generate thermal stresses that significantly reduce the lifecycle of the PV panels. The electrochromic filter can be controlled using an electrical signal that depends on the panel temperature. This is a different optimization problem but similar in concept to the optimization process discussed above that is based on maximizing the output power. The electrochromic layers can be monolithically integrated with the PV material, where both, the PV cells and the filter layers are combined into a single unit. This would improve the light transmittance through the layers than stacking two units (PV panel and electrochromic glass) on top of each other.
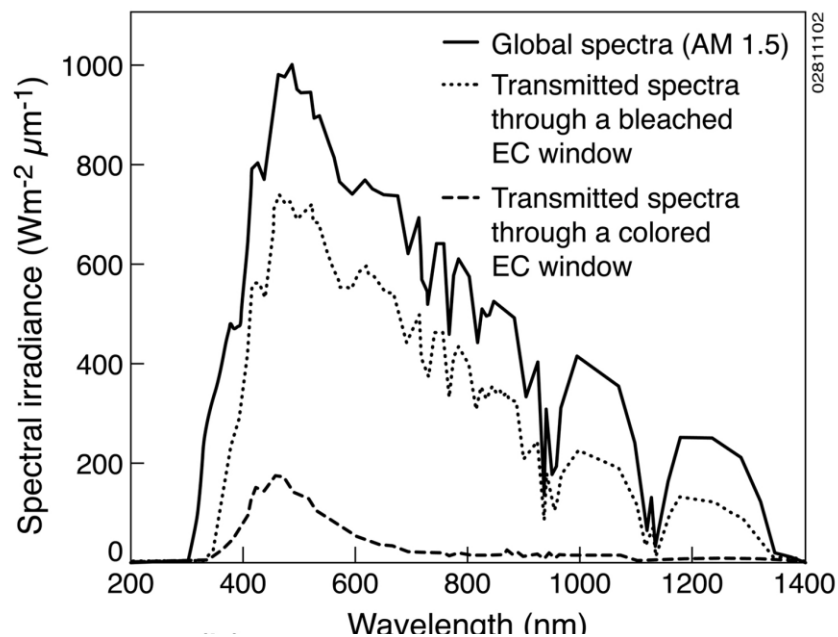
Figure 6.17. Effect of electrochromic smart glass on solar spectrum [113]

In conclusion, the currently available optical technologies do not highly assist to implement the desired active optical filter. However, this creates new opportunities for future joint projects with other engineering disciplines and research fields such as optics which may lead to create such an application.

127

CHAPTER 7.

CONCLUSIONS AND CONTRIBUTIONS

In this chapter, the research dissertation is concluded. The progress achieved in the goals and objectives of this work and the accomplished milestones are discussed. The contributions to the photovoltaic (PV) research communities are highlighted. In addition, recommendations for future research opportunities are proposed.

7.1. Research goals status

As proposed in Chapter one, the main objective of this research is to enhance the efficiency of the photovoltaic modules and increasing their lifecycle. In this research, a thermoelectrical wavelength-based model is developed as a fundamental prerequisite for optical filtering. This model shows the contribution of each wavelength in the solar spectrum to the PV module temperature and output power. Accordingly, the model is capable of quantifying the effects of optical filters that are either passive or active. Therefore, this model is a key milestone toward designing and optimizing these filters. The contribution of both, the model and the optical filter are an important foundation toward achieving the research main objective. The following are the goals used to measure the progress of research work to develop the model and the optical filter:

1. Understanding and observing the photovoltaic effect of converting light into electricity

2. Understanding the limitations of light-to-electricity conversion efficiency especially the ones that are related to thermal aspects, and addressing the conducted efforts of the researchers to override these limitation

3. Developing a mathematical model that uses computational methods to predict the temperature of the PV module, and its effects on the output power. This model should reflect the individual contribution of the solar spectrum wavelengths on the module efficiency

4. Designing and building the required experimental setup to validate the wavelength-based developed model

5. Using the validated model to proof that active filtering scheme would be effective in increasing the productivity of the photovoltaic process

6. Obtaining a penalty function that accurately reflects the contribution of various parameters to the photovoltaic process

7. Designing an active controller filter using the optimization techniques to get the optimal values of the variables of the penalty function obtained in number 6

8. Exploring different means that could be used in order to physically implement the designed active controlling filter

9. Building the described filter if it is physically and economically feasible

The goals listed from 1 to 8 are completed. In Chapter six, it is concluded that the goal number 9 is not feasible using the available optical technologies. However, more research work in this area is promising to achieve this goal.

7.2. Conclusions

The following conclusions are observed while working on this research:

1. The proposed thermoelectrical model is able to predict the interaction between the module temperature and its output power.

2. It is observed that understanding the light behavior within the module is critical toward developing a wavelength-based model.

3. It is found that selecting the appropriate heat transfer coefficient model is a critical factor for the accuracy of the results.

4. The parameterization methodology proposed in this work to characterize the developed model represents a road map for characterizing the model for any given PV module at various locations and meteorological conditions.

5. The proposed model is capable of predicting the module temperature for various loading conditions, including open circuit, resistive, and maximum power point loadings.

6. The proposed model is capable of predicting the module temperature output power for various light angles of incidence. This would extend the model to be used over the entire day.

7. It is learned that the ultraviolet light degrades the performance of the PV module more than it contributes to generate electrical current. On the other hand, the infrared light with wavelengths longer than the PV material response may degrade the module performance if absorbed in other layers.

8. It is observed that optical filtering enhances the performance and the lifecycle of the PV module. The optical filtering can be passive or active.

9. Active optical filtering has an advantage over the passive filter, where based on some operational conditions, the filter performance can be optimally controlled to maximize the output power.

10. It is found that the available optical and smart glass technologies are not reliable to be utilized to implement the active optical filter for photovoltaic applications.

7.3. Contributions

The work conducted in this research is expected to have an impact on the PV research community through the following contributions:

1. Developed and validated a wavelength-based thermoelectrical model that predicts the effects of the spectrum wavelengths on the PV module performance

2. Developed an optical model that is able to predict the overall optical properties of the PV module using the optical properties of its layers

3. Designed and built a portable data acquisition system that can be used to measure the PV module temperature, output power, IV-characterization curve, and finds the maximum output power loading point

4. Validated the concept of active optical filtering for photovoltaic applications

5. Designed an active optical filter and optimized it for maximum output power performance. It is predicted that the efficiency of the PV module increased for some meteorological conditions by 0.73% over 72 minutes of applying the filter

6. Developed a large scale solar simulator and built two monocrystalline silicon solar modules

7. Presented in the 37th and 38th IEEE Photovoltaic Specialist Conferences, and nominated for the best student presentation award. The two papers are published in the conference proceedings

8. Published two journal papers, modeling and characterization, in the IEEE Journal of Photovoltaics

The contributions listed from 1 to 5 can be considered of high impact on the photovoltaic research community. The rest of the contributions are of high impact on the academic performance of the student.

7.4. Recommendations and future work

The most novel aspect of the proposed wavelength-based electrothermal model is the method of calculating the absorption coefficients of the module layers as a function of wavelength which can be very useful in many photovoltaic researching areas. Since the photovoltaics have emerged as a promising renewable energy source, many research areas of solar energy are continuously developing and many others come into sight. In this research, several researching fields are recognized and recommended to be a continuous effort for the work started herein. The following are recommended developing opportunities where the work conducted in this research can be extended:

1. Investigate the feasibility of implementing the "ideal" active optical filter jointly with the optical fields' experts.

2. Validate the active filtering concept using experimentally designed filter and compare with predicted results.

3. Develop the model to be capable of predicting the temperature and output power of the III-V multijunction PV modules.

4. Develop the active filtering concept to be applicable to the III-V multijunction PV modules. It is expected that the active filtering concept will be more beneficial for these PV materials since they target wide and different ranges of the solar spectrum.

5. Apply the model and its filtering capabilities to predict the performance of the PV module when shading is occurring due to clouds existence. Clouds deteriorate the solar spectrum and apply random filters that degrade the output power of the module. The behavior of the PV module under this condition can be predicted using the proposed model.

6. Develop the model to be applicable for space applications, where the extraterrestrial irradiance hits the module surface with harmful UV and IR light. Filtering the light in space applications will be more effective and more efficient than it appears for the terrestrial solar irradiance.

7. Investigate the effect of the light filtering on the lifecycle of the PV module. Two aspects can be recognized as major lifecycle factors; temperature effects and harmful light.

REFERENCES

[1]   Anonymous, " International Energy Agency Outlook 2010," ed: U.S. Energy
        Information Administration (EIA), 2010.

[2]   Anonymous, "U.S. Energy Facts," ed: U.S. Energy Information Administration
        (EIA), 2010.

[3]   Anonymous, "Non-renewable energy," ed: U.S. Energy Information
        Administration (EIA), 2010.

[4]   E. Radziemska, "Thermal performance of Si and GaAs based solar cells and
        modules: a review," *Progress in Energy and Cumbusion Science* vol. 29, pp. 407-
        424, 2003.

[5]   W. Smith, "Society Telecom Engineering," vol. 2, 1873.

[6]   D. Chapin, C. Fuller, and G. Pearson, "A new silicon p-n junction photocell for
        converting solar radiation into electronical power," *Journal of Applied Physics,*
        vol. 25, pp. 676-677, 1954.

[7]   S. Bowden and C. Honsberg. (2010). *PVCDROM website*. Available:
        http://pvcdrom.pveducation.org/index.html

[8]   B. Norton, P. Eames, T. Mallick, M. Huang, S. McCormack, J. Mondol, and Y.
        Yohanis, " Enhancing the performance of building integrated photovoltaics,"
        Solar Energy, vol. doi: 10.1016/j.solener, 2010.

[9]   Anonymous. (September 2010). *U.S. Energy Information Administration (EIA)*.
        Available: http://www.eia.doe.gov/energyexplained/index.cfm?page=solar_where

[10]   N. Lewis. (2008). *Chemical Challenges in Renewable Energy*. Available:
http://nsl.caltech.edu/energy

[11]   E. Bucher, "Solar cells materials and their base parameters," *Journal of Applied Physics,* vol. 17, pp. 1-25, 1978.

[12]   V. P. Singh and J. F. Jordan, "Sprayed Zinc-Cadmium Sulfide Films for Cu2s-Znxcd1-Xs Heterojunction Solar-Cells," *Electron Device Letters,* vol. 2, pp. 137-138, 1981.

[13]   V. P. Singh, D. L. Linam, D. W. Dils, J. C. McClure, and G. B. Lush, "Electro-optical characterization and modeling of thin film CdS-CdTe heterojunction solar cells," *Solar Energy Materials and Solar Cells,* vol. 63, pp. 445-466, Aug 31 2000.

[14]   J. Fritsche, A. Klein, and W. Jaegermann, "Thin film solar cells: Materials science at interfaces," *Advanced Engineering Materials,* vol. 7, pp. 914-920, Oct 2005.

[15]   R. S. Singh, V. K. Rangari, S. Sanagapalli, V. Jayaraman, S. Mahendra, and V. P. Singh, "Nano-structured CdTe, CdS and TiO2 for thin film solar cell applications," *Solar Energy Materials and Solar Cells,* vol. 82, pp. 315-330, May 1 2004.

[16]   V. P. Singh, R. S. Singh, B. Parthasarathy, A. Aguilera, J. Anthony, and M. Payne, "Copper-phthalocyanine-based organic solar cells with high open-circuit voltage," *Applied Physics Letters,* vol. 86, pp. -, Feb 21 2005.

[17]   A. Imenes and D. Mills, "Spectral beam splitting technology for increased conversion efficiency in solar concentrating systems, a review " *Solar Energy Materials and Solar Cells,* vol. 84, pp. 19-69, 2004.

[18]   V. Salas, E. Olias, A. Barrado, and A. Lazaro, "Review of the maximum power point tracking algorithms for stand-alone photovoltaic systems," *Solar Energy Materials and Solar Cells,* vol. 90, pp. 1555-1578, Jul 6 2006.

[19]   C. Ababei, S. Yuvarajan, and D. L. Schulz, "Toward integrated PV panels and power electronics using printing technologies," *Solar Energy,* vol. 84, pp. 1111-1123, Jul 2010.

[20]   H. Mousazadeh, A. Keyhani, A. Javadi, H. Mobli, K. Abrinia, and A. Sharifi, "A review of principle and sun-tracking methods for maximizing solar systems output," *Renewable and Sustainable Energy Reviews,* vol. 13, pp. 1800-1818, Jan. 2009.

[21]   M. Peters, J. C. Goldschmidt, P. Loper, B. Gross, J. Upping, F. Dimroth, R. B. Wehrspohn, and B. Blasi, "Spectrally-Selective Photonic Structures for PV Applications," *Energies,* vol. 3, pp. 171-193, Feb 2010.

[22]   E. Radziemska, "Thermal performance of Si and GaAs based solar cells and modules: a review," *Progress in Energy and Combustion Science,* vol. 29, pp. 407-424, 2003.

[23]   B. Norton, P. Eames, T. Mallick, M. Huang, S. McCormack, J. Mondol, and Y. Yohanis, "Enhancing the performance of building integrated photovoltaics," *Solar Energy,* vol. doi: 10.1016/j.solener, 2010.

[24]   A. Hasan, S. J. McCormack, M. J. Huang, and B. Norton, "Evaluation of phase change materials for thermal regulation enhancement of building integrated photovoltaics," *Solar Energy,* vol. 84, pp. 1601-1612, Sep 2010.

[25]   J. Smith and L. Reiter, "Non-numerical approach for the review of photovoltaic system performance models," in *Proc. Joint ASME-ASES Solar Energy Conference* 1985, pp. 220-226.

[26]   J. Gow and C. Manning, "Development of a photovoltaic array model for use in power-electronics simulation," *Electric Power Applications,* vol. 146, pp. 193-200, Mar. 1999.

[27]   M. Zagrouba, A. Sellami, M. Bouaicha, and M. Ksouri, "Identification of PV solar cells and modules parameters using the genetic algorithms: Application to maximum power extraction," *Solar Energy,* vol. 84, pp. 860-866, May 2010.

[28]   O. Shekoofa and M. Taherbaneh, "Modeling of silicon solar panel by MATLAB/Simulink and evaluating the importance of its parameters in a space application," presented at the 3rd International Conference IEEE on Recent Advances in Space Technologies June 16 2007, pp. 719-724.

[29]   G. Omar and O. Eduardo, "A General Purpose Tool for Simulating the Behavior of PV Solar Cells, Modules and Arrays," presented at the 11th IEEE Workshop on Control and Modeling for Power Electronics, August 17, 2008, pp.

[30]   A. Jones and C. Underwood, "A thermal model for photovotaic systems," *Solar Energy,* vol. 70, pp. 349-359, Feb. 2001.

[31]   G. Tina and S. Scrofani, " Electrical and thermal model for PV module temperature evaluation," in *Proc. Electrotechnical Conference the 14th IEEE Mediterranean*, 2008, pp. 585-590.

[32]   G. Charalambous, G. Maidment, A. Kalogirou, and K. Yiakoumetti, "Photovoltaic thermal (PV/T) collectors: A review," *Applied Thermal Engineering,* vol. 27, pp. 275-286, Feb 2007.

[33]   M. Green, "Silicon solar cells: evolution, highefficiency design and efficiency enhancements," *Semiconductor Sience and Technology,* vol. 8, pp. 1-12, 1993.

[34]   M. Green, "The path to 25% silicon solar cell efficiency: history of silicon cell evolution," *Progress in Photovoltaics: Research and applications,* vol. 17, pp. 183-189, 2009.

[35]   R. Ohl, " Light-sensitive electric device," USA Patent 2402622, 1941.

[36]   E. F. Kingsbury and R. S. Ohl, "Photoelectric Properties of Ionically Bombarded Silicon," *Bell System Technical Journal,* vol. 31, pp. 802-815, 1952.

[37]   Anonymous, *Bell Labs Records,* p. 436, 1954.

[38]   J. Mandelkorn, C. McAfee, J. Kesperis, L. Schwartz, W. Pharo, and "Fabrication and characteristics of phosphorus-diffused silicon solar cells," *Electrochemical Society Journal,* vol. 109, pp. 313-318, 1962.

[39]   P. Iles and D. Zemmrich, "Improved performance from thin silicon solar cells," in *Proc. IEEE Photovoltaic Specialests Conference, 10th*, 1973, pp. 200-206.

[40]   Mandelko.J and J. H. Lamneck, "New Electric-Field Effect in Silicon Solar Cells," *Journal of Applied Physics,* vol. 44, pp. 4785-4787, 1973.

[41]   M. P. Godlewski, C. R. Baraona, and H. W. Brandhorst, "Low-High Junction Theory Applied to Solar-Cells," *Solar Cells,* vol. 29, pp. 131-150, Aug 1990.

[42]   J. Lindmayer and J. Allison, "The violet cell: an silicon solar cell," COMSAT Technolgy 31, 1973.

[43]   J. Haynos, J. Allison, R. Arndt, and A. Meulenberg, "Comsat non-reflective silicon solar cell: a second generation improved cell," in *Proc. International Conference on Photovoltaic Power Generation*, 1974, pp. 487-500.

[44]   E. Rittner and R. Arndt, "Comparison of silicon solar cell efficiency for space and terrestrial use," *Journal of Applied Physics,* vol. 47, pp. 2999-3002, 1976.

[45]   M. Green, A. Blakers, S. Wenham, S. Narayanan, M. Willison, M. Taouk, and T. Szpitalak, " Improvements in silicon solar cell efficiency," in *Proc. Eighteenth IEEE Photovoltaic Specialists Conference*, 1985, pp. 39-42.

[46]   R. Sinton, Y. Kwark, S. Swirhun, and R. Swanson, " Silicon point contact concentrator solar cells," *Electron Device Letters,* vol. EDL-6, pp. 405-407, 1985.

[47]   R. Sinton, R. Crane, S. Beckwith, A. Cuevas, and P. Gruenbaum, "Developments in module ready Si backside-contact solar, cells," in *Proc. Twenty First IEEE Photovoltaic Specialists Conference* 1990, pp. 302-306.

[48]   R. Stinton, Y. Kwark, J. Gan, R. Swanson, and E. Howe, "27.5 % Si concentrator solar cells," *Sunworld,* vol. 10, pp. 78-80, 1986.

[49]   M. Green, S. Wenham, and A. Blakers, "Recent advances in silicon solar cell performance," presented at the The Nineteenth IEEE Photovoltaic Specialists Conference, 1987, pp. 6-12.

[50]   E. Radziemska, "The effect of temperature on the power drop in crystalline silicon solar cells," *Renewable Energy,* vol. 28, pp. 1-12, Jan. 2003.

[51]   M. Shaltout, M. El-Nicklawy, A. Hassan, U. Rahoma, and M. Sabry, "The temperature dependence of the spectral and efficiency behavior of Si solar cell under low concentrated solar radiation," *Renewable Energy,* vol. 21, pp. 445-458, Nov-Dec 2000.

[52]   E. Skoplaki and J. Palyvos, "On the temperature dependence of photovoltaic module electrical performance: A review of efficiency/power correlations," *Solar Energy,* vol. 83, pp. 614-624, 2009.

[53]   F. Gaithom, F. Ndiritu, P. Muriithi, R. Ngumbu, and J. Ngareh, "Effect of thermal conductivity on the efficiency of single crystalsilicon solar cell coated with an anti-reflective thin film," *Solar Energy,* vol. 83, pp. 1290-1293, 2009.

[54]   E. Karatepe, M. Boztepe, and M. Colak, "Neural network based solar cell model," *Energy Conversion and Management,* vol. 47, pp. 1159-1178, Sep. 2005.

[55]   H. Fahmy, " Mathematical and numerical model for PV cell steady state temperature distribution," in *Proc. International Solar Energy Conference*, 1998, pp. 225-231.

[56]   H. Patel and V. Agarwal, "Matlab-based modeling to study the effects of partial shading on PV array characteristics," *IEEE Transaction on Energy Conversion,* vol. 23, pp. 302-310, 2008.

[57]   M. Gonzalez and J. Carroll, "Solar cell efficiency variation with varying atmospheric conditions," *Solar Energy,* vol. 53, pp. 395-402, 1994.

[58]   R. Balog, Y. Kuai, and G. Uhrhan, "A photovoltaic module thermal model using observed isolation and meteorological data to support a long life highly reliable module-integrated inverter design by predicting expected operating temperature " in *Proc. Energy Conversion Congress and Exposition (ECCE)* 2009, pp. 3343-3349.

[59]   S. Armestrong and W. Hurley, "A thermal model for photovoltaic panels under varying atmospheric conditions," *Applied Thermal Engineering,* vol. 30, pp. 1488-1495, Mar. 2010.

[60]   S. Fahr, C. Ulbrich, T. Kirchartz, U. Rau, C. Rockstuhal, and F. Lederer, "Optimization of Rugate filters for ultra light-trapping in solar cells," in *Proc. Photonics for Solar Energy Systems II*, 2008, pp. 1-9.

[61]   S. Fahr, C. Ulbrich, T. Kirchartz, U. Rau, C. Rockstuhal, and F. Lederer, "Rugate filter for light-trapping in solar cells," *Optics Express,* vol. 16, pp. 9332-9343, Jun. 2008.

[62]   M. Green and A. Ho-Baillie, "Forty three percent composite split-spectrum concentrator solar cell efficiency," *Progress in Photovoltaics: Research and applications,* vol. 18, pp. 42-47, 2010.

[63]   M. Peters, J. Goldschmidt, T. Kirchartz, and B. Blasi, "The photonic light trap-Improved light trapping in solar cells by angularly selective filters," *Science Direct: solar energy materials and solar cells,* vol. 93, pp. 1721-1727, Jun. 2009.

[64]   L. Zeng, Y. Yi, C. Hong, J. Liu, N. Feng, X. Duan, and L. Kimerling, "Efficiency enhancement in Si solar cells by textured photonic crystal back reflector," *Applied Physics Letters,* vol. 89, pp. 11111(1-3), Sep. 2006.

[65]   A. Geotzberger, J. Goldschmidt, M. Peters, and P. Loper, "Light trapping, a new approach to spectrum splitting," *Solar Energy Materials and Solar Cells,* vol. 92, pp. 1570-1578, 2008.

[66]   A. Barnett, "Very high efficiency solar cell modules," *Progress in Photovoltaics: Research and Applications,* vol. 17, pp. 75-83, Oct. 2008.

[67]   C. Ulbrich, S. Fahr, J. Upping, and M. Peters, "Directional selectivity and ultra-light-trapping in solar cells," *Physica Status Solidi Applications,* vol. 205, pp. 2831-2843, Dec. 2008.

[68]   H. Yoon*, et al.*, "Application of infrared reflecting (IRR) coverglass on multijunction III-V solar cells," presented at the IEEE 4th World Conference on Photovoltaic Energy Conversion, Waikoloa, HI, May, 2006, pp. 1861-1864

[69]   W. Beachamp and T. Hart, "UV/IR Reflecting solar cell cover," USA Patent 5449413, 1995.

[70]   Y. Anjaneyulu and D. Yoon, " Liquid crystal window to control the solar energy," in *Proc. Optical material technology for energy efficiency and solar conversion IV, SPIE*, 1985, pp. 10-14.

[71]   C. Y. Chen and Y. L. Lo, "Integration of a-Si:H solar cell with novel twist nematic liquid crystal cell for adjustable brightness and enhanced power characteristics," *Solar Energy Materials and Solar Cells,* vol. 93, pp. 1268-1275, Aug 2009.

[72]   L.-M. Huang, C.-W. Hu, H.-C. Liu, C.-Y. Hsu, C.-H. Chen, and K.-C. Ho, "Photovoltaic electrochromic device for solar cell module and self-powered smart glass applications," *Solar Energy Materials and Solar Cells,* vol. 99, pp. 154-159, Apr. 2012.

[73]   T. Soderstrom, F. J. Haug, V. Terrazzoni-Daudrix, and C. Ballif, "Optimization of amorphous silicon thin film solar cells for flexible photovoltaics," *Journal of Applied Physics,* vol. 103, pp. -, Jun 1 2008.

[74]   F. Newman, D. Aiken, P. Patel, Dan Chumney, I. Aeby, R. Hoffman, and P. Sharps, "Optimization of inverted metamorphic multijunction solar cells for field-deployed concentrating PV systems," in *Proc. 34th IEEE Photovoltaic Specialists Conference*, 2009, pp. 1611-1616.

[75]   I. Visa, D. Diaconescu, A. Duta, and V. Popa, "PV tracking data needed in the optimal design of the azimuthal tracker's control program," in *Proc. 11th International Conference on Optimization of Electrical and Electronic Equipment*, 2008, pp. 449-454.

[76]   M. Balzani and A. Reatti, "Neural network based model of a PV array for the optimum performance of PV system," in *Proc. PhD Research in Microelectronics and Electronics* 2005, pp. 323-326.

[77]   K. Koizumi, K. Yoshioka, and T. Saitoh, "Performance improvement of light-trapping type concentrator modules for circular cells," in *Proc. International Solar Energy Conference*, 2003, pp. 475-481.

[78]   Y. P. Chang, "Optimal design of discrete-value tilt angle of PV using sequential neural-network approximation and orthogonal array," *Expert Systems with Applications,* vol. 36, pp. 6010-6018, Apr 2009.

[79]   S. Mokkapati, F. Beck, A. Polman, and K. Catchpole, "Designing periodic arrays of metal nanoparticles for light-trapping applications in solar cells," *Applied Physics Letters,* vol. 95, 2009.

[80]   Q. Zhao, P. Wang, and L. Goel, "Optimal pv panel tilt angle based on solar radiation prediction," in *Proc. IEEE 11th International Conference on Probabilistic Methods Applied to Power Systems*, 2010 pp. 425-430.

[81]   M. Park and I.-K. Yu, "A study on the optimal voltage for MPPT obtained by surface temperature of solar cell," in *Proc. 30th Annual Conference of IEEE Industrial Eelctronics Society*, 2004, pp. 2040-2045.

[82]   Y. M. Xuan, X. Chen, and Y. G. Han, "Design and analysis of solar thermophotovoltaic systems," *Renewable Energy,* vol. 36, pp. 374-387, Jan 2011.

[83]   V. Andreev, V.Grilikhes, and V. Rumyantsev, *Photovoltaic conversion of concentrated sunlight*. New York, NY: John Wiley & Sons, 1997.

[84]   M. Green, *Solar cells: operating principles, technology, and system applications*. Englewood Cliffs, NJ: Prentice-Hall, 1982.

[85]   H. Fahmy, "Mathematical and numerical model for PV cell steady state temperature distribution," in *Proc. International Solar Energy Conference*, Albuquerque, NM, 1998, pp. 225-231.

[86]   S. Krauter, R. Hanitsch, P. Campbell, and S. Wenham, "Optical modelling, simulation and improvement of PV module encapsulation," in *Proc. 12th European Photovoltaic Solar Energy Conference*, 1994, pp. 1194-1197.

[87]   P. Batagiannis and C. Gibbons, "Thermal assessment of silicon-based composite materials used in photovoltaics," in *Proc. Renewable Energy Conference*, Maritime Island Climates, 2001, pp. 151-157.

[88]   K. Bucher, "Site dependence of the energy collection of PV modules," *Solar Energy Materials and Solar Cells,* vol. 47, pp. 85-94, Oct. 1997.

[89]   G. Tina and S. Scrofani, "Electrical and thermal model for PV module temperature evaluation," in *Proc. Electrotechnical Conference the 14th IEEE Mediterranean*, Melecon, 2008, pp. 585-590.

[90]   S. Churchill, "A comprehensive correlating equation for laminar, assisting, forced and free convection " *Journal of American Institute of Chemical Engineers,* vol. 23, pp. 10-26, 1976.

[91]   Y. Kemmoku, T. Egami, M. Hiramatsu, Y. Miyazaki, K. Araki, N. Ekins-Daukes, and T. Sakakibara, "Modelling of module temperature of a concentrator PV system " in *Proc. 19th European Photovoltaic Solar Energy Conference*, Paris, 2004.

[92]   J. Zhao and A. Green, "Optimized antireflection coatings for high-efficiency silicon solar-cells," *IEEE Transactions on Electron Devices,* vol. 38, pp. 1925-1934, Aug. 1991.

[93]   S. Dimitrijev, *Principles of semiconductor devices*. New York, NY: Oxford University Press, 2006.

[94]   H. Tsai, C. Tu, and Y. Sun, "Development of generalized photovoltaic model using Matlab/Simulink," in *Proc. World Congress on Engineering and Computer Science* , San Francisco, CA, 2008, pp. 846-851.

[95]   M. Green, "Solar-cell fill factors - general graph and empirical expressions," *Solid-State Electronics,* vol. 24, pp. 788–789, Jan. 1981.

[96]   A. Green and J. Keevers, "Optical-Properties of Intrinsic Silicon at 300 K," *Progress in Photovoltaics,* vol. 3, pp. 189-192, May-Jun 1995.

[97]   Anonymous, "Optical coatings," in *Material Properties*, ed: Melles Griot, 2011, pp. 5.1-5.36.

[98]   Anonymous. (2012, Jan.). *Overview of materials for acrylic, extruded*. Available: http://www.matweb.com/search/DataSheet.aspx?MatGUID=632572aeef2a4224b5 ac8fbd4f1b6f77&ckck=1

[99]   Anonymous, "Solaphire PV high-transmissive glass," PPG Industries Inc., Cheswick, PA   2010.

[100]   M. Guvench, C. Gurcan, K. Durgin, and D. Macdonald, "Solar simulator and I-V measurement system for large area solar cell testing," in *Proc. American Society for Engineering Education Annual Confference & Exposition*, Salt Lake City, UT, 2004, pp. 12747-12753.

[101]   S. Aljoaba, A. Cramer, and B. Walcott, "Thermoelectrical modeling of light wavelength effects on photovoltaic cell performance," Unpublished.

[102] C. Gueymard, "The sun's total and spectral irradiace for solar energy applications and solar radiation models," *Solar Energy,* vol. 76, pp. 423-453, Aug. 2004.

[103] C. Gueymard and D. Myers, "Simple Model of Atmospheric Radiative Transfer of Sunshine (SMARTS)," 2.9.5.i1 ed: NREL, 2006.

[104] C. Honsberg and S. Bowden. (2010). *PVCDROM, PV Education.Org*. Available: http://www.pveducation.org/pvcdrom

[105] C. Gueymard, "The sun's total and spectral irradiace for solar energy applications and solar radiation models," *Soalr Energy,* vol. 76, pp. 423-453, 2004.

[106] W. U. Inc. (2011). *History for Lexington, KY*. Available: http://www.wunderground.com/history/airport/KLEX/2010/6/15/DailyHistory.html?req_city=NA&req_state=NA&req_statename=NA

[107] C. Gueymard and D. Myers, "SMARTS," ed: NLRE, 2010.

[108] C. A. Gueymard, "Parameterized transmittance model for direct beam and circumsolar spectral irradiance," *Solar Energy,* vol. 71, pp. 325-346, 2001.

[109] Anonymous. (2012, Dec.). *Overview of materials for polystyrene, extrusion grade*. Available: http://www.matweb.com/search/DataSheet.aspx?MatGUID=1c41e50c2e324e00b0c4e419ca780304

[110] Anonymous. (02/02/2012). *Weather History for Lexington, KY*. Available: http://www.wunderground.com/history/airport/KLEX/2010/6/15/DailyHistory.html?req_city=NA&req_state=NA&req_statename=NA

[111] L. Wei, T. Alkeskjold, and A. Bjarklev, "Electrically tunable bandpass filter based on liquid crystal photonic bandgap fibers," presented at the 2010 Conference on

Optical Fiber Communication, Collocated National Fiber Optic Engineers Conference, San Diego, CA, 21 March, 2010, pp. 1-3.

[112] S. Matsumoto, K. Hirabayashi, S. Sakata, and T. Hayashi, "Tunable wavelength filter using nano-sized droplets of liquid crystal," *IEEE Photonics Technology Letters,* vol. 11, pp. 442-444, Apr. 1999.

[113] S. Dep, "Photovoltaic-integrated electrochromic device for smart-window applications," presented at the World Renewable Energy Congress VI, Brighton, UK, July, 2000, pp.

[114] R. Vergaz, J.-M. Sanchez-Pena, D. Barrios, C. Va´zquez, and P. Contreras-Lallana, "Modelling and electro-optical testing of suspended particle devices," *Solar Energy Materials and Solar Cells,* vol. 92, pp. 1483-1487, May 2008.

[115] Anonymous. (2011, Jan.). *Polymer dispersed liquid crystal devices*. Available: http://www.smartwindows.info/liquid-crystal-devices.html

[116] B. Lamontagne, P. Barrios, and C. Py, "The next generation of switchable glass: the micro-blinds," in *Proc. Glass Performance Days*, Finland, 2009, pp. 637-639.

VITA

SHARIF ZIDAN AHMAD ALJOABA

Place of Birth: Hebron, Palestine

EDUCATION

- **University of Kentucky (UK),** Lexington, Kentucky**,** May 2013

  - PhD of Electrical Engineering
  - Dissertation: "Active Optimal Control Strategies for Increasing the Efficiency of Photovoltaic Cells"
  - GPA: 3.93/4.0

- **University of Kentucky (UK),** Lexington, Kentucky**,** December 2009

  - Master of Manufacturing Systems Engineering
  - Thesis: "Experimental Investigation and Modeling of Friction Stir Processing using 3D CFD Analysis"
  - GPA: 4.0/4.0

- **Palestine Polytechnic University (PPU),** Hebron, Palestine, July 2007

  - Bachelor degree in Mechatronics Engineering-Mechanical Engineering
  - Project: Design and Control of Power Assisted Jib Crane
  - GPA: 89.3/100

ACADEMIC HONOURS:

- **Scholarship for Doctoral Degree**, 2010-2013: Full Scholarship for the graduate degree (PhD in Electrical Engineering). Provided by University of Kentucky, USA.
- **Best Student Presentation Award Finalist** at 38th IEEE Photovoltaic Specialists Conference, 2012

- **Scholarship for Masters Degree**, 2008-2010: Full Scholarship for the graduate degree (Master in Manufacturing Systems Engineering). Provided by University of Kentucky, USA.
- **Scholarship for Undergrad Education,** 2003-2007: 8 semesters of honor with full scholarship, and passed in first class with distinction. Provided by Palestine Polytechnic University, Palestine.

PROFESSIONAL EXPERIENCE

1- **On-Board Diagnostics Development Engineer,** Cummins Inc.
  Columbus, IN, USA, 06/2012-Present

2- **Research and Development Engineer,** UK
  Lexington, KY, USA, 01/2008-06/2012
  - **Photovoltaic Cells Research and Development Engineer,** *09/2009-06/2012*
  - **Technical Advisor**, *01/2011-05/2012*
  - **Process Design Engineer**, *05/2008-09/2009*

3- **Lean Manufacturing Engineer**, Aichi Forge USA Inc.
  Georgetown, KY, *01/ 2009-04/2009*

PUBLICATIONS AND CONFERENCE PROCEEDINGS

- Published, "Thermoelectrical Modeling of Light Wavelength Effects on Photovoltaic Module Performance, Part I: Model", IEEE Journal of Photovoltaic, March, 2013.
- Published, "Experimental Parameterization of Wavelength-Based Thermoelectrical Model of PV Modules, Part II: Parameterization", IEEE Journal of Photovoltaic, March, 2013.
- Published, "Experimental Characterization of a Thermo-electrical Model of Photovoltaic Modules", 38th IEEE PVSC, Austin, June, 2012.
- Published, "Thermo-Electrical Modeling of Light Wavelength Effects on Photovoltaic Cell Performance", 37th IEEE PVSC, Seattle, June, 2011.
- Published, "Modeling of Friction Stir Processing with in Process Cooling using Computational Fluid Dynamics Analysis", CIRP, Abu Dhabi, UAE, 2011.
- Published, "Modeling the Effects of Coolant Application in Friction Stir Processing on Material Microstructure Using 3D CFD Analysis", Journal of Materials Engineering and Performance, July, 2010.
- Published, "Modeling of Friction Stir Processing Using 3D CFD Analysis",

Material Forming 12th ESAFORM Conference, Netherlands, April, 2009.

SKILLS

- Laboratory Skills:
  - o Experienced the advanced embedded systems laboratory (signal generator, oscilloscope, microcontroller kits, etc.).
  - o Mastered the design and implementation of **electrical** and **control** circuitry.
  - o Experienced **electrical** and **mechanical bench testing.**
  - o Carried out advanced material forming (Friction Stir Welding and Processing, Superplasticity).
  - o Skilled Material Processing Laboratory (Metallographic).
  - o Conducted Machining Operations (CNC lath and milling machines).
- Simulation Toolkits: Professional expertise: **SPICE, STAR CCM+, ANSYS 11,** and **MATLAB 8.1**/**SIMULINK.**
- Programming: Skilled in **C/C++** and **CNC Programming**.
- Computer Aided Design (CAD): Highly certified in **CATIA V5** and **AUTOCAD 2006.**
- Certified with the fundamentals of the **Diesel Engines** and their **After Treatment Catalyst System.**
- Applied Lean Manufacturing Methodologies.
- Skilled team work, communicating, time planning.

CLUBS AND ACTIVITIES

- Co-organizer at the 38th IEEE Photovoltaic Specialists Conference (PVSC), Austen, 2012
- Member of the Golden Key International Honor Society (GKIHS)
- Member of Institute of Electrical and Electronics Engineers (IEEE)
- Judge of Kentucky Junior Academy of Science for 2010 and 2011
- Leader soccer team for indoor 2010/2011 competition

LANGUAGE SKILLS

- Arabic language.
- High skills in reading, writing, listening, and speaking of English language

- The basics of Hebrew language.

PROFESSIONAL REFERENCES

- **Prof. Dr. Bruce Walcott**
  Associate Dean for New Economy Initiatives and Innovations Management
  Engineering Alumni Association Professor
  University of Kentucky, College of Engineering
  Department of Electrical and Computer Engineering
  221 DMB, Lexington, KY 40506-0503
  Phone: (859) 257 1182
  Email: walcott@engr.uky.edu
  Dr. Walcott is the chair of the advisory committee of my PhD degree, the supervisor of my research and the counselor of my degree's academic requirements.

- **Dr. Aaron Cramer**
  Assistant Professor
  University of Kentucky, College of Engineering
  Department of Electrical and Computer Engineering
  687B FPAT, Lexington, KY 40506-0503
  Phone: (859) 257 9113
  Email: cramer@engr.uky.edu
  Dr. Cramer is my co-advisor of my PhD degree. He is highly involved in my research. Dr. Cramer and I have worked together on different tasks and sub-objectives in the Photovoltaic modules research.

- **Prof. Dr. I.S. Jawahir**
  Director of Institute for Sustainable Manufacturing
  James F. Hardymon Chair in Manufacturing Systems Professor
  University of Kentucky, College of Engineering
  Department of Mechanical Engineering
  414C, CRMS Building, Lexington, KY 40506-0503
  Phone: (859) 323 3239
  E-mail: jawahir@engr.uky.edu
  Dr. Jawahir is my Co-advisor of my MS degree. He was highly involved in my manufacturing field research. He directed and advised me while working on the objectives of my project.

- **Prof. Dr. M.K. Khraisheh**
  Professor and Dean of Engineering
  Masdar Institute of Science and Technology
  Mechanical Engineering

Abu Dhabi, UAE
Phone + 971 2 810 9322
E-mail (Preferred): mkhraisheh@mist.ac.ae
Dr. Khraisheh is the chair of my MS degree committee and the Co-advisor of my research and the counselor of my degree's academic requirements.